2012-05-09

Refining Vibrationally-Resonant Sum Frequency Generation Spectroscopy for Studies of Interfacial Interactions

Alexander D. Curtis
Brigham Young University - Provo

Refining Vibrationally-Resonant Sum Frequency Generation Spectroscopy

for Studies of Interfacial Interactions

Alexander Dean Curtis

A dissertation submitted to the faculty of
Brigham Young University
in partial fulfillment of the requirements for the degree of

Doctor of Philosophy

James E. Patterson, Chair
Matthew C. Asplund
Steven R. Goates
Juliana Boerio-Goates
Matthew R. Linford

Department of Chemistry and Biochemistry

Brigham Young University

June 2012

ABSTRACT

Refining Vibrationally-Resonant Sum Frequency Generation Spectroscopy
for Studies of Interfacial Interactions

Alexander D. Curtis
Department of Chemistry & Biochemistry, BYU
Doctor of Philosophy

Many phenomena of interest to science and engineering occur at interfaces; however, access to, or discrimination of, interfacial interactions has been challenging, especially at buried interfaces. Vibrationally resonant sum-frequency generation (VR-SFG) spectroscopy is a powerful tool for investigating the molecular structure of free or buried interfaces, but spectral analysis has relied on many assumptions. To claim accurate new insights, practitioners must be able to make unique determinations from the data without experimental artifacts affecting the final results. For example, two independent and overlapping studies for the polystyrene/air interface were carried out, but reported different surface structures. Initially, this difference was attributed to the use of different substrates, but we have shown that the surface structure is independent of substrate by experimental suppression of the interfering nonresonant signal. These results show difficulties in SFG analysis that have led to faulty determinations of structural changes. Similar problems have been observed in systems assumed to have negligible nonresonant interference, demonstrating the need for proper experimental design instead of relying solely on post-experimental analysis of the data. We have investigated the inherent limitations imposed on the technique from the nature of the signal generation and nonresonant interference, and have developed methods to overcome such difficulties, depending on what is desired from the data.

By nature of nonlinear spectroscopy, the desired frequency response is affected by overlapping interactions in the time domain, and these time domain interactions can be exploited to overcome challenges in analysis. By delaying the upconverting pulse, the nonresonant signal can be removed to enable accurate qualitative comparison or even quantify change; however this removal results in incomplete upconversion, or apodization, of the resonant signal, causing distortion in the observed resonant response. If absolute parameters are desired, additional work is necessary to correct the distortion of the resonant response. Correction can be accomplished by further exploiting time domain effects by collecting spectra at various delay times of the upconverting pulse, and this additional data also aids in interpretation of congested spectra. Many practical applications, however, only require a means to quantify change, and measurements of change are unaffected by the effects of apodization. These techniques have been used to more accurately analyze polystyrene and octadecylsilane surfaces.

Keywords: sum frequency spectroscopy, polystyrene, nonresonant signal, surface science

ACKNOWLEDGEMENTS

CONTENTS

CHAPTER 1: INTRODUCTION AND BACKGROUND

1.1. MOTIVATION IN USING SUM FREQUENCY GENERATION SPECTROSCOPY FOR INTERFACIAL STUDIES

Many interfacial processes such as friction, lubrication, and adhesion are of significant interest in science and engineering applications, but have been difficult to access for direct analytical study. Three requirements must be simultaneously met for accurate study of these interfacial interactions. First, there must be adequate discrimination between interfacial and bulk molecules to study the desired interface. Second, information must be accessible from the buried interface without destruction of that interface. Third, high sensitivity is required to produce a clear response with the fewer molecules that are present at the interface to understand what processes are involved.

These requirements, if taken alone, can be met with a variety of techniques, but techniques that can accomplish all three requirements simultaneously are limited. Surface science techniques, such as atomic force microscopy or x-ray photoelectron spectroscopy, can provide high discrimination of the surface from the bulk, but these techniques fail to provide access to the buried interface without first destroying that interface. For studying an interfacial property such as adhesion, if the adhesive interface is broken to provide a free surface of study, the adhesive interactions have also been destroyed and the desired properties are no longer present to study. Many spectroscopic techniques provide access to buried interfaces as long as one substrate material is transparent to the frequencies of light used, but most techniques cannot often provide adequate discrimination between the interfacial molecules involved in the interactions and the bulk molecules.

1.1.1. Advantages of sum-frequency generation spectroscopy

Study of buried interfaces is now possible with the development of sum-frequency generation (SFG) spectroscopy.[1] SFG is a nonlinear optical process using two different input beams to produce a new output beam whose frequency is the sum of the two input frequencies (see Figure 1-1). SFG utilizes high power lasers that negate a simple approximation of material permittivity with an electric "constant" and induces higher order polarizations that must be used to describe the response. In linear optics the input and output frequencies and polarizations are the same, but in nonlinear optics, a nonlinear polarization is created that generates an output beam with a different frequency and may also change the polarization. Because SFG is a nonlinear process involving two input frequencies, it is dependent on a nonlinear polarization that is governed by the $\chi^{(2)}$ tensor as shown in the following equation.

$$\vec{P}^{(2)}(\omega_3) = \chi^{(2)} : \vec{E}_1(\omega_1)\vec{E}_2(\omega_2) \tag{1}$$

The $\chi^{(2)}$ tensor, shown in equation 1, provides SFG with interfacial discrimination. Under the electric dipole approximation, the $\chi^{(2)}$ tensor (shown in Figure 1-2) produces no signal in a centrosymmetric medium. This requirement for lack of centrosymmetry can be seen by applying physical constraints to the mathematical model that is used. Many materials, such as atactic polymers, possess an isotropic bulk, so the mathematical model must also show that all directions and symmetries are equal in the bulk. For example, if we place ourselves at the origin, looking right must be the same as looking left, which can be mathematically represented as +x=-x. The only way for this to be true is for x=0. As this symmetry operation is applied to all three indices, it can be seen that the tensor element of xxx must be 0 because xxx=-x-x-x=-xxx. As similar symmetry operations are applied to all 27 elements of the tensor, for a completely isotropic medium, all elements will go to 0.
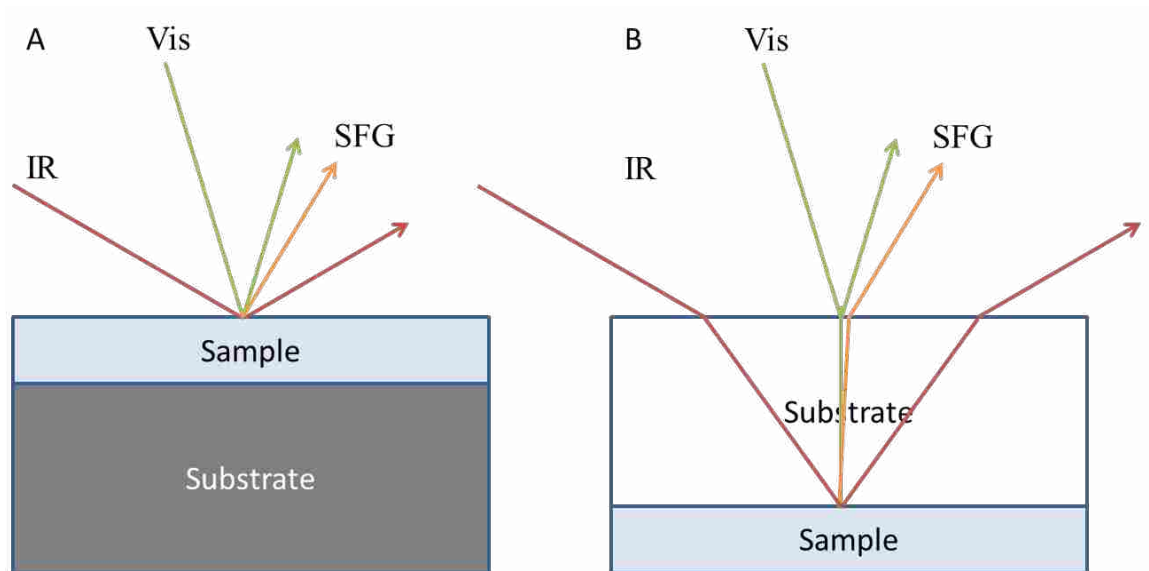
Figure 1-1 SFG is generated by the combination of the two input frequencies. Panel A illustrates SFG generated from a free surface while panel B shows SFG from a buried interface.
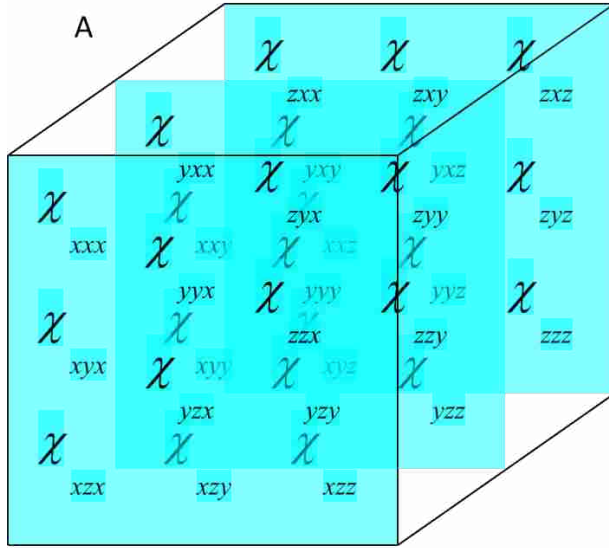
$$\chi_x = \begin{bmatrix} \chi_{xxx} & \chi_{xxy} & \chi_{xxz} \\ \chi_{xyx} & \chi_{xyy} & \chi_{xyz} \\ \chi_{xzx} & \chi_{xzy} & \chi_{xzz} \end{bmatrix}$$

$$\chi_y = \begin{bmatrix} \chi_{yxx} & \chi_{yxy} & \chi_{yxz} \\ \chi_{yyx} & \chi_{yyy} & \chi_{yyz} \\ \chi_{yzx} & \chi_{yzy} & \chi_{yzz} \end{bmatrix}$$

$$\chi_z = \begin{bmatrix} \chi_{zxx} & \chi_{zxy} & \chi_{zxz} \\ \chi_{zyx} & \chi_{zyy} & \chi_{zyz} \\ \chi_{zzx} & \chi_{zzy} & \chi_{zzz} \end{bmatrix}$$
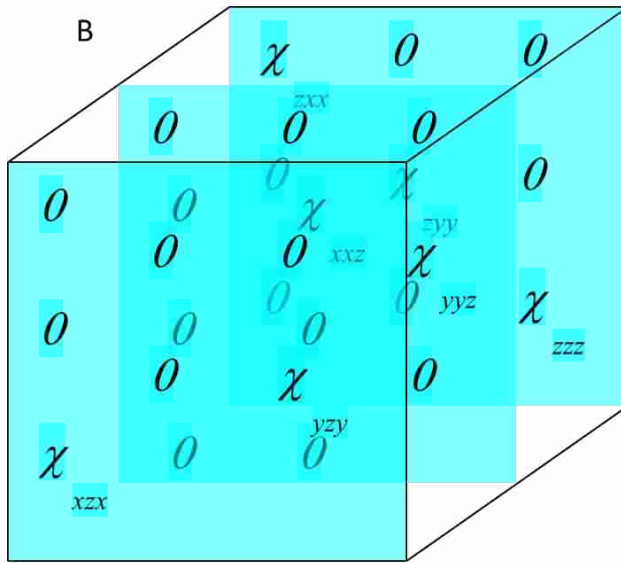
$$\chi_x = \begin{bmatrix} 0 & 0 & \chi_{xxz} \\ 0 & 0 & 0 \\ \chi_{xzx} & 0 & 0 \end{bmatrix}$$

$$\chi_y = \begin{bmatrix} 0 & 0 & 0 \\ 0 & 0 & \chi_{yyz} \\ 0 & \chi_{yzy} & 0 \end{bmatrix}$$

$$\chi_z = \begin{bmatrix} \chi_{zxx} & 0 & 0 \\ 0 & \chi_{zyy} & 0 \\ 0 & 0 & \chi_{zzz} \end{bmatrix}$$

Figure 1-2 The $\chi^{(2)}$ tensor shown in part A contains all 27 elements. After assuming an isotropic bulk and azimuthal symmetry at the broken interface, it reduces to the seven elements shown in B, only four of which are independent.

At an interface, where one plane of symmetry has been broken, 7 elements remain that are nonzero (i.e. xxz, yyz, xzx, yzy, zxx, zyy, and zzz). These 7 remaining elements require the assumption that the interface possesses azimuthal symmetry, meaning all neighboring molecules on left and right are the same with the broken symmetry only resulting from down being different than up. Of those 7 elements, the azimuthal symmetry dictates that that xxz=yyz, xzx=yzy, and zxx=zyy, so only 4 independent elements remain nonzero, including zzz.

Different elements of the $\chi^{(2)}$ tensor can be selectively probed by using different polarizations of light to isolate specific information. Each index in the tensor represents a different beam of light with its respective polarization and conventional ordering used to describe the polarization combination goes from short wavelength to long wavelength. The *p* polarization indicates a polarization parallel to the plane of incidence (which includes x and z elements) and *s* polarization is perpendicular to the plane of incidence (y elements). For example, an *ssp* polarization means an *s*-polarized SFG beam results from an *s*-polarized visible beam and a *p*-polarized IR beam that probes the yyz element of the tensor (which is equivalent to the xxz).

Because the resonant excitation is caused by the IR beam, the *ssp* combination is best suited for probing of upright molecules while the *sps* combination is more sensitive to molecules that are lying down. This is because molecules that are more upright relative to the surface are more in line with the plane of incidence and will be more sensitive to the *p* polarization, while molecules that are lying near the surface, or more perpendicular to the plane of incidence, benefit more from *s* polarization. The *ppp* polarization samples all 4 independent elements (zzz, xzx, xxz, and zxx) of the $\chi^{(2)}$ tensor because of the symmetry relations at an interface. As such, *ppp* can be considered as the most information rich, but behavior relating to any specific tensor element is difficult to determine causing a practical constraint that compromises the extraction of

information. The *ssp* and *sps* polarizations can be more useful in analysis because only a single tensor element is probed, so there is a more definitive source of the observed signal to link with molecular symmetry.

A potential restriction on SFG spectroscopy is that the vibrational modes which are observed must possess both IR and Raman activity. Signal generation in SFG involves an excitation by the IR light to provide the resonant response that is then upconverted by the visible beam through a Raman process. Because both IR and Raman processes are required, neither the IR dipole moment nor the change in Raman polarizability can be 0 for SFG signal to be generated. This seems to be a large restriction because IR and Raman intensity often have a significant trade-off in intensity that would greatly minimize the applicability of this technique; however, this trade-off occurs only when the probed molecules possess inversion symmetry. This difficulty is negated because the $\chi^{(2)}$ tensor that governs the SFG process dictates that signal can only be produced by areas of broken symmetry. This overcomes the intensity trade-off and allows most materials to provide an SFG response.

The SFG technique can provide access to molecular level information at surfaces and interfaces without interference from the bulk of the sample. Not only does this technique allow for the investigation of free surfaces, but it also allows access to the buried interface as long as the material covering that interface is transparent to the probe beams (see Figure 1-B). Chemical information can be obtained as in other spectroscopic techniques, but additional information about the physical structure of the molecules is extracted because the differing polarizations of light will interact differently with the molecules dependent on their physical orientation. This aspect of the technique makes it possible to gain information about both the chemical and physical mechanisms involved in interfacial interactions.

1.1.2. *Processes involved in SFG*

Because the visible and IR photons interact nearly simultaneously to generate SFG light, coherence is maintained which boosts sensitivity and affects the observed line-shapes and interferences. Although non-linear processes are inherently weaker than linear processes, the coherent nature of the response allows the entire signal to be collected to help mitigate the weaker response. The signal generated produces two types of responses, termed the resonant and nonresonant contributions. The resonant signal results from the interactions of light that produced SFG from molecular vibrations that are resonant with the IR frequencies present in the pulse. Nonresonant contributions result from light interactions that are not resonant with the molecular vibrations and have been commonly attributed to much faster electronic responses that are also excited by the IR pulse. The resulting signal is often modeled according to the following equation.

$$I_{SFG} = \left| \chi_{NR}^{(2)} + \chi_{R}^{(2)} \right|^2 = \left| B_{NR} e^{i\Phi} + \sum_k \frac{A_k}{\omega - \omega_k + i\Gamma_k} \right|^2 \qquad (2)$$

In equation 1-2, I_{SFG} represents the intensity of the SFG signal with χ_{NR} and χ_R representing the nonresonant and resonant interactions. These interactions are typically modeled as B_{NR} being the response of the nonresonant signal, with A_k, w_k, and Γ_k representing the amplitude, central frequency, and half-width at half-max of a Lorentzian lineshape respectively. The $e^{i\Phi}$ term accounts for the phase difference between the resonant and nonresonant signal. It should also be noted that for a Lorentzian line-shape in this form, A is only proportional to the amplitude and is coupled to the linewidth (specifically, A=sqrt(amplitude) x Γ). Furthermore, the Γ parameter additionally relates to the vibrational lifetime of the mode, specifically $\Gamma=(4\pi T_2)^{-1}$ which will be explicitly utilized in chapter 6.

1.1.3. *Frequency scanning versus broadband SFG systems*

The first applications of SFG utilized frequency scanning experiments[1] with long duration pulses (nanosecond) for both the visible and IR beams. Both resonant and nonresonant responses are continually driven throughout the duration of the IR pulse. Due to the physical relationship between frequency and time, the long IR pulse is only able to excite a very narrow range of frequencies at one time. This process necessitates multiple scans across a range of frequencies to build up the spectral response from a sample. Because the visible pulse is also long, it is able to upconvert all of the response driven by the IR pulse and potentially yield resolution dependent only on the peak widths. However, the resolution obtained from this process is realistically dependent on how many frequency points are scanned to build up the spectrum, so the number of data points collected by the experimenter often dictates the resulting resolution.

Later on, the broadband SFG technique[2,3] was developed and allows for faster collection of data. In the broadband technique, shorter pulses (often around 100 femtoseconds) are used. A shorter IR pulse allows excitation over a broad band of frequencies allowing for simultaneous collection without the need for scanning. However, when the visible pulse is also short, the visible frequency is also broad leading to very poor frequency resolution. It is possible to scan across multiple times to build up the full time response which can then be transformed into the frequency response to provide higher resolution,[4] but the speed advantages of broadband collection are lost.

To improve resolution the visible beam is lengthened in time, which causes it to spectrally narrow in frequency. This can be accomplished by either passing it through a narrow slit (a common procedure to improve frequency resolution and maintains a Gaussian profile) or by passing it through a Fabry-Perot etalon (which imposes an exponential decay of the signal). As

the longer visible pulse is convolved with the IR response, it is able to upconvert more of the signal in time resulting in high resolution spectra that can simultaneously detect a broad band of frequencies. This method allows for faster detection because there is often no need for scanning (some scanning may be necessary if a larger frequency range is desired than the intensity profile covers), and higher time resolution experiments can be performed with the shorter pulses.

1.1.4. *Analyzing SFG data*

The common means of analysis for SFG data is to fit the spectral response to equation 2, but accurate analysis with nonlinear curve-fitting procedures requires most of the parameters to be known and constrained;[5] however, known constraints are not often present in the analysis of SFG data. When fitting spectra, constraints can be applied from previous experiments that were performed to comprehensively determine peak parameters, such as a definitive line-width or frequency position; however, because SFG contains an inherent sensitivity to areas of broken symmetry, a different environment is being probed. This different environment often results in deviations from known parameters determined in bulk probing techniques such as IR or Raman spectroscopy.

The deviations of SFG data from linear techniques are manifest in multiple ways: shifts in peak frequency, changes in line-width, and even the presence or absence of specific vibrational modes. Additionally, the interference of the nonresonant signal can cause peaks to adopt a derivative line-shape, which further complicates the determination of central frequencies or the number of peaks to be used. These additional factors in SFG data may compromise previously known constraints that could be used in fitting of spectroscopic data. Most often, the fit parameters are extracted from SFG data without applying any definitive constraints to the model

9

in equation 2, and a more thorough discussion and analysis of this analytical routine will be given in chapter 2.

To determine physical information from the extracted peak parameters, such as molecular tilt angle, a ratio between peak amplitudes is used. This can be accomplished in multiple ways, such as comparing the amplitudes of the same peak in two different polarizations, or by comparing orthogonal vibrational modes in a single polarization. The analysis presented here uses single polarization data, and incorporates fundamental relations formulated by Hirose et al.[6] with additional mathematical work performed by Duffy et al.[7] on those relations. This work was algebraically manipulated into a single equation by Gautam et al.[8] This particular equation invokes the assumption of C_{2v} symmetry and reduces the number of unknowns by assuming that the twist angles of molecular groups are randomly oriented and can be averaged out. This allows a single unknown tilt angle to be determined using the ratio between different vibrational modes within the *ssp* polarization according to the following equation:

$$R = \left| \frac{A_{II}}{A_{I}} \right| = \left| \frac{\beta_{caa,II}}{\beta_{aac,I}} \left(\frac{2(\langle \cos 3\theta \rangle - \langle \cos \theta \rangle)}{(7+2r)\langle \cos \theta \rangle + (1-2r)\langle \cos 3\theta \rangle} \right) \right| \qquad (3)$$

In the above equation, R denotes the observed ratio of peak amplitudes, A_{II} and A_{I} are the amplitudes of the type II and type I vibrations (also known as B_1 or A_1 vibrations, respectively, in character tables), β is the hyperpolarizability for the vibrational mode possessing the molecular indices noted (*caa* or *aac* and can be mapped to the lab frame of reference, in this case xxz), and *r* is the hyperpolarizability ratio β_{ccc}/β_{aac} for the same type I vibration. The downside is that hyperpolarizabilites are often ambiguous in determination; however, this difficulty is common to other analysis techniques as well. If hyperpolarizabilites are known, orientational information can then be determined from data within a single polarization by the above equation.

Polystyrene has been of particular interest in our studies, but understanding why requires a critical analysis of the work that has been performed. Understanding of adhesive interactions is one of the primary interests of our lab and polystyrene has been involved in studies to correlate molecular structure to adhesive performance.[9] However, it should be noted that the conclusions of the adhesive study are potentially compromised by an unresolved issue of the surface structure of polystyrene.[8,10] Two independent studies investigated the surface structure of polystyrene at nearly the same time, but reported two completely different orientations. This discrepancy should have raised concerns about the use of the technique, but the issue seems to have been largely ignored without any direct investigation into the differences. If these issues remain unresolved, it is difficult to claim that SFG data can provide accurate information.

1.2.1. Initial polystyrene report

The first investigation of the surface structure of polystyrene with SFG spectroscopy was performed by Gautam et al.[8] The samples for this study were produced by spin-coating polystyrene onto sapphire prisms. The film thickness for the samples was 160 nm (no uncertainty range given). Molecular structures for both the PS/air (free) interface and PS/sapphire (buried) interface were reported. By changing the incident angles of the beams, they claimed interface selectivity by enhancement of the Fresnel factors from the interface of interest. They collected data using *ssp* and *ppp* polarizations in this study, but as stated previously in section 1.1.1, *ppp* is not as informative in SFG studies due to inadequate discrimination in data analysis, although it does often provide the most intense signal. The reasoning for the additional *ppp* investigation was never stated.

To test which surface was being observed, spectra of the surface were collected before and after a short plasma treatment. If the spectrum remained unchanged after plasma treatment, they concluded that the buried interface was being observed. Likewise, if the spectrum changed after plasma treatment, they concluded that the free interface was observed. They neglected to show the spectra before and after plasma treatment for the reader to verify. In a separate study by a different group that did show before and after spectra,[11] there were small, but noticeable changes to the spectra that were likely discredited as noise (the other group neglected any change as well). Our group has since shown[12] that plasma treatment is not a valid test for surface specificity, but this was not known at the time.

The method used for determining orientation in this study is outlined in section 1.1.4. They invoke the assumption that their annealing process of 110° C for 4 hours was sufficient to allow for the random distribution of twist angles required. The unknown hyperpolarizabilites were determined in this study by a combination of theoretical and fitting constraints. The r ratio was calculated theoretically for the ν_{7a} mode, which was fit as a negative peak at 3037 cm^{-1}. The hyperpolarizability ratio of a type II mode to a type I mode was determined by post-experimental data processing and comparing to all possible values for the β_{II}/β_{I} ratio within their peak ratios obtained from fitting. The fitting results of their PS/sapphire interface provided a lower bound constraint to the hyperpolarizability values, while the upper bound was set by standard IR and Raman intensities. The middle of these bounds was used as the needed ratio for analysis.

The tilt angles calculated from their spectra were interpreted as the phenyl group at the buried interface being tilted 70° from the surface normal (or 20° relative to the surface) and 20° from the surface normal (70° from surface) at the free interface. The strength of the signal form the phenyl rings and lack of signal from the methylene groups was surprising to this group and

went against their prediction of methylene dominance at the surface. They expected the methylene modes to be more dominant at the free surface because they are more hydrophobic than the phenyl groups to provide a favorable interaction with the air. Because they did not observe a strong methylene signal they concluded that the methylene groups must be in a disordered state.

1.2.2. Conflicting report on polystyrene orientation

A conflicting report on the free surface structure of PS was published by Briggman et al.[10] from a NIST group in Maryland. In this study, SFG was also used to investigate the surface structure of polystyrene, this time on silicon. In the NIST paper they report the free surface phenyl groups being tilted about 57° from the surface normal (33° from surface), which is nearly 3 times larger than what Gautam et al.[8] reported. This second paper also claims to be the first measurements of the molecular orientation of the polystyrene surface, but the nearness of publication dates likely means that this group was not aware of the initial polystyrene study. The lack of awareness of the initial study is actually beneficial because it is often the tendency to not repeat what has already been done. More interesting than the claim of who was really first to study the surface of polystyrene is the fact that the two papers do not agree in their results.

The NIST group claimed that the interface being investigated by SFG can be determined by the film thickness. The assumption made is that as long as the thickness exceeds 6 times the radius of gyration for the polymer, the molecular structures are independent of film thickness. This claim came from cited papers using neutron scattering experiments that show the substrate no longer has an influence after 5 times the radius of gyration. Since their chosen thickness of 350nm is well beyond that requirement (radius of gyration being 13 nm), they claim investigation of the free surface of polystyrene independent of other influences that may result

from film thickness or bulk properties. Also, they state repeatedly in this paper that the signal coming from the free interface is significantly higher than any that may come from the buried interface to justify their free interface selectivity.

As part of their investigation, the phase dependence of Fresnel factors were calculated for various thicknesses of polystyrene films. However, as will be shown in chapter 5, this thickness dependence can be attributed to an effect of thin film interference without a need to invoke Fresnel factors. The orientation analysis of the surface was determined from a film that is 350 nm thick because they claim a maximum of signal intensity resulting from both phase and Fresnel factors at that thickness for all polarizations.

This group additionally claimed determination of an absolute orientation of the phenyl peaks by comparison to a phenylsiloxane self-assembled layer. This method allows determination of an absolute orientation by comparison of phase relations to the vibrational modes in a reference material of known orientation, thus constraining an absolute up versus down alignment of the molecules.[13] In this study there is an assumption that the phenyl groups of the phenylsiloxane layer are pointed up. It should be noted, however, that they used a triethoxyphenylsilane which can polymerize in solution. Because polymerized triethoxyphenylsilane is not confined to a single monolayer, many orientations are possible, which compromises the usefulness as a reference material for orientation.

Orientational analysis was performed by fitting the data of both the *ssp* and *sps* spectra and comparing the ratios of peak amplitudes in the different polarizations. They acknowledge the fact that rough surfaces could distort the analysis and claim that their surfaces are sufficiently smooth to avoid that problem (RMS roughness less than 1 nm). However, they also report a roughness of the phenylsiloxane layer that is greater than 1 nm, which from their own report, is great enough

to potentially cause problems, but that seems to be ignored in analysis. They also acknowledge that their results differ from previously reported near-edge X-ray absorption fine structure spectroscopy (NEXAFS) determinations on the structure of polystyrene and attribute that to an inability for NEXAFS to really determine phenyl group orientation.

A review written by Chen et al.[14] claimed that the difference in the two nearly simultaneous studies must result from the different substrates used. This claim could account for part of the difference if film thickness is also a factor because the polystyrene films of Gautam et al.[8] were 160 nm and could have experienced more influence at the surface from the substrate; however, if the assumption based on the radius of gyration is correct the substrate should not have had an influence since both films were above 6 times the radius of gyration. Other possible causes could include the different annealing conditions used in the two studies, or because the two groups used different mode assignments for their spectra and analysis.

1.2.3. A new model suggesting multiple resonant interferences

Another complication in the analysis of SFG spectra of thin polymer films was suggested by the same NIST group when they published a paper suggesting interferences from two resonant signals due to the presence of two different interfaces.[11] In this paper, they claim the observed SFG signal is actually a composite of two resonant signals, one from the light reflected by the interface of interest, and the second from the light that travels through the bulk and generates a second signal at the other interface. This claim conflicts with the numerous statements in their previous paper that the signal intensity is significantly weaker at the buried interface and can be neglected.[10] Under the new claims of their publication, SFG analysis without correction for interference from the second resonant signal at the other interface is inaccurate.

To account for the possible interference problem from signal coming from two different interfaces, a layer of spin-on-glass (SOG) was placed in-between a 129 nm thick PS film and a reflective gold substrate to create another interfering signal (see Figure 1 - 3). By varying the thickness of the SOG, they claimed that the transmitted signal from the polymer/glass interface could destructively interfere and cancel with the reflected signal from the same interface so that the observed signal is solely from the free surface. Likewise, they claimed they could alter the SOG thickness to cancel out the signal from the free surface with the transmitted signal to allow only the observation of the buried PS/SOG interface. The spectra shown in the paper were clearly different, which they claim as verification that this method achieves interface specificity. In addition, when adding in an extra interface into the fitting equation better fits are obtained, which is used as further justification.

Although the interference model showed a valid concern and provided a potential solution to the discrepancy of the polystyrene surface structure determined by SFG data, it still lacked any direct testing to confirm such a cause. This potential solution assumes that the spectral difference only results from the different SFG signal produced by the buried polymer interface, and the structure of the buried interface is dependent on the substrate. The spectra from the two papers on polystyrene structure actually possess a similar appearance except for the higher resolution in the initial study (due to use of a frequency scanning system), but inaccuracy in the data model or inconsistency in analysis was not proposed as a potential problem despite the similarities of the spectra. As shown in later chapters, analysis is at the heart of the problem.
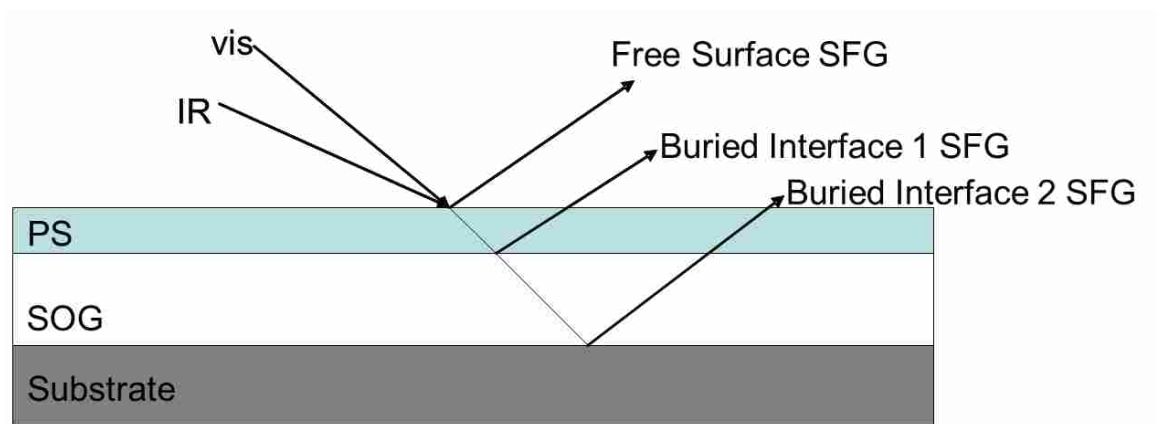
Figure 1 - 3 Under the new model for multiple interferences, there will be a resonant signal generated from both the PS-air interface as well as the PS-substrate interface. By adding in a transparent layer of spin on glass, they claim creation of a new SFG signal that can cancel with either the air or buried interfacial signal for isolation.

The evidence of this multiple interference model seems compelling, but key factors have not been considered. First off, their buried interface spectrum looks very similar to what is typically observed in broadband SFG for a pure nonresonant signal (and they did utilize a broadband system), which could suggest that they only altered interference between resonant and nonresonant signal. The nonresonant signal will dominate as thin-film interference causes most of the resonant signal to cancel and they may have labeled the spectra in which the nonresonant signal dominated as the buried interface. This alternative possibility, however, goes against one of the dominant assumptions at the time that the nonresonant signal is generated solely from the substrate. So, despite the nearly identical appearance, it is likely that because the "buried" signal did not appear to come solely from the substrate, the signal is attributed to a resonant contribution from the buried interface.

Furthermore, previous SFG papers (including the initial polystyrene study by Gautam) have tested their interface specificity for a buried signal by exposing the free surface to plasma, ozone, or UV for alteration or destruction. Despite the new evidence we have collected compromising such an interpretation of surface specificity,[12] this interference model still does not agree with the observations in such tests. In the interference paper, isolation of the response required a third SFG signal to be created to selectively cancel out the undesired interfacial signal. If SFG signal is actually an interference of resonant signal from both interfaces, then altering the free surface should also alter the signal observed when supposedly looking at the buried interface without the third signal used for selective destruction; however, this extra effort was not used in previous studies that still showed negligible change. Additionally, an improvement in curve fitting is not a valid proof of the physical model because doubling the number of parameters should always result in an improvement to the fit, as discussed explicitly in chapter 2.

Although the potential for interference is an important claim that required consideration, and the testing was primarily in agreement with the knowledge concerning SFG at the time, their conclusions are inconsistent with other studies. It should also be noted that this paper is in contradiction to studies using angle-resolved electron spectroscopy that show that there is no ordering of the polymer until it is sufficiently thick (around 27 nm), at which point the free surface starts ordering.[15] The logical implication of the electron spectroscopy study is that there is no preferred order at the buried interface (however, this thickness requirement is for polymers and not for monolayers which often utilize a direct chemical attachment to the substrate that requires ordering at single molecular layers). Despite the lack of consistency that this interference model has with other studies, and even self-consistency within SFG studies as I have pointed out, the interference model has gained a lot of support as the accepted model for SFG analysis.[11,16–21] However, there is no possible way to obtain accurate information from this method of analysis, as illustrated in chapter 2.

1.2.4.   Application of Orientational Information to Adhesion

Determining interfacial molecular structure alone may be sufficient to satisfy scientific curiosity, but the real power of any scientific technique lies in the application of the scientific information gained from the studies. Application of scientific knowledge to practical problems additionally serves as confirmation of the scientific claims. If any trends in polymer surface structure can be determined, this knowledge of structure changes should be applicable to the determination of factors affecting adhesive properties. Such knowledge could be directly applied to engineering of adhesives or lubricants without the need for empirical optimization routines. As was previously stated at the beginning of section 1.2, correlation between molecular structure and adhesive performance for polystyrene has been reported by the same NIST group.[9] Specific

claims regarding the adhesive mechanism were presented despite the still unresolved issue of the free surface structure of the polymer. Although such definitive claims are potentially premature without resolving the discrepancy in SFG analysis of polystyrene, this study illustrates practical uses of SFG that are of general interest.

For their adhesion study, the molecular structure and adhesive strength of PS were investigated on hydrophobic and hydrophilic surfaces. This was accomplished by spin-coating polystyrene (now ~200 nm thick) on various surface-modified glass substrates. Adhesive strength was determined qualitatively by a peel test, which a coating passes if it cannot be removed with adhesive tape, and fails if it is removed with the tape. The glass used in this study, Spin-on-glass (SOG), is natively hydrophobic due to termination with a Si-H group; however, after subjection to UV-ozone treatment for approximately five minutes, the surface composition changes to Si-OH and becomes hydrophilic. Water contact angles were measured to verify the hydrophobicity or hydrophilicity of the surface. RMS roughness was determined for both the glass and the PS film to verify that roughness was not a factor in the analysis.

When coated on hydrophilic surfaces, polystyrene passed the peel test, but on hydrophobic surfaces it did not. In order to link molecular structure to these observed adhesive properties, SFG spectra were collected from what they believed to be the buried interface. The resulting spectra were normalized to a gold mirror coated with deuterated PS as an intensity profile reference.

The observed spectrum of polystyrene on a hydrophilic substrate was clearly different than that of the polymer on a hydrophobic substrate. The data was fit using the interference model previously suggested by this group. On a hydrophobic substrate, they claimed both the free and buried interface possessed similar amplitudes but differed by a phase factor. This

suggested that the orientation of the phenyl groups at both interfaces was similar because they were pointing away from the bulk PS. Broader peaks for the buried interface suggested more heterogeneity than at the free surface. For a hydrophilic substrate, they concluded that the phenyl rings oriented themselves more parallel to the surface to maximize the intermolecular bonding between the surface hydroxyl groups and the pi electrons of the phenyl groups. They state that the spectrum for this buried interface on a hydrophilic substrate is similar to the one observed for the study performed by Gautam[8] on a sapphire substrate. They attribute this spectrum to simply be the characteristic structure of PS for hydrophilic substrates.

Although this paper may seem to resolve the discrepancy between this group's original polystyrene report and Gautam's polystyrene report, their determination lacks confirmational testing and self-consistency. Their polystyrene tests were performed on silicon, which is also a very hydrophilic substrate, but their silicon studies do not agree with the proposed structures on hydrophilic substrates. This study reports that polystyrene on a hydrophilic substrate results in a tilt angle of 40° relative to the surface normal, which, if in reference to the buried interface (it wasn't entirely clear) is almost half of what was claimed for the buried interface by Gautam,[8] who claimed a buried interface tilt of 70°, and if referring to the free surface is double what was reported by Gautam. They also report a torsional angle of 30° relative to the backbone at the buried interface, which, if true, would mean that it may have been incorrect to assume that this angle was random and could be neglected in the original polystyrene studies. However, solving for both a tilt and a torsional angle provides an additional unknown that cannot be determined from a single equation, independent of the method of orientational analysis being used. Significant complications in these determinations result from the models used for analysis that allow multiple interpretations of the data.

Because multiple interpretations of the data are possible, many models can be made to fit the data, only one of which can be correct. This flexibility in interpretation requires validation of the proposed science, such as providing predictive power that can be tested. However, this adhesion study is only a proposed mechanism of what specifically occurs with polystyrene phenyl rings when adhesion (or lack thereof) is already occurring. Previous to the NIST adhesion study, it has been common knowledge that hydrophilic surfaces enhance adhesion, and the results obtained did not conflict with this knowledge. There are no testable properties or modifications reported to provide predictive power, only a proposed mechanism to explain what already occurs for a specific molecule. Without providing any predictive power, the proposed mechanism is arbitrary. The plausibility of the mechanism serves to somewhat support this interpretation of orientation from the spectra, but cannot be confirmed. Without a more definitive means to interpret spectra and determine molecular structure at interfaces, the technique does not possess the power to elucidate new information.

Some mechanisms, though correct, go against conventional knowledge and require a restructuring of thought. For example, the thermodynamic explanation of why a rubber band releases heat when stretched is initially counter-intuitive, but fully explained by thermodynamics. Most materials require heat to overcome the breaking of intermolecular causing the material to cool when it expands and to release of heat as it recompresses and reforms the bonds. The rubber band behaves oppositely because the molecules are in the higher entropy state when relaxed, but form energetically favorable interactions upon stretching. The simple experiment of stretching a rubber band definitively illustrates an exception to the general trend of many materials and serves as a valuable example to more thoroughly understand materials and thermodynamics.

Similarly, a technique claiming new insights must be able to independently provide new information that may challenge conventional wisdom, but is nonetheless true.

Although the adhesive study focuses on an engineering application, if the model used for analysis is inaccurate, the results are likely inaccurate. The results of the proposed mechanism for polystyrene adhesion have not been used in predicting anything new to add validity to the claims, compromising the support that is gained from the plausibility of the mechanism. It is unlikely that they would have reached the same conclusions if they had not used a multiple interface model and the analysis is strongly dependent on the set of assumptions invoked. Further experiments are still necessary to confirm the validity of such assumptions and models.

1.3. CONCLUSIONS AND OUTLINE FOR FUTURE CHAPTERS

SFG has been used for polymer studies to obtain information regarding interfacial interactions at the molecular level, but there are still challenges to be worked out. The disagreement on the reported surface structure of polystyrene and what factors may affect that structure are crucial issues that bring into question the validity of using this technique for practical analysis. If two different groups studying the same material arrive at two different conclusions, then accurate analytical capability cannot yet be claimed. The justification of substrate influence was proposed without any direct testing and this suggestion does not provide adequate justification to disagree with determinations already made with other techniques. Many experimental factors differed in the two polystyrene studies that could also potentially result in different orientations. Additionally, differences in modeling and analysis of the results will also result in different interpretations of data even in the absence of orientational differences. Furthermore, much of the analysis performed in the field has been based upon theoretical

predictions, but if the experiment does not possess the capability to independently disprove the theory, then the experiments can provide no additional information.

A series of experiments were performed to further investigate the stated difficulties with SFG spectroscopy and resolve these issues so that greater confidence can be given to analytical results obtained from this technique. These investigations have invalidated many of the assumptions used in previous studies, thus compromising many of the scientific insights claimed. In chapter 2, I will show the general problem with relying on curve fitting for accurate analysis of spectroscopic data and how this problem is amplified in nonlinear techniques. Chapter 3 contains detailed information regarding the experimental setup, sample preparation, and programming of the curve fitting routines. Chapter 4 will present our first published paper showing polystyrene samples on multiple substrates without a nonresonant signal and directly answering the question of why different results were obtained. Chapter 5 will detail further investigations into the nonresonant response and the inherent limitations it places on accuracy of SFG analysis. Chapter 6 will detail a new experimental method to overcome many of the challenges present with congested spectra and/or nonresonant interference to obtain accurate peak parameters. Chapter 7 will provide new insights into the vibrational modes probed with SFG in the aromatic region of polystyrene and correct the mode assignments that have been used. Chapter 8 illustrates that the problems presented herein are not specific to polystyrene or large nonresonant producing substrates, but also occur with model chromatography systems that have been assumed to contain negligible nonresonant contribution. Chapter 9 summarizes the current status of our ongoing work and additional challenges.

1.4. REFERENCES

(1) Zhu, X. D.; Suhr, H.; Shen, Y. R. *Phys. Rev. B* **1987**, *35*, 3047-3050.

(2) van der Ham, E. W. M.; Vrehen, Q. H. F.; Eliel, E. R. *Optics Letters* **1996**, *21*, 1448-1450.

(3) Richter, L. J.; Petralli-Mallow, T. P.; Stephenson, J. C. *Optics Letters* **1998**, *23*, 1594-1596.

(4) Laaser, J. E.; Xiong, W.; Zanni, M. T. *Journal of Physical Chemistry B* **2011**, *115*, 2536-2546.

(5) Meier, R. J. *Vibrational Spectroscopy* **2005**, *39*, 266-269.

(6) Hirose, C.; Akamatsu, N.; Domen, K. *Applied Spectroscopy* **1992**, *46*, 1051-1072.

(7) Duffy, D. C.; Davies, P. B.; Bain, C. D. *Journal of Physical Chemistry* **1995**, *99*, 15241-15246.

(8) Gautam, K. S.; Schwab, A. D.; Dhinojwala, A.; Zhang, D.; Dougal, S. M.; Yeganeh, M. S. *Physical Review Letters* **2000**, *85*, 3854-3857.

(9) Wilson, P. T.; Richter, L. J.; Wallace, W. E.; Briggman, K. A.; Stephenson, J. C. *Chemical Physics Letters* **2002**, *363*, 161-168.

(10) Briggman, K. A.; Stephenson, J. C.; Wallace, W. E.; Richter, L. J. *Journal of Physical Chemistry B* **2001**, *105*, 2785-2791.

(11) Wilson, P. T.; Briggman, K. A.; Wallace, W. E.; Stephenson, J. C.; Richter, L. J. *Appl. Phys. Lett.* **2002**, *80*, 3084-3086.

(12) Calchera, A. R.; Curtis, A. D.; Patterson, J. E. *ACS Applied Materials and Interfaces* **2012**, *submitted*.

(13) Ward, R. N.; Davies, P. B.; Bain, C. D. *Journal of Physical Chemistry* **1993**, *97*, 7141-7143.

(14) Chen, Z.; Shen, Y. R.; Somorjai, G. A. *Annual Review of Physical Chemistry* **2002**, *53*, 437-465.

(15) Dowben, P. A.; Xu, B.; Choi, J.; Monkawa, E. *Characterizaton and Spectroscopy of Thin Films*; Academic Press: San Diego; Vol. 2.

(16) Lambert, A. G.; Neivandt, D. J.; Briggs, A. M.; Usadi, E. W.; Davies, P. B. *Journal of Physical Chemistry B* **2002**, *106*, 5461-5469.

(17) Ye, S.; Morita, S.; Li, G.; Noda, H.; Tanaka, M.; Uosaki, K.; Osawa, M. *Macromolecules* **2003**, *36*, 5694-5703.

(18) McGall, S. J.; Davies, P. B.; Neivandt, D. J. *Journal of Physical Chemistry B* **2004**, *108*, 16030-16039.

(19) Holman, J.; Neivandt, D. J.; Davies, P. B. *Chemical Physics Letters* **2004**, *386*, 60-64.

(20) Lu, X.; Li, D.; Kristalyn, C. B.; Han, J.; Shephard, N.; Rhodes, S.; Xue, G.; Chen, Z. *Macromolecules* **2009**, *42*, 9052-9057.

(21) Tong, Y.; Zhao, Y.; Li, N.; Osawa, M.; Davies, P. B.; Ye, S. *The Journal of Chemical Physics* **2010**, *133*, 034704-034704-13.

CHAPTER 2: MATHEMATICAL LIMITATIONS TO OBTAINING PHYSICAL MEANING FROM SFG SPECTRA

When spectroscopic information is believed to be rich in information, justifying additional fitting parameters is tempting, but trying to glean additional information with extra fit parameters does not often provide analysis that is physically meaningful.[1] Claiming information-rich data to justify additional fit parameters usually creates data that is effectively information-poor because the ability to uniquely discriminate an accurate analysis is lost by creation of multiple solutions. There are many claims of SFG providing information-rich data with multiple levels of molecular information to extract;[2] however, such claims create multiple solutions in analysis without any means of isolating the accurate model. All peak parameters used in the analysis of SFG data, in addition to the parameters of the interfering nonresonant signal, have been extracted from nonlinear fitting analyses, but nonlinear curve fitting does not provide unique solutions with this lack of constraints. Attempts at data analysis in our initial experiments using the accepted fitting models further motivated the studies that have been performed and published. The analysis of SFG data is highly dependent on assumptions regarding the relative amount and phase of the interference from the nonresonant signal and the number of peaks to be used, both of which are not definitively known. Determination of factors that can be reasonably neglected in data analysis must be accomplished to accurately obtain the desired interfacial information.

2.1. CURVE FITTING

Despite the high resolution capabilities of our system, the nonlinear fitting analysis previously shown in equation 2 of chapter 1 contains multiple solutions, but with no physical constraints to determine an accurate analysis. Peak amplitudes are the desired parameters for analysis of the molecular orientation, but accurate peak amplitudes also depend on accurate

central frequencies, widths, and hyperpolarizabilities. Previously known peak constraints with linear spectroscopic techniques, such as IR and Raman, are not always applicable to data obtained from SFG because linear techniques probe the entire material without regards to broken symmetry. Without the ability to discriminate the areas of broken symmetry, the larger amount of bulk material dominates signal generation and is effectively indicative of the bulk environment only. The different environment at areas of broken symmetry, such as a free surface, contain fewer molecules and are likely less densely packed than the bulk material. Different environments can change the coupling of vibrational modes that results in altered central frequencies and/or peak widths. Determination of accurate peak amplitudes in SFG is further complicated by dependence on the often unknown hyperpolarizabilities of the vibrational modes.

A conventional curve fitting analysis was applied to our polystyrene data, but with multiple solutions that provide good fits as shown in Figure 2-1. All fitting results used an equally rigorous analysis, applying literature precedent to determine the number of peaks and acceptable frequency shifts of the vibrational modes. Different reports have employed a different number of peaks while investigating polystyrene. The first report by Gautam et al.[3] used five phenyl modes to fit their data, whereas Briggman et al.[4] used seven modes by invoking an additional two combination bands. I applied a fitting analysis using both 5 and 7 peaks, either allowing both positive and negative amplitudes, or fitting with all positive peaks. All three attempts provided mathematically good fits, but with different results in the resonant parameters. Some results have differences up to 100% in the amplitude values for the same peak. The significant differences from the fitting results are highlighted in Table 2-1.

Due to the unknown hyperpolarizability values and the orientational dependence on amplitude, even the number of peaks that should be used is not definitively known when

5 peaks SSE: 3. 76e-3
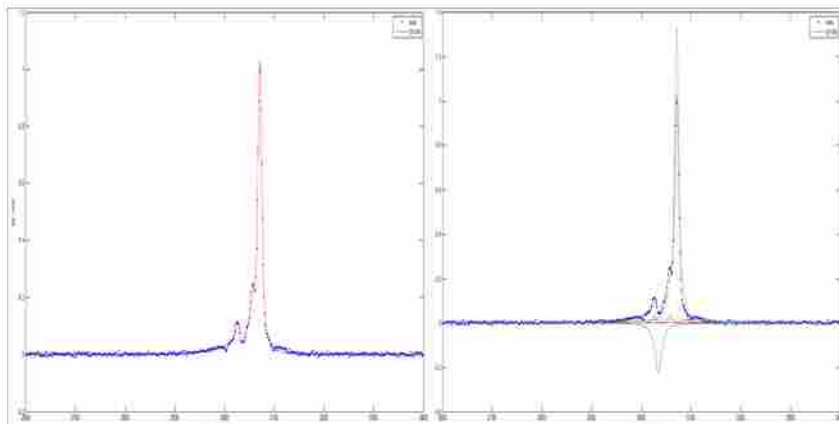
7 peaks SSE: 2.70e-3
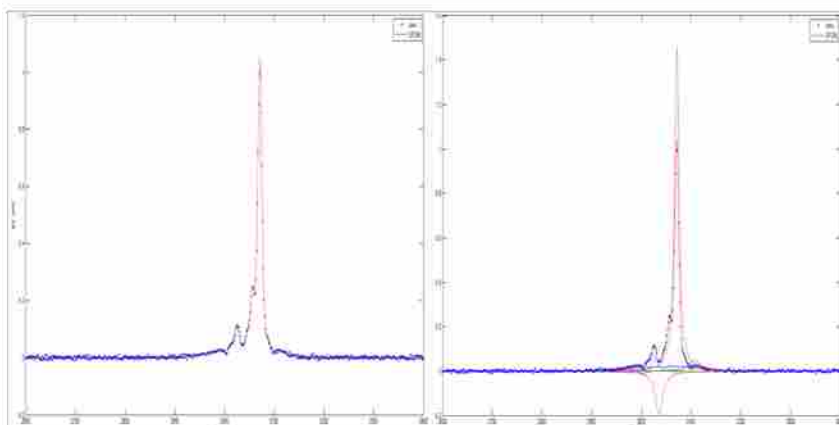
7 peaks(2) SSE: 3.48e-3
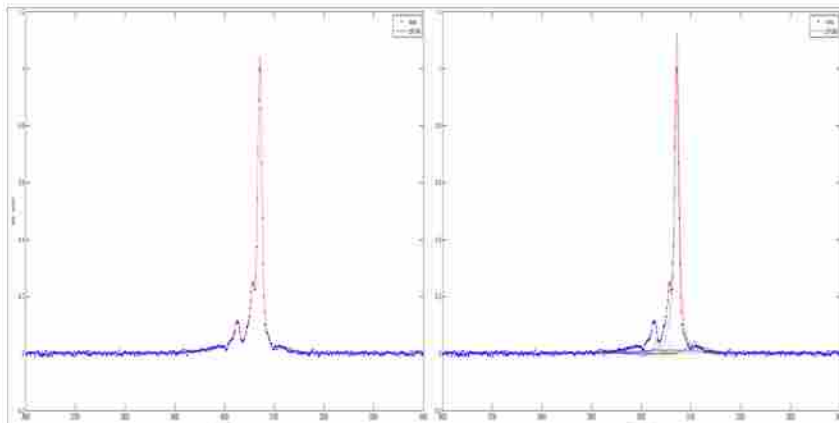
Figure 2-1 A single polystyrene spectrum be fit in three different ways with equal scientific justification.

The left side shows the overall fit while the right side shows the individual peaks.

Table 2-1 Parameters extracted from three different fits to the same data

5 peaks			7 peaks			7(2) peaks		
ω_0	A	Γ	ω_0	A	Γ	ω_0	A	Γ
			3004	-0.01245	5.598	3004	-0.006081	7.869
3026	0.03318	3.633	3027	0.06873	5.532	3031	0.04833	5.334
3034	-0.2222	8.053	3036	-0.1952	9.294	3048	0.003169	7.008
3059	0.04145	3.519	3059	0.04674	3.762	3058	0.04339	3.519
3071	1.354	5.053	3071	1.47	5.204	3071	1.135	5.087
3090	0.01269	6.999	3086	0.01316	4.153	3088	0.01108	3.815
			3107	0.04988	15.26	3107	0.0419	13.13
NR	0.1312		NR	0.1489		NR	0.1116	

analyzing SFG data. The hyperpolarizability of a vibrational mode may be too weak to provide a detectable signal and/or the molecular orientation may result in no coupling of certain vibrational modes with the polarization of the incident radiation to produce a signal. Additionally, with peaks that are around 4 cm^{-1} wide, a shift in central frequency that is about the size of the peak is also quite significant.

2.2. MULTIPLE INTERFACE MODEL

To complicate matters further, if the model of interference from multiple interfaces[5] is applied (as previously discussed in chapter 1.2.3), the number of peaks that needs to be used is doubled and even more solutions that provide good fits are attainable. I have applied such an analysis as shown in Figure 2-2, but no physical meaning can be extracted from this model. Without performing multiple fits, the evidence for multiple solutions is readily seen in the confidence intervals above 100% for the parameters shown in Table 2-2. These confidence intervals show an extremely high covariance, or the value of any parameter being dependent on the values of the other parameters. High covariances allow nearly any arbitrary value to be set for a parameter and the other parameter values can change to account for it. However, there is only one physically correct model to generate the underlying peak parameters.

Even if the detected signal does contain additional interferences from a second resonant response, it cannot be used in a fitting analysis to extract any meaningful parameters. Doubling the number of peaks beyond what is resolvable cannot result in a single answer, independent of the spectroscopic technique used. It is impractical to directly show this for every possible system with multiple fits, so I have performed a mathematical proof showing the relations that allow an infinite number of working solutions when using double the number of observed peaks for all three possible methods of fitting analysis. The possible methods to fit data using double the

Figure 2-2 Polystyrene fit with 14 peaks, allowing 7 peaks for the free surface and an additional 7 for

the buried interface. Though this does provide the best sum of squared errors, confidence levels on the

parameters indicate no physical meaning has been gained.

Table 2-2 Selected parameters extracted from the 14 peak interference fit.

ω_0	A	Γ
3057 (3057,3058)	**0.03094 ±95%** (0.001617, 0.06027)	**3.679 ±28%** (2.643, 4.716)
3069 (3067, 3070)	**0.1501 ±243%** (-0.2143, 0.5144)	**3.951 ±27%** (2.879, 5.024)
3053 (3050, 3055)	**0.004451 ±312%** (-0.009452, 0.01835)	**5.746 ±86%** (0.7822, 10.71)
3071 (3070, 3072)	**0.215 ±264%** (-0.3522, 0.7822)	**3.632 ±53%** (1.698, 5.566)
3032 (-1.32e+006, 1.326e+006)	**-5.285e-4 ±3e7%** (-163.2, 163.2)	**3.694 ±2e7%** (-6.069e+005, 6.069e+005)

number of resolvable peaks can occur with no constraints, allowing only peak amplitudes to differ, or to only constrain peak frequencies allowing both amplitudes and widths to differ. All three methods result in further underdetermined systems with an infinite number of solutions.

2.2.1.   Doubling the number of peaks used with no constraints

For all methods of analysis, we will simplify the fitting equation to analysis of a single observed peak that is assumed to be an interference of two resonant peaks from the two interfaces. It is readily observed that the same relations determined with this simple model will hold as more peaks are used. The first method of analysis that allows for multiple interferences is to simply allow double the number of peaks to be used without constraining any parameters. The mathematical representation of this approach is below:

$$\left| \frac{\sqrt{A_1} \times \Gamma_1}{\omega - \omega_1 + i\Gamma_1} + \frac{\sqrt{A_2} \times \Gamma_2}{\omega - \omega_2 + i\Gamma_2} \right|^2 = \left| \frac{\sqrt{A_T} \times \Gamma_T}{\omega - \omega_0 + i\Gamma_T} \right|^2 \tag{1}$$

This method is subject to a commonly accepted error of obtaining a mathematically better fit with additional peaks, but at the loss of the model having any physical meaning. The mathematical measure of goodness of fit in this case is the sum of squared errors. It is possible to reach a sum of squared errors value of 0 if a peak is utilized for every data point obtained, but this extreme has no physical basis and the peak parameters contain no physical meaning. Allowing for double the number of peaks without any constraints still follows the same underlying logic, because without any constraints, the mathematical model is clearly underdetermined. There are 6 parameters to modify from the two peaks to obtain the 3 parameters observed in the resolved peak, and no unique solution can possibly exist.

2.2.2. *Allowing only amplitudes to differ*

Another method of analysis would be to constrain the peak position and peak width, but allow for different amplitudes that would be indicative of the peak differences at the two interfaces. The mathematical representation of this analysis is as follows.

$$\left| \frac{\sqrt{A_1} \times \Gamma_T}{\omega - \omega_0 + i\Gamma_T} + \frac{\sqrt{A_2} \times \Gamma_T}{\omega - \omega_0 + i\Gamma_T} \right|^2 = \left| \frac{\left(\sqrt{A_1} + \sqrt{A_2}\right) \times \Gamma_T}{\omega - \omega_0 + i\Gamma_T} \right|^2 = \left| \frac{\sqrt{A_T} \times \Gamma_T}{\omega - \omega_0 + i\Gamma_T} \right|^2 \qquad (2)$$

This method is easily shown to lack a unique solution because the amplitudes are directly additive, i.e. as long as $A_1 + A_2 = A_T$ a mathematically acceptable solution exists. This again lacks any physical meaning though because it is equivalent to putting forth $x + y = 5$ and being told to uniquely determine x and y. There are again an infinite number of solutions.

2.2.3. *Constraining only the central frequency*

The last method is to constrain the central frequency and allow both amplitude and width to differ. The proof for the inability to obtain unique answers for constraining only the peak frequencies is a little more complicated, but still shows that a unique answer cannot be obtained. Because of the complexity, a direct proof is not currently available, but I have worked this out as a proof by contradiction. The mathematic representation for this model of interference is shown below.

$$\left| \frac{\sqrt{A_1} \times \Gamma_1}{\omega - \omega_0 + i\Gamma_1} + \frac{\sqrt{A_2} \times \Gamma_2}{\omega - \omega_0 + i\Gamma_2} \right|^2 = \left| \frac{\sqrt{A_T} \times \Gamma_T}{\omega - \omega_0 + i\Gamma_T} \right|^2 \qquad (3)$$

The assumption that must be made for this model to work and that will lead to a contradiction is that the value inside the brackets on the left-hand side of the equation will provide a unique solution to the values of the form on the right side of the equation. To begin evaluation, a common denominator must be chosen to allow direct addition, which leads to:

$$\left|\frac{\sqrt{A_1}\times\Gamma_1\times(\omega-\omega_0+i\Gamma_2)+\sqrt{A_2}\times\Gamma_2\times(\omega-\omega_0+i\Gamma_1)}{(\omega-\omega_0+i\Gamma_1)\times(\omega-\omega_0+i\Gamma_2)}\right|^2=\left|\frac{\sqrt{A_T}\times\Gamma_T}{\omega-\omega_0+i\Gamma_T}\right|^2 \quad (4)$$

$$\left|\frac{\omega(\sqrt{A_1}\Gamma_1+\sqrt{A_2}\Gamma_2)-\omega_0(\sqrt{A_1}\Gamma_1+\sqrt{A_2}\Gamma_2)+i\Gamma_1\Gamma_2(\sqrt{A_1}+\sqrt{A_2})}{\omega^2-2\omega\omega_0+i\omega(\Gamma_1+\Gamma_2)+\omega_0^2-\Gamma_1\Gamma_2}\right|^2=\left|\frac{\sqrt{A_T}\times\Gamma_T}{\omega-\omega_0+i\Gamma_T}\right|^2$$

For this to be mathematically true, there must be a way to make the denominator factor into two factors, one of which shows the same form as the denominator on the right. In addition, the numerator must be able to factor out a term that will cancel with the denominator term, so that only a denominator in the form of the right side remains. To illustrate this process, the denominator and numerator will be evaluated separately at first.

The denominator can actually be factored into a square as follows:

$$\omega^2-2\omega\omega_0+i\omega(\Gamma_1+\Gamma_2)-i\omega_0(\Gamma_1+\Gamma_2)+\omega_0^2-\Gamma_1\Gamma_2=(\omega-\omega_0+i\frac{\Gamma_1+\Gamma_2}{2})^2 \quad (5)$$

This now gives the relationship necessary for the two gamma values, namely that

$$\frac{\Gamma_1+\Gamma_2}{2}=\Gamma_T \quad (6)$$

For example if $\Gamma_T=5$ and $\Gamma_1=4$, then $\Gamma_2=6$. However, if you expand out the right side of equation 3-5, it gives:

$$(\omega-\omega_0+i\frac{\Gamma_1+\Gamma_2}{2})^2=\omega^2-2\omega\omega_0+i\omega(\Gamma_1+\Gamma_2)-i\omega_0(\Gamma_1+\Gamma_2)+\omega_0^2-\frac{(\Gamma_1+\Gamma_2)^2}{4} \quad (7)$$

So, from Eq. 3-5 and 3-7, we obtain the relation that $\Gamma_1\Gamma_2=\frac{(\Gamma_1+\Gamma_2)^2}{4}$ or equivalently

$$\frac{\Gamma_1+\Gamma_2}{2}=\sqrt{\Gamma_1\Gamma_2} \quad (8)$$

This relation is strictly true only if $\Gamma_1=\Gamma_2$; however, if they are not equal, the above relation still gets sufficiently close for real world applications. For example, plugging in the

example values above gives $\frac{6+4}{2} = 5 \approx \sqrt{6 \times 4} = 4.9$ or if you use values further apart, like 3 and

7 it results in 4.6 (the error gets even less as larger numbers are used). These error values are

smaller than the confidence intervals of many published fits and are therefore negligible in actual

analysis of experimental data.

The numerator must contain a factor of the denominator that will cancel out, and the

leftover numerator values will constitute the value of the numerator in the single peak function.

This can be shown by factoring the numerator as follows:

$$\omega(\sqrt{A_1}\Gamma_1 + \sqrt{A_2}\Gamma_2) - \omega_0(\sqrt{A_1}\Gamma_1 + \sqrt{A_2}\Gamma_2) + i\Gamma_1\Gamma_2(\sqrt{A_1} + \sqrt{A_2}) = (\omega - \omega_0 + i\frac{\Gamma_1+\Gamma_2}{2})(\sqrt{A_1}\Gamma_1 + \sqrt{A_2}\Gamma_2)$$

After multiplying the right side out, it can be seen that for this to be true we must have

$$\frac{\Gamma_1+\Gamma_2}{2}(\sqrt{A_1}\Gamma_1 + \sqrt{A_2}\Gamma_2) = \Gamma_1\Gamma_2(\sqrt{A_1} + \sqrt{A_2}) \qquad (9)$$

This can be simplified to:

$$\sqrt{A_1}\Gamma_1 = \sqrt{A_2}\Gamma_2 \ or \sqrt{A_1} = \sqrt{A_2}\frac{\Gamma_2}{\Gamma_1} \qquad (10)$$

Another equation is still required for determining what A_1 must be, which can be obtained after

applying all the above relations to equation 3 as shown below:

$$\frac{(\omega - \omega_0 + i\frac{\Gamma_1+\Gamma_2}{2})(\sqrt{A_1}\Gamma_1 + \sqrt{A_2}\Gamma_2)}{(\omega - \omega_0 + i\frac{\Gamma_1+\Gamma_2}{2})^2} = \frac{(\sqrt{A_1}\Gamma_1 + \sqrt{A_2}\Gamma_2)}{(\omega - \omega_0 + i\frac{\Gamma_1+\Gamma_2}{2})} = \frac{\sqrt{A_T}\Gamma_T}{\omega - \omega_0 + i\Gamma_T}$$

So there is also the additional relation that:

$$\sqrt{A_1}\Gamma_1 + \sqrt{A_2}\Gamma_2 = \sqrt{A_T}\Gamma_T \qquad (11)$$

And now there are two equations for two unknown amplitudes. From these relations, we

can select a Γ_1 and Γ_2 will be determined by the relation shown in equation 6. The amplitudes

will be determined by the solutions to equations 10 and 11 to satisfy the single peak value that

we observe spectrally. Likewise, we could pick a single amplitude factor and determine what the other amplitudes and gammas must be using the derived relations to make everything work. Due to the arbitrary nature of our initial guesses for interfering peaks 1 and 2, multiple solutions are attainable with these mathematical relations leading to the contradiction of unique analysis.

2.2.4.   Inability to provide meaningful results

Considering the above mathematics, even if interference from multiple interfaces were occurring, it is impossible to account for it in any fitting analysis and maintain physically meaningful information. Fitting a single peak with two functions will always yield a large number of solutions that are equally valid. This will be magnified by the fact that these determinations allow for nearly perfect fits to noiseless data, but without that perfection the number of acceptable parameters increases even more. Additionally, this analysis neglects the added interference of nonresonant signal that will also increase the number of acceptable parameters.[6] So, even though interference from multiple resonant signals is potentially occurring, it cannot be used to obtain any physically useful analysis of data.

The difficulties presented with fitting indicate a large underlying problem in analysis of SFG data. It is not possible to adequately constrain the analysis of spectral data to provide unique information if accounting for the possibility of multiple interferences, and additionally, at least for polystyrene, there is not enough known information to provide unique analysis even without the added complication of interference. To overcome this problem, the equation used for analysis must be simplified in some way, but to accurately simplify the analysis requires experimental conditions that physically allow a simplification to the modeling of signal generation from SFG.

2.3. Nonresonant Suppression

Many of our samples provide a relatively large nonresonant response, so we utilized the recently developed technique of nonresonant suppression[7] for these studies. This technique provides cleaner looking spectra with higher resolution by minimizing the interference between the resonant and nonresonant signal. To understand how this experimental process works requires looking at both frequency and time-domain interactions.

In Figure 2-3, a simulated resonant response of polystyrene and the interacting pulses are modeled. Time and frequency are related by the Fourier transform, and sharp features in frequency are longer lived in time. The sharp peaks of polystyrene in the frequency domain (top-left) lead to a relatively long lived response when viewed in the time domain (bottom-left). The nonresonant signal is believed to occur from fast electronic responses that last only as long as the IR pulse is present. This leads to a broad frequency response shown in the middle panel, which is identical in shape with the intensity profile of the IR pulse. The broad frequency profile is correlated to an extremely short-lived time response. The frequency response of the visible pulse is shown in the top-right panel, and the time response contains the lifetime and shape shown in the bottom-right panel due to passage through two etalons. This causes additional convolutions of the signal as will be discussed in section 3.1.5

When the IR pulse interacts with the sample before the visible pulse, both resonant and nonresonant responses are excited without the immediate upconversion of any signal. This technique works because the nonresonant response is short lived, but the resonant response maintains coherence after the IR pulse has ceased interaction with the material. Delaying the visible pulse relative to the IR pulse prevents upconversion of the earlier response, which contains the nonresonant signal, as shown in Figure 2-4.
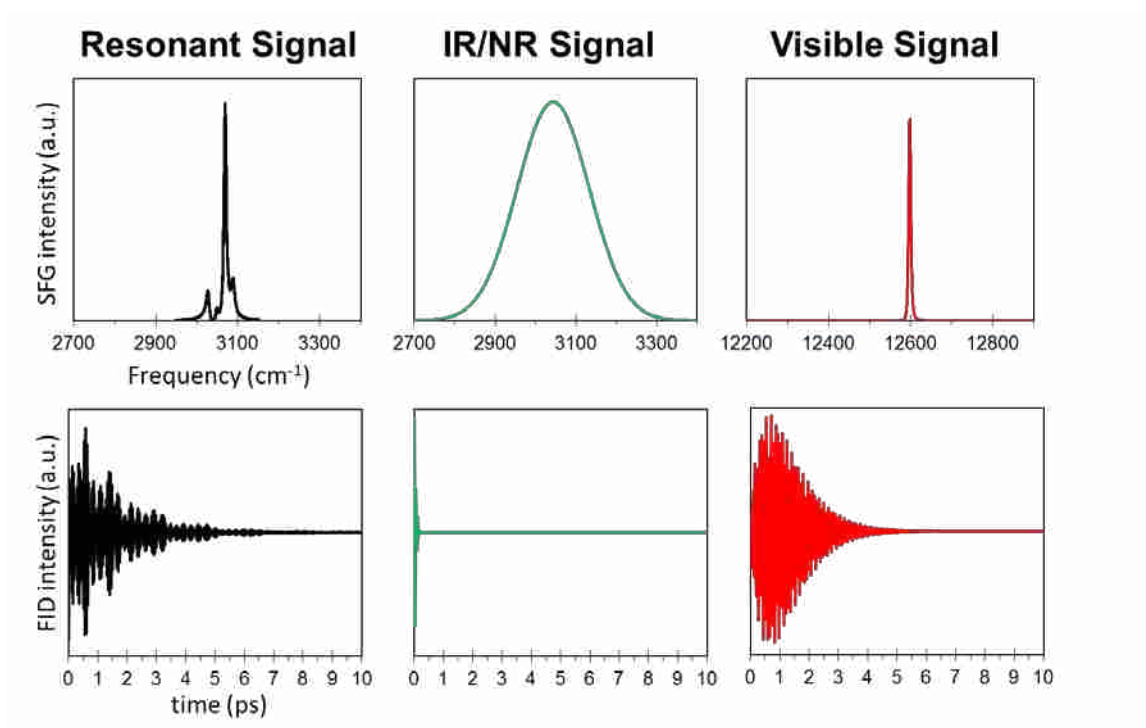
Figure 2-3 Simulations of the various responses involved in the SFG process in both frequency and time. The top row is modeled responses in frequency and the bottom row shows the corresponding response in time.
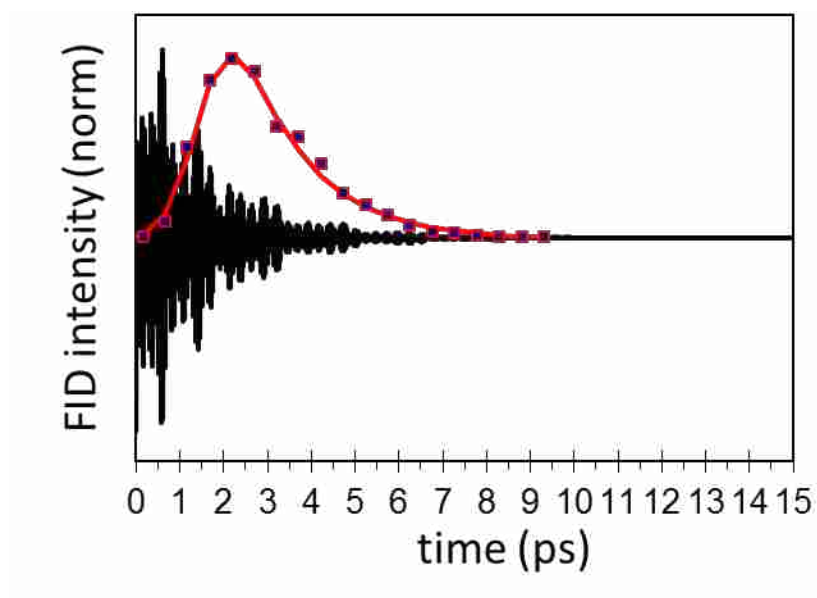
Figure 2-4 By delaying the visible pulse, shown in red, you can prevent upconversion of the initial response that contains the nonresonant signal. The purple data points shown on the visible pulse come from our measurements of the temporal profile. *(Reproduced from* Curtis et al. **J. Phys. Chem. C.** *2011,* **115,** 11550-11559*.)*

2.3.1. *Resolution improvements from suppression of the nonresonant signal*

Delay of the visible pulse also provides additional resolution from a more complete use of its temporal profile. Frequency resolution is directly dependent on the lifetime of the resonant signal, and when all of that response is detected, the maximum resolution that is governed by the vibrational lifetimes is obtained. However, the visible pulse has a finite duration that alters the observed lifetime by incomplete upconversion of the resonant response.[8] Delaying the visible pulse relative to the IR pulse allows the initial time portion of the visible pulse that was previously unused (i.e. the amplitude before the peak maximum) to take part in the upconversion process. The full usage of the visible pulse in time is necessary to achieve the full resolution that is anticipated from the frequency profile of that pulse.

In SFG experiments, the pulse overlap is often set by maximizing the signal from a large nonresonant generator such as gold, but this does not provide the expected resolution. The maximum nonresonant response from gold occurs when the temporal profile of the nonresonant response is overlapped with the maximum of the visible pulse in time, but this overlap only utilizes a portion of the visible pulse. If the visible pulse is symmetric in time, only half of the pulse is used and resolution is actually only half of what is expected from the frequency profile. More complete use of the visible pulse can be obtained with an assymetric pulse shape because there is a sharper rise time leading to less waste of the pulse in standard experiments and less resonant signal being lost in experiments involving nonresonant suppression.

2.3.2. *Minimal signal loss from Nonresonant suppression*

Because of the more complete use of the upconverting visible pulse, resonant signal is not often significantly reduced by the suppression technique. Although a purely nonresonant signal produced from materials such as gold decreases significantly, because the resonant signal is

longer lived, more of the resonant response is being upconverted by the visible pulse. The greater amount of resonant signal upconversion partially negates the loss of the more intense response from the initial times. Additionally, because the upconverting pulse is not flat, the added intensity from the upconverting maximum will change with the time delay providing additional intensity to whatever portion of the resonant signal is being probed.

2.4. EXPERIMENTAL MODIFICATIONS TO ANALYSIS

Initially, we suppressed the nonresonant contribution by decreasing the pure nonresonant signal measured from gold to about 10% of its maximum value before scanning samples. This amount of suppression was chosen because it provides more resolved peaks (particularly in quality, but ocassionally in number as well), does not require a longer integration time, and still has a small nonresonant signal visibly present that could potentially provide absolute phase information. The smaller nonresonant signal was assumed to be properly dealt with in curve fitting procedures. However, all resonant data presented in this chapter were acquired under these conditions and show the problems associated with any interfering nonresonant signal.

More accurate analysis of spectra is obtainable with an effectively complete suppression of the nonresonant signal. Without the additional nonresonant interference in data analysis, there are fewer unknown parameters to determine and the resonant interactions are made explicitly clear without the interfering nonresonant response. This is beneficial not only for quantitative determination, but is also essential for qualitative determinations as well.

2.5. REFERENCES

(1) Meier, R. J. *Vibrational Spectroscopy* **2005**, *39*, 266-269.

(2) Shultz, M. J. In *Advances in Multi-Photon Processes and Spectroscpy*; World Scientific Publishing Co. Pte. Ltd.: Singapore, 2008; Vol. 18, pp. 133-200.

(3) Gautam, K. S.; Schwab, A. D.; Dhinojwala, A.; Zhang, D.; Dougal, S. M.; Yeganeh, M. S. *Physical Review Letters* **2000**, *85*, 3854-3857.

(4) Briggman, K. A.; Stephenson, J. C.; Wallace, W. E.; Richter, L. J. *Journal of Physical Chemistry B* **2001**, *105*, 2785-2791.

(5) Wilson, P. T.; Briggman, K. A.; Wallace, W. E.; Stephenson, J. C.; Richter, L. J. *Applied Physics Letters* **2002**, *80*, 3084-3086.

(6) Busson, B.; Tadjeddine, A. *Journal of Physical Chemistry C* **2009**, *113*, 21895-21902.

(7) Lagutchev, A.; Hambir, S. A.; Dlott, D. D. *Journal of Physical Chemistry C* **2007**, *111*, 13645-13647.

(8) Stiopkin, I. V.; Jayathilake, H. D.; Weeraman, C.; Benderskii, A. V. *Journal of Chemical Physics* **2010**, *132*, 234503-234503-9.

CHAPTER 3:   BUILDING THE SFG SYSTEM, SAMPLE PREPARATION PROCEDURES, AND CURVE FITTING PROGRAMS

There were three requirements allow experimental investigations to initiate: Building the spectroscopic system to enable collection of SFG, establishing sample preparation procedures to reproducibly provide uniform sample coatings, and writing programs to enable analysis of the data from the nonlinear curve fitting procedures.

Many details regarding our SFG system as well as the experimental methods used in sample preparation are published in the supporting information section of our initial paper in the *Journal of Physical Chemistry Letters* (chapter 4).However, a more detailed description is included in this chapter to further explain the reasoning behind the setups that we have tried in the past with their various pros and cons as well as the justification for the current SFG setup.

3.1. SET-UP & INSTRUMENTATION

3.1.1. *Building the SFG system*

I built our SFG system to allow broadband experiments and the ability to experimentally suppress the nonresonant signal, with L. Robert Baker assisting in the first setup. For SFG to occur, the laser pulses must be powerful enough to drive the weaker nonlinear process, and ideally be powerful enough to allow splitting of the initial pulse to provide both pulses required. The broadband application of SFG requires a short (femtoseconds) IR pulse with a longer visible pulse to provide the resolution needed as described in chapter 2. Additionally, the two pulses must be overlapped spatially and temporally for SFG to occur. Because the broadband technique utilizes pulses that are extremely short in time, this requires an equal pathlength for the two pulses to ensure temporal overlap at the sample. To minimize the loss of signal requires an asymmetric visible pulse with a sharp leading edge.

The vibrationally resonant sum-frequency generation (VR-SFG) spectroscopy system uses an amplified Ti:sapphire laser system (Quantronix, Integra C) that produces approximately 795 nm pulses with around 2.7 mJ per pulse (the actual power varies day to day, and generally decreases over time) at 1 kHz. Pulse duration is ~130 fs. The output from this laser is split to provide the two pulses necessary for sum frequency generation. Part of the split output pumps a broad band IR optical parametric amplifier (Quantronix, TOPAS-C), with the other portion used as the "visible" pulse (the actual wavelength is technically outside the defined visible range, but is still sufficiently close and visible to the naked eye due to intensity). The visible pulse is stretched in time and given the asymmetric lineshape by passing through a Fabry-Perot étalon. The étalon provides the lineshape and frequency utilizing two closely spaced mirrors that provide constructive interference for a specific wavelength and cause destructive interference of other wavelengths. Temporal overlap is obtained by using a delay stage that can finely adjust the pathlength (micrometer precision for manual stages, nanometer precision for electronic stages) allowing for equal time traveled by both pulses as long as the two paths are within one inch of each other.

3.1.2. *The first operational SFG setup*

Our first SFG setup involved all power from the Integra laser going into the TOPAS, using both the converted IR light and the "waste" visible light from the TOPAS as the two beam sources. The waste light that does not get converted is typically dumped into an absorbing material, which can be removed if the extra light is desired for use. This setup was advantageous because both pulses passed through the added length provided by the TOPAS instrument and maintained a similar path length over a much larger distance. This required fewer optics to be used and less work to ensure simultaneous arrival at the sample. Although this setup worked to

produce SFG signal, the visible beam was unstable and contained local hot spots that eventually burned our Fabry-Perot étalon used for frequency narrowing of the visible beam. This beam instability forced us to adopt a different optical configuration.

3.1.3.   The current SFG setup

The current optical configuration involves a beam splitter before the TOPAS, so the visible light used at the sample never passes through the TOPAS. This setup has provided a much more stable visible beam without any apparent hot spots. Initially, this split was accomplished with a 50/50 beam splitter; however, there was an excess of visible light that burned the samples. The burning was overcome with significant defocusing of the visible light at the sample, but such defocusing also means that much of the available power is wasted. Because the TOPAS does not fully convert the input light, if more power is sent into the TOPAS, more IR power can be gained, but without as much power present at the sample. A 70/30 beam splitter is now used with the majority pumping the TOPAS to provide additional IR power to improve signal while maintaining non-destructive probing of the samples. A general schematic of the SFG system is given in Figure 3 - 1.

3.1.4.   Optimizing signal intensity

Initially, the delay stage was used on the IR path; however, the path with the delay stage necessitates more mirrors to be used and the IR mirrors are less efficient reflectors than the visible mirrors. Although we would initially measure fairly high powers (~30 µJ) right out of the TOPAS, only a small fraction of that power of IR light remained at the sample. By minimizing the number of optics used in the IR path, which included switching the delay stage to the visible path, this loss was noticeably decreased.
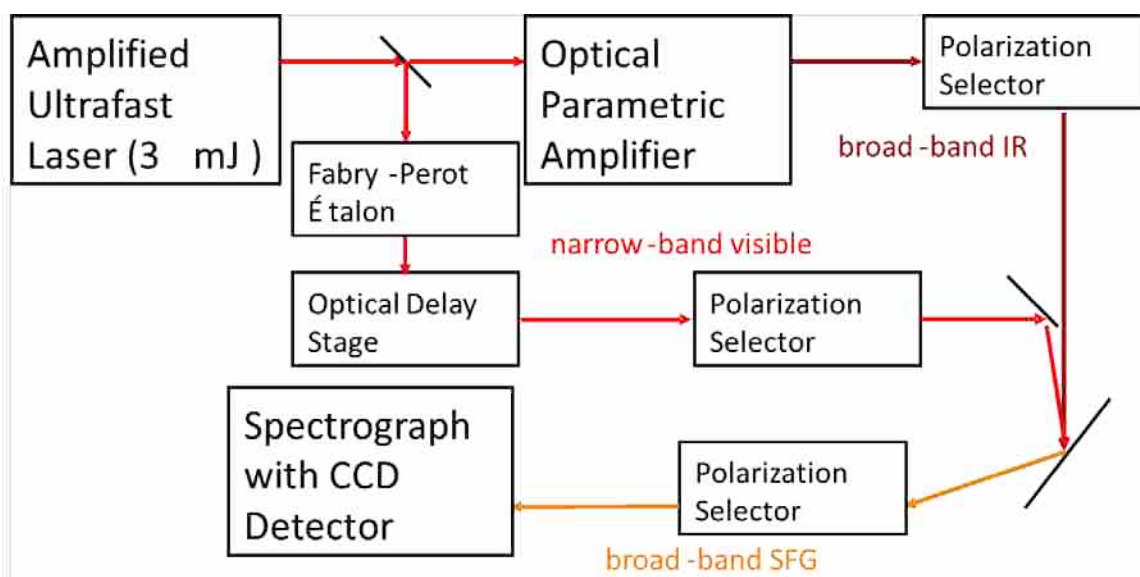
Figure 3-1. Simplified schematic of our broadband SFG system. The optical parametric amplifier generates the broadband IR light, the étalon allows for frequency narrowing of the visible pulse, and the delay stage is used to ensure temporal overlap of the pulses. The polarization selectors allow different polarization combinations to be used to probe different tensor elements.

Working with Arthur D. Quast, we additionally negated loss of IR power replacing optics initially used in that path with more efficient materials. The loss of IR power along the path can only be due to two factors: absorption of light through the air, or loss at each reflection. Absorption of light by water in the air is a common loss of IR power, but the wavelength of light used in our experiments is resonant with C-H vibrations and not water. We confirmed that water is not the significant loss mechanism by building a purge box which filtered out water and CO_2, but our power and SFG signal did not improve. The problem lies in the materials used for the IR optics. Initially, germanium materials were used for both a filter window (to filter out yellow and green light that is also produced from the TOPAS) and the focusing lens.

Germanium is often used in IR applications because of its high IR transmission; however, the applications for which germanium is highly efficient are for longer wavelengths of IR light than are used for our applications. IR power was significantly increased by replacing the germanium optics with silicon optics, and SFG signal doubled with such replacements. For similar reasons, gold mirrors are not actually the most ideal for the IR wavelengths used in these experiments, but are sufficient considering the financial costs required for replacement with optimal IR mirrors.

3.1.5. *Improving resolution of the SFG signal*

The IR light from the TOPAS allows us to perform broad band SFG experiments with a bandwidth of ~150 cm^{-1} (Gaussian full-width half-max), but the resolution is dependent upon the upconverting visible pulse. We initially used a single Fabry-Perot étalon that narrowed our visible pulse to about 10 cm^{-1} (Lorentzian full-width half-max) with a detector grating of 600 lines/mm, but as seen in Figure 3-2A this setup did not provide much resolution. By switching
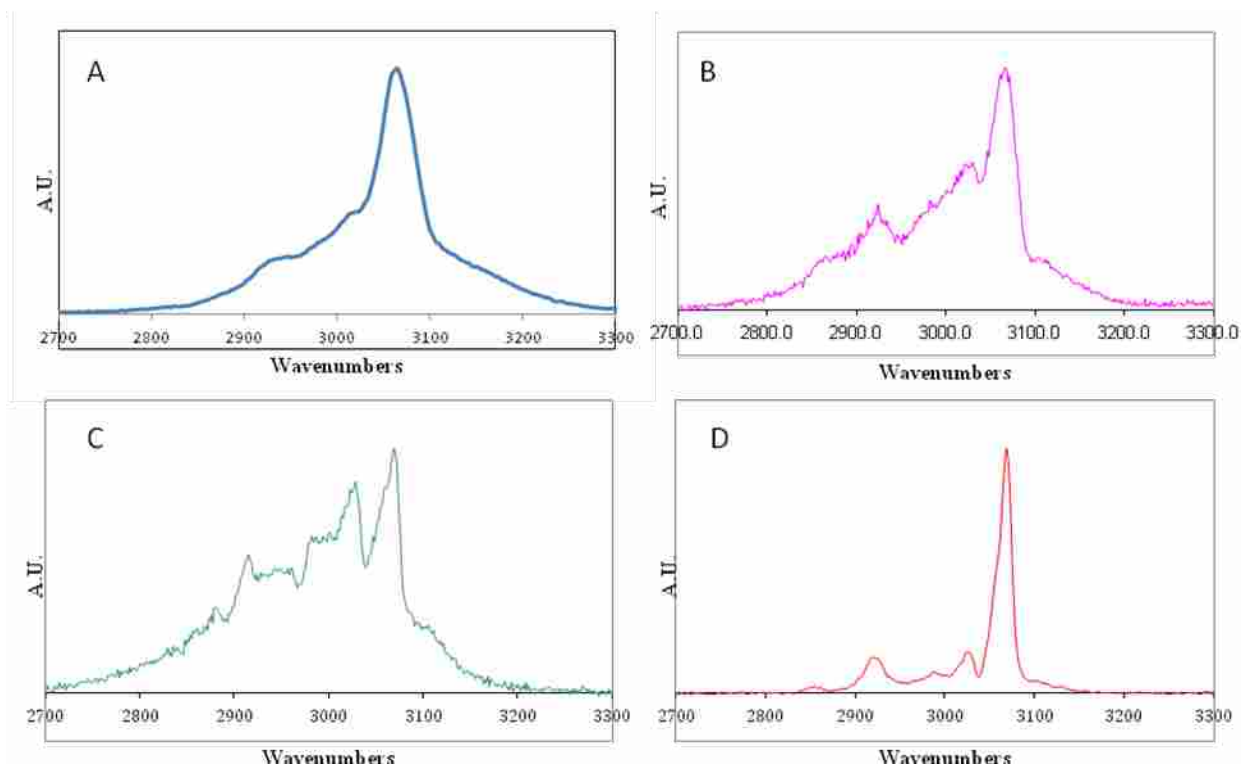
Figure 3-2. Progression in the resolution of our SFG system is shown with polystyrene spectra. Panel A shows the resolution attainable with a single étalon on the 600 l/mm grating; B shows what can be gained by simply switching to the 1200 l/mm grating; C shows the spectral resolution attained with two étalons on the 1200 l/mm grating, but without isolation of a single wavelength; D shows the resolution that has been achieved with two étalons isolating a wavelength, includes some nonresonant suppression, and uses the 600 l/mm grating.

the grating to 1200 lines/mm, much more resolution is gained as seen in Figure 3-2B, but is still not enough resolution to adequately resolve the modes present in polystyrene.

A second étalon was purchased to narrow the frequency spectrum of the visible pulse further, but this étalon did not provide a large enough free spectral range to isolate a single wavelength, shown in Figure 3-3. If a single wavelength is not isolated, additional visible peaks will combine with the resonant signal providing weaker SFG duplicates at slightly different wavelengths. The difficulties this posed in scanning polystyrene are shown in Figure 3-2C, with the apparent flat portions of the spectrum indicative of spectral shadowing problems. This étalon was replaced with another étalon that had a larger free spectral range to isolate the pulse to the single wavelength of interest. The double étalon configuration now provides a full-width half-max of about 5 cm^{-1}, also shown in Figure 3-3. As stated in 2.3.1, the full resolution is only attainable with some amount of visible delay/nonresonant suppression, and the spectra resulting from a visible delay have much higher resolution even if the 600 lines/mm grating is used as shown in Figure 3-2D. Although a less dispersive grating can be used to boost signal, to ensure that no extra resolution is accidentally being missed, all experimental scans have been performed with the 1200 lines/mm grating.

It should also be noted that the pulse resulting from two étalons is no longer Lorentzian, but takes on more Gaussian character. This is because each étalon convolves the input signal with an exponential decay. The first étalon produces a signal that is dominated by the exponential decay resulting in a Lorentzian lineshape, but after convolution with the second exponential decay by the second étalon, the decay takes on more Gaussian character. In time, this results in the assymetric gaussian profile shown in chapter 2. Visible power after both étalons is around 17.5 μJ, and is slightly defocused to ensure upconversion of the full area probed by the IR pulse.
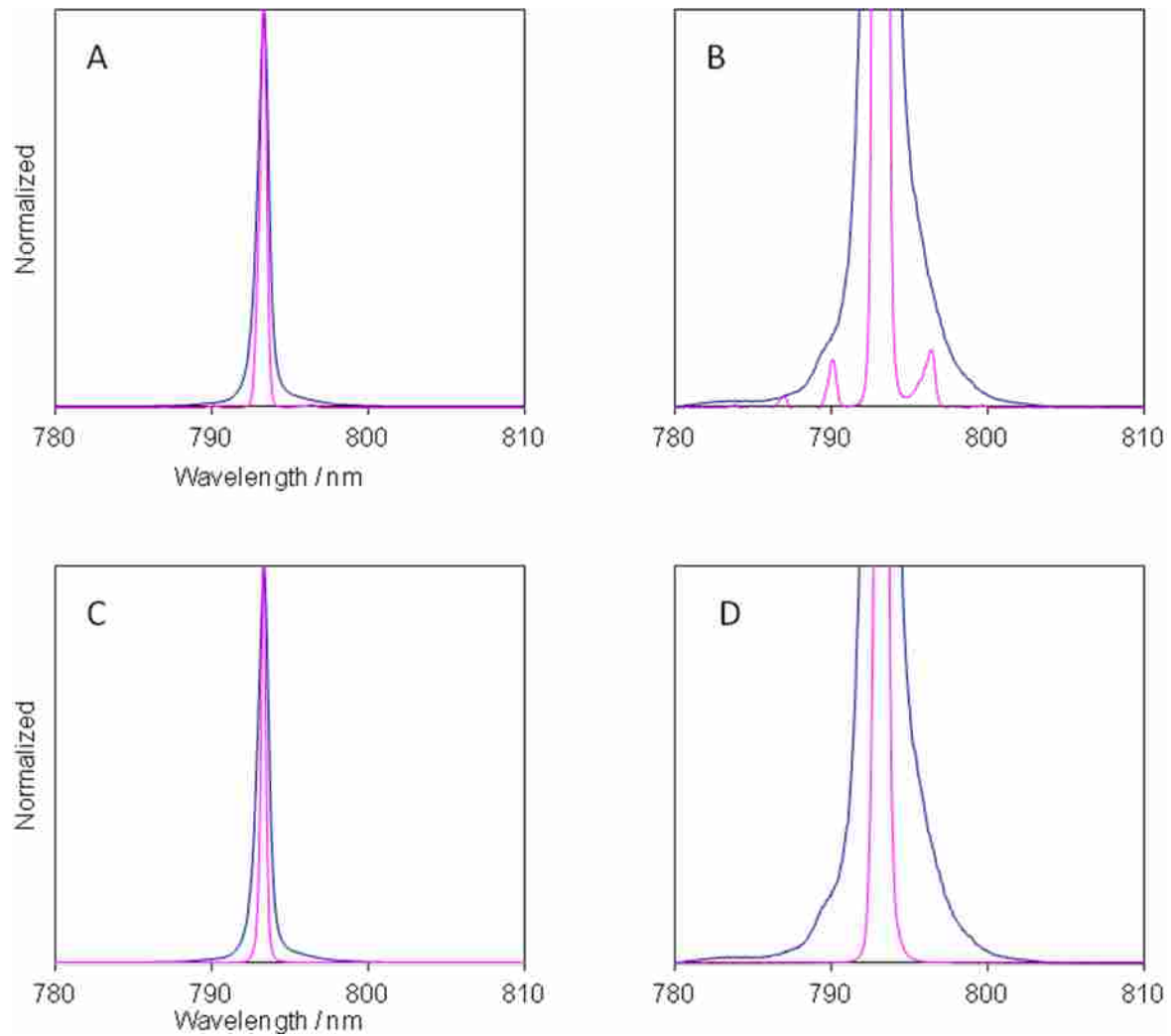
Figure 3-3. Panel A shows the first setup using two etalons, but the second etalon failed to isolate a single wavelength, as shown in panel B that zooms in at the base. Panels C and D show a properly isolated wavelength using the same amount of base magnification.

3.1.6.   Polarization Control

Polarization control of both the IR and visible beams has been accomplished with periscopes. All published experiments involve *p*-polarized IR, and *s*-polarized visible beams. This input combination only produces *s*-polarized SFG (assuming bulk centrosymmetry), which was rotated 90° by a half waveplate for optimal detection by the spectrometer (Andor Shamrock) and CCD (Andor iDus). A short-pass optical filter is placed before the spectrometer to remove any reflected or scattered light from the visible beam.

Recently, I have added a half waveplate to the visible path for polarization control so that polarizations can be easily switched without any changes to the beam path. Because the path of the visible beam can no longer change with a change in polarization (which did occur when using the periscope for polarization control), changes between *ssp* and *ppp* can be made quickly without any need for re-optimization of the signal. Switching to *sps* or *pss* combinations still require rotation of the IR periscope and optimization of the signal resulting from the slightly different IR path.

3.1.7.   Experimental Scanning Geometry

The SFG system has also been constructed with two different probing geometries. Initially the system was built so that the IR beam was slightly above the visible beam until the last reflection and arrived in a quasi-collinear geometry with both IR and visible pulses being 60° to surface normal. The last IR mirror before the sample dropped the beam height to the same spot on the sample as the visible pulse. This configuration simplifies finding the SFG pulse because conservation of momentum causes the directionality of the SFG pulse to be more influenced by the visible pulse and SFG can be easily found by tracing the visible pulse. Only a small vertical offset is necessary for finding and detecting the SFG signal.

This configuration worked flawlessly for front surface measurements; however, when used for back surface measurements, additional nonresonant signal occurred in the substrate material as shown in Figure 3-4. These effects were minimized by increasing the separation angle of the two input pulses to prevent overlap in the substrate before the sample. With this added spatial separation, both beams are now at the same height and separated horizontally instead of vertically. All scans used in the published experimental data use an IR beam that contains and incident angle at approximately 60° to the surface normal and the visible beam is about 17°. This geometry is used because it provides front and backsurface scans that are nearly identical. Now that we have the means to effectively remove all nonresonant signal (as discussed in the previous chapter), the original scanning geometry could possibly be restored, but has not yet been tested.

3.1.8.   *Intensity Correction of VR-SFG Signal*

Because the TOPAS output is not constant over all wavelengths, the VR-SFG spectra may require correction for the intensity profile of the IR beam. The intensity profile is obtained by collecting the nonresonant spectrum off a gold mirror, which is indicative of the up-converted spectrum of the TOPAS output. Prior to our first set of published data, multiple scans of gold were taken over 5 hours to check for possible drift in the intensity profile within a day, but no change was observed. These checks have been repeated occasionally over time with similar results, but it should be noted that this stability has not been present if scans were taken prior to two hours of warm-up time for the laser.

Prior to each experimental run, a reference spectrum from the gold mirror is collected. To correct for the IR intensity profile, each sample spectrum can be divided by the gold signal; however, when sample spectra were well centered and narrow enough in relation to the intensity
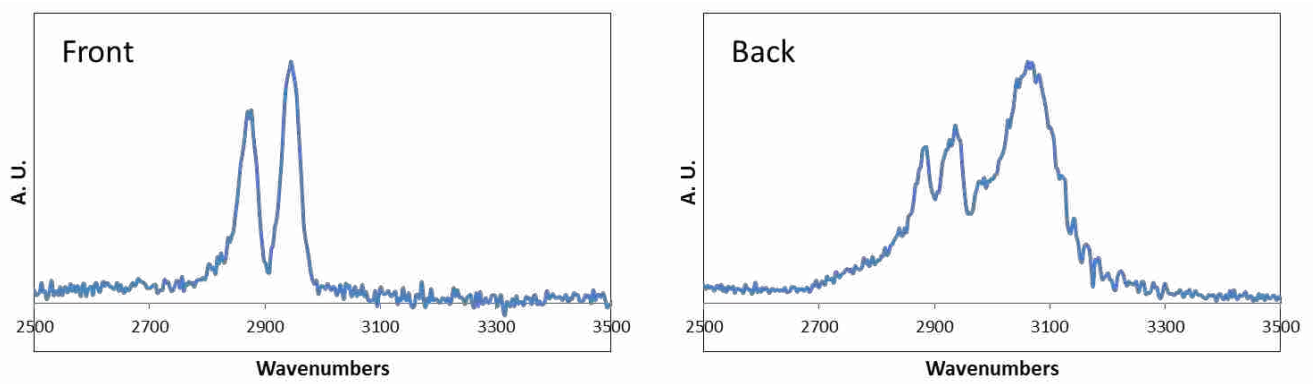
Figure 3-4. Spectra of octadecylsilane collected with quasi-collinear input pulses. The panel on the left shows the spectrum obtained if collecting from the free surface. The right panel shows the significant amount of nonresonant interference obtained if collecting through the backsurface in the same geometry.

profile, very little difference after intensity correction can be seen as shown in Figure 3-5.

Because correction by division amplifies noise and provides no significant difference to the relative intensity of resonant features, unless otherwise stated the spectra are not corrected by the gold profile. However, any fits applied to the data do incorporate the intensity profile into the fitting procedure for correction. Not correcting for the IR profile also makes the nonresonant effects more apparent because they can be easily distinguished from the baseline.

3.2. SAMPLE PREPARATION

The majority of experiments performed in this work used thin films of polystyrene. Films of polystyrene in the nanometers range can be created by spinning substrates that are coated with dilute solutions of dissolved polystyrene at high speeds. This process spins off the solvent leaving a thin film of the sample material on the substrate. Thin films of polystyrene were prepared using the cleaning and spin-coating procedures detailed below.

3.2.1. Materials

Polystyrene (MW 230,000) and Chromasolv water (HPLC grade) were obtained from Sigma-Aldrich. Toluene (spectrograde 99.9%) and hydrogen peroxide (30%) were obtained from Fischer Scientific. All materials were used as received. Rinsing water was obtained from a Millipore Milli-Q RG water system with a resistivity of 18 MΩ-cm. Silicon wafers were obtained from University Wafer and cut into smaller, roughly 1 in^2, samples. Sapphire windows were obtained from Meller Optics and fused silica windows were purchased from Quartz Scientific.

3.2.2. Cleaning substrates

New wafers and windows were initially cleaned with soap and water, but now are used in the next cleaning steps as long as there is no coating on the substrate. Testing showed that cleaning
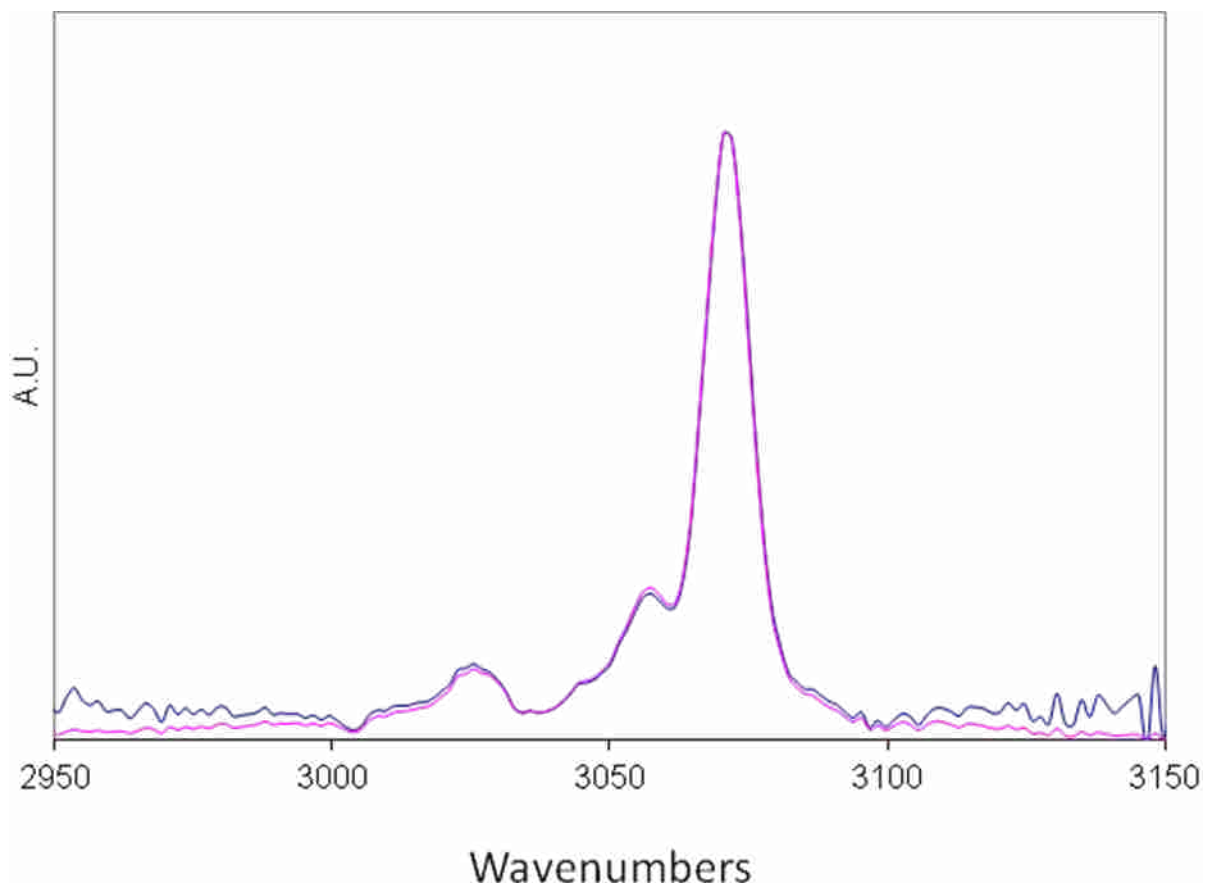
Figure 3-5 Intensity correction of the resonant response. The broadest range of spectra that is typically collected result from the vibrational modes present in the phenyl rings of polystyrene shown above. The raw data is the pink line and the intensity corrected data is in blue. As long as the data is well centered within the intensity profile over a range of frequencies this broad, intensity correction is negligible.

substrates with soap and water is often unnecessary, providing no additional cleanliness when skipped. If a polymer coating is present from a previous use, the substrate is rinsed with a suitable solvent to remove the coating (such as rinsing with chloroform to remove a polystyrene coating) followed by a rinse with water, using soap if needed to ensure a clean appearance to the naked eye. The substrates are then immersed in freshly made *piranha* solution (3:1 sulfuric acid and hydrogen peroxide) for one hour. (*Cautionary Note: Piranha* solution is very corrosive and extreme care must be used when handling.) The wafers were then immersed in HPLC grade water for at least one hour. This cleaning procedure removes any organic contamination that may confuse the spectroscopic measurements. This cleaning process was verified by scanning substrates with SFG to detect hydrocarbons in either the aromatic or aliphatic regions before and after cleaning.

Initially, substrates were subjected to further plasma cleaning after the previous steps involving cleaning solutions to supposedly remove any residual contamination that is not visible to the naked eye. Upon testing with SFG this proved to be a counterproductive step. Initial word of mouth information claimed that about 30s of plasma cleaning would remove all organic contamination to further ensure sample cleanliness. Before the first set of published experiments, the cleaned substrates were scanned after plasma cleaning with SFG looking in the aliphatic C-H region and found that significant C-H signal was present, indicating that 30s was inadequate. One minute also frequently failed to remove the C-H contamination, and I found that only after 3 minutes was the sample regularly free of aliphatic contamination. I then scanned samples after being removed from piranha and copiously rinsed with water followed by drying with nitrogen and found that samples were clean after those steps. Scanning the same clean samples after exposure to the plasma chamber, it was found that the plasma treatment was often introducing

contamination of the samples when subjected to the shorter treatment times, and hence this step is now left out entirely.

3.2.3. Spin-coating procedures

Immediately before the spin-coating process, samples were removed from water, dried with nitrogen, rinsed with Milli-Q water and dried again. The longer a sample is exposed to air, the more contamination it gains so the coatings were applied as quickly as possible to the cleaned substrates. Random substrates have been scanned on the VR-SFG system to ensure there is no surface contamination following this cleaning process before the coating procedure. Thickness of the SiO_2 layer is measured by ellipsometry immediately before spin coating; for a clean sample, 1.5 - 2.0 nm SiO_2 is typically observed (greater SiO_2 "thicknesses" are obtained for dirty samples with equally good fits, but this higher reading is due to the addition of contamination layers, such as the observed aliphatic contamination, not additional SiO_2 thickness, which has been confirmed by SFG scans). PS was spin-coated (Laurell Technology, CZ650) at various speeds from various weight percent solutions in toluene to achieve the desired thickness.

Additional experiments were performed with polystyrene dissolved in chloroform (99.8% from Mallinckrodt) to confirm that SFG signal was coming from polystyrene and not residual toluene solvent. No significant differences were observed in the spectra, and toluene was used in all the experiments reported. Toluene was chosen over chloroform because spin-coating procedures are less sensitive to the exact polystyrene concentrations in toluene solutions than in chloroform for film thickness and this solvent provides a more uniform film.

To obtain a good coating free of irregulaties, such as streaks or comets, some trial and error is required. A dynamic dispense, or applying solution while the spin-coater was already spinning, was most often recommended in the literature for clean coatings, but this method was also for

thicker photoresist solutions and frequently failed to provide the desired results in coating quality for our applications. By covering the entire substrate with solution before beginning the spin process, I was able to consistently achieve uniform films with that spin coater. I will note, however, that although this method worked perfectly on Prof. Matt Linford's spin coater, this same method failed to produce the same results when we later acquired a spin coater of our own. Angela Calchera worked out the best method for our spin coater, which does require a form of dynamic dispense. Spin-coating still requires a lot of guess work to make the best coatings, and is dependent on the sample, the solvent, and the specific spin-coater used.

3.2.4. *Characterization of polymer film thickness*

We used the ellipsometer of Prof. Matt Linford's lab as our primary characterization of the cotaing thickness for our thin films. The ellipsometer records the change in elliptical polarization over a range of wavelengths, and with known optical constants, can fit that data to determine film thickness. Prior to my experiments, no model providing the optical constants required for polystyrene was present in the local ellipsometer files, thus requiring creation of a new model. Although the ellipsometer can fit both the thickness and the optical constants to create a model, as previously stated, with no constraints, no unique solution is obtainable from fitting and the extracted information does not contain physical meaning. With definitive knowledge of the thickness, the optical constants can be extracted and used for the model to measure films of different thicknesses, but an independent measurement is required. An independent measure can be gained by physical techniques that are able to measure relative film thickness to the zero point of the substrate.

The film thickness of polystyrene was independently measured using a profilometer and used to build the ellipsometer model. Although the most accurate physical characterization of

film thickness would come from use of atomic force miscroscopy, the high sensitivity of that technique comes at the price of lowering the distance of scanning and requires a sharper film edge than can be readily produced. An edge on the film can be created by either masking part of the substrate during coating or dissolving part of the film after coating. Profilometry is similar technique for physical measurement that uses a needle-like probe to image surfaces and identify height relative to a reference point. Profilometry has lower sensitivity than AFM, but allows scanning ranges great enough to map over the zero thickness at the substrate, the film edge, and the area where the film thickness becomes essentially uniform. The profilometer used does have an innate uncertainty of approximately 5 nm due to inherent noise present in the scans over the needed range. Despite the 5 nm uncertainty, this provided thickness constraints that were used to build the ellipsometer model for easier and faster characterizations in subsequent film measurements.

Ellipsometry measurements showed that the sample procedures developed often resulted in sample consistency within about 2 nm; however, I do acknowledge that it is questionable to claim a definitive consistency greater than the information used to make the model (primarily because there is no definitive check on such consistency). Either way good consistency is maintained in preparing samples that is definitively within 5 nm.

3.3. DATA ANALYSIS OF THE SPECTRAL RESPONSE

There was no program available to provide the curve-fitting analysis routines needed for our data, requiring an in-house development. I worked with Prof. Matthew C. Asplund to develop routines to accomplish the curve-fitting procedures required for our data in Matlab. A couple of these routines are included in appendix 1 to show the direct programming script for the fitting programs.

The fitting programs request the spectra of the gold response and the sample data to accomplish fits with intensity correction built in to the routine. Instead of dividing by the gold signal for intensity correction, which consequently amplifies the baseline noise of the sample spectra, the gold profile is used as a known parameter in a multiplication routine. Each individual data point of the fit function is multiplied by the corresponding gold intensity at that frequency. Data that is within the more intense portions of the intensity profile do not acquire as large of amplitudes from the fit parameters because a larger multiplier from the intensity profile is present. Likewise, the data contained in less intense portions of the intensity profile are fit with larger amplitudes to compensate for being coupled to smaller multipliers. This is mathematically identical to correction by division of the intensity profile, but does not amplify noise.

These programs require more manual input than commercial programs (e.g. Grams32, Origin, etc.). Manual input is required to establish a vector containing initial guesses for the peak parameters, another vector stating the maximum parameter values allowed, and another vector containing the minimum parameter value constraints. Without good initial guesses and constraints, the program often settles into an unrealistic local minimum such as fitting the baseline only. If more peaks are desired than what is currently present in the script file, the user must manually add the additional peaks; however, that is not a difficult task since it only requires a copy of a previously programmed peak with a change in the indexing numbers. I initially programmed scripts to fit Lorentzian profiles with the addition of the nonresonant signal; however, as more was discovered regarding the nature of the signal, I was required to program more complex scripts as will be discussed in chapters 4 and 6.

With the experimental requirements now met, the studies of the remaining chapters were performed.

CHAPTER 4:   UNDERSTANDING THE ROLE OF NONRESONANT SUM-FREQUENCY GENERATION FROM POLYSTYRENE THIN FILMS*

4.1. ABSTRACT

The nonresonant (NR) portion of sum-frequency generation (SFG) spectra of polystyrene (PS) thin films is shown to contain physical information and affect the analysis of the surface structure. When the NR signal is suppressed, PS thin films on three different substrates produce the same spectrum, suggesting the same structure at the free surface. Annealing or aging of PS films on silicon causes the NR signal to increase significantly compared to a fresh sample, indicating that the substrate is not the sole source of NR signal. A method is proposed for improved analysis of SFG spectra. First, spectra obtained with NR suppression are used to determine the resonant parameters. After these are constrained, the nonresonant amplitude and phase parameters are determined more uniquely from un-suppressed spectra. NR-SFG must be properly handled in order for the analysis of SFG spectra to be mathematically unique and physically meaningful.

4.2. ARTICLE

Many scientifically and technologically important phenomena, such as lubrication and adhesion, involve molecular interactions at surfaces and interfaces. Although much has been done to improve our macroscopic understanding of these processes, we lack a general theory of exactly what governs them at the molecular level. Such a model would allow for strategic design of new lubricants, adhesives and other materials. We lack this molecular-level understanding in part because of the challenges of accessing a buried interface to probe these systems *in situ*.

Sum-frequency generation (SFG) spectroscopy, first demonstrated in 1986,[1] has developed into a powerful tool for probing both free and buried interfaces. In one noteworthy example, correlations were established between the orientation of polystyrene at the buried interface and the strength of the adhesive interactions.[2] The nonlinear nature of this technique, however, often leads to complications in analysis and interpretation of the experimental results. Nonresonant SFG can be particularly problematic and, as we show in this paper, must be dealt with properly to ensure correct interpretation of the data.

Consider the case of determining the molecular structure of the free surface of polystyrene (PS) thin films, specifically the orientation of the pendant phenyl groups. Two different orientations for the phenyl group at the PS-air interface have been reported; nearly parallel[3] vs at a 57° tilt,[4] with respect to the surface normal. The question remains as to why the reported structures are different, but a comparison of the two studies reveals some important considerations. First, two different substrates were used; sapphire prisms in the first and Si wafers in the second. The choice of substrate may affect the structure of the polymer/air interface,[5] however once the polymer film is thick enough, the structure at the free surface should be independent of the substrate material. In fact, the idea that the substrate influences the free polymer surface actually complicates the interpretation of the results. If the free surface depends on the substrate, there may be some preferential order throughout the film, which would lead to sum-frequency generation in the bulk and result in a loss of surface selectivity. Second, the film thickness was 160 nm in the sapphire experiments and 370 nm in the silicon study. It is possible that the thin samples were too thin and the surface structure was still being influenced by the substrate. Given these differences between the two samples, the surfaces may in fact be very different and a simple, direct comparison may not be warranted. Finally, since the substrates

have different optical properties, including how much nonresonant SFG is produced from each, it is possible that different assumptions and analysis procedures led to different conclusions even though both structures were in fact the same.

In the technique of broad-band vibrationally resonant sum-frequency generation (VR-SFG) spectroscopy, two laser beams are incident on the sample; one is a narrow-band visible (~790 nm) beam and the other is a broad-band (150 cm^{-1} FWHM) IR beam centered at ~3050 cm^{-1}. When the two pulses overlap in space and time, a non-linear polarization generates a new beam at the sum of the two incident frequencies. This process is resonantly enhanced when the IR frequency coincides with the vibrational frequency of molecules in the sample. Within the electric dipole approximation, no SFG signal is produced in an isotropic medium, such as a glassy polymer, allowing us to probe the molecular structure of the surface.

There are, in fact, two sources of sum-frequency signal: the resonant response of molecules at the interface and the nonresonant response of the materials. The overall SFG signal is typically modeled as

$$I_{SFG} \propto \left| \chi_{NR}^{(2)} + \chi_{R}^{(2)} \right|^2 = \left| B_{NR} e^{i\phi} + \sum_q \frac{A_q}{v_{IR} - v_q + i\Gamma_q} \right|^2 \tag{1}$$

where $\chi_{NR}^{(2)}$ and $\chi_{R}^{(2)}$ are the nonresonant and resonant nonlinear susceptibilities, respectively, B_{NR} is the amplitude of the nonresonant contribution, $e^{i\phi}$ governs the interference between the resonant and nonresonant signal with ϕ as a phase factor, and A_q, v_q, and Γ_q represent the amplitude, center frequency, and half-width half-max linewidth, respectively, of a Lorentzian line shape of the resonant features. The sum is over all the normal modes of the molecules and v_{IR} is the frequency of the IR beam. Because both the resonant and nonresonant terms are complex, they interfere with each other. This can be seen more clearly if the equation is expanded:

$$I_{SFG} \propto \left| \chi_{NR}^{(2)} \right|^2 + \left| \chi_{R}^{(2)} \right|^2 + 2 \left| \chi_{NR}^{(2)} \right| \left| \chi_{R}^{(2)} \right| \cos\left[\phi - \delta(\nu) \right] \qquad (2)$$

where $\delta(\nu)$ is a frequency dependent phase term. Generally, the nonresonant SFG (NR-SFG) is treated as a frequency independent background signal with the intensity depending on multiple factors, such as sample composition, orientation, visible wavelength, etc. Interference between the resonant and nonresonant signal allows for absolute orientational analysis, however, in some cases the nonresonant signal can overwhelm the resonant signal, making spectra difficult to interpret. Nonlinear curve fitting is typically used to extract the parameters of the resonant signal, as well as the nonresonant amplitude and phase, but care must be taken to make certain that the set of spectral parameters is mathematically unique, or the interpretation of the results may not be valid.[6]

Lagutchev et al.[7] have developed a method to suppress the nonresonant signal with a pulsed broadband SFG system. NR-SFG is produced only when both the visible and IR pulses are incident on the sample, whereas the resonant free induction decay is typically much longer than the sub-picosecond IR pulse length. Delaying the two pulses still allows for interaction between the visible beam and the IR polarization but reduces the amount of nonresonant signal. By suppressing the nonresonant signal, the resonant spectrum can be acquired directly rather than being extracted through post-processing. It has also been shown that delaying the visible pulse results in narrower[8] and more symmetric line shapes.[9] In many cases, particularly when T_2 is long, the resonant signal does not decrease substantially[7,10,11] and may increase.[9] However, in cases of rapid dephasing, due to intrinsically short lifetimes, fast molecular reorientation,[12-16] or energy transfer,[17] the resonant signal will decrease with this delay. In this paper we show that judicious suppression of nonresonant SFG reveals physical information about polystyrene thin films and improves our confidence in the results of curve fitting analysis.

We prepared ~90 nm PS thin films by spin coating from toluene solution on three

substrates: silicon wafers, sapphire windows and fused silica windows. (For additional

experimental details, see the Supporting Information.) Our broadband vibrationally resonant

sum-frequency generation (VR-SFG) system is very similar to that described in reference 10. We

first acquired spectra with 90% nonresonant suppression by delaying the visible pulse 0.68 ps.

This delay suppresses the nonresonant signal of a gold reference to ~10% of its maximum.

Replicate spectra were acquired in random order to remove any experimental bias and

representative spectra of the three types of samples are shown in Figure 4-1a. All spectra were

acquired with the *ssp* polarization combination (*s*-polarized SFG and visible, *p*-polarized IR).

Apparent differences in the spectra suggest that the structure of the free surfaces may be

influenced by the substrate material.

To completely remove the possibility of interference between the resonant and

nonresonant signals, we suppressed the nonresonant signal even more. Figure 4-1b shows

representative normalized spectra of the three samples taken with the visible pulse delayed by

2.2 ps. With the nonresonant signal fully suppressed, the spectra are virtually identical,

suggesting that the surface structure is in fact the same for all three substrates. Signal levels are

significantly higher on silicon because the reflective substrate allows us to collect the SF signal

generated in the forward direction; this signal is not collected from the transparent substrates. It

also appears that all significant SF signal is produced only at the free surface. Because the

nonlinear Fresnel factors are necessarily different for each material, SFG from the buried

interface should vary with the substrate. This light should interfere with that from the free

surface, affecting the measured spectrum,[18] but the fact that all three resonant spectra appear
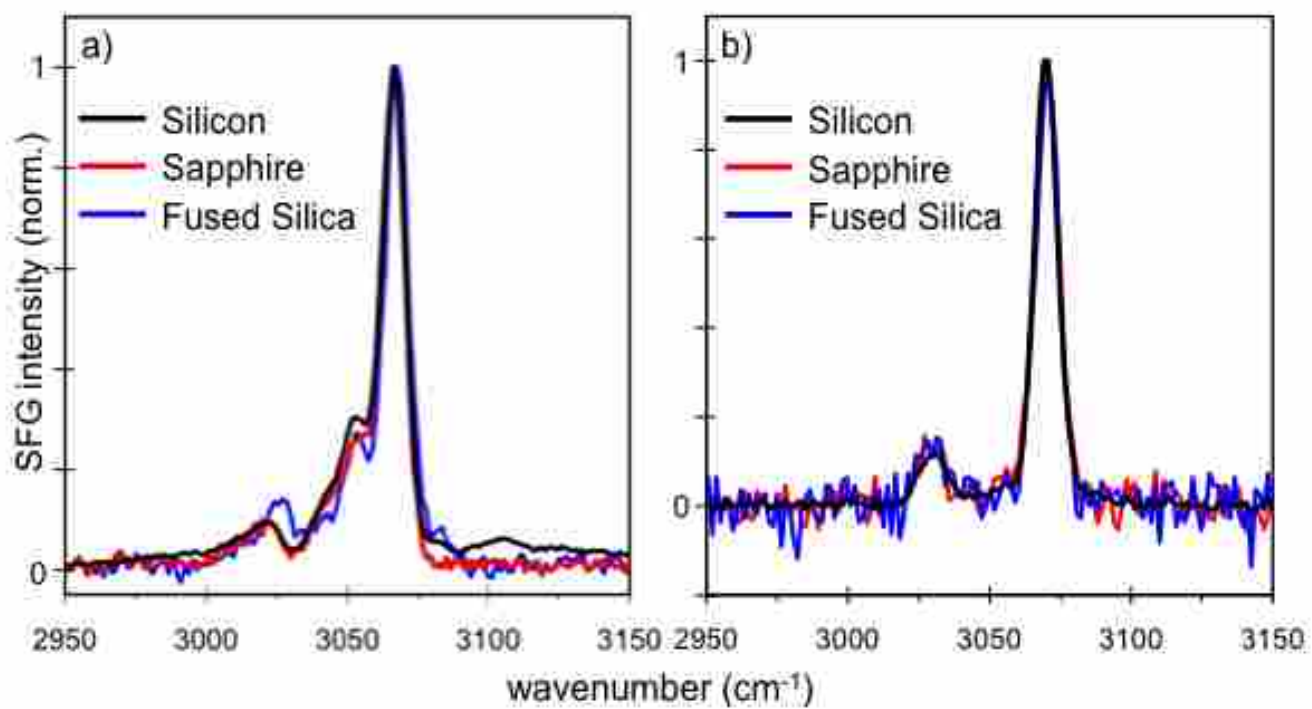
Figure 4-1. a) Normalized VR-SFG spectra (*ssp* polarization combination) of 90 nm PS on Si sapphire, and fused silica with 10% NR contribution; b) the same samples with full NR suppression.

identical suggests there is no such interference with these samples, or that there is no significant signal generated from the buried interface.

Suppression of the nonresonant signal also allows us to explore other aspects of how the thin film is affected by sample preparation and handling. Polymer thin films are typically annealed after spin coating to remove residual stress in the film. Figure 4-2a contains spectra of three PS samples on Si substrates. The first sample was fresh and scanned shortly after it was prepared with no further processing. A second sample was annealed at 120°C for 2 hrs, followed by cooling under vacuum overnight. Another sample was aged for 1 week with no annealing. All spectra were acquired with full nonresonant suppression. The signal from the annealed sample is about 35% less intense, and the aged sample is about 27% less intense, compared to the fresh sample. The normalized spectra, shown in Figure 4-2b, appear identical, suggesting that the surface structure remains the same in all three cases. One possible explanation is that the interfacial layer is deeper in the fresh, unannealed sample, meaning the SFG process probes more material. Annealing and aging may allow more molecules near the surface to adopt an isotropic bulk-like configuration and thereby reduce the SFG signal because a thinner layer is being probed.

Reintroduction of the nonresonant component, however, leads to changes in the spectra, as shown in Figure 4-3a; annealing and aging cause a significant increase in the NR signal compared to the fresh sample. This increase in NR-SFG occurs along with the decrease in the resonant signal, again suggesting that more of the material is "bulk-like" rather than "interface-like". The NR signal leads to apparent shifting of the peak positions (see Figure 4-3b), but this is merely a result of the interference.[11,19] These interference effects can also lead to the creation of "ghost peaks",[6] such as the apparent peak at ~3105 cm^{-1}, which completely disappear when
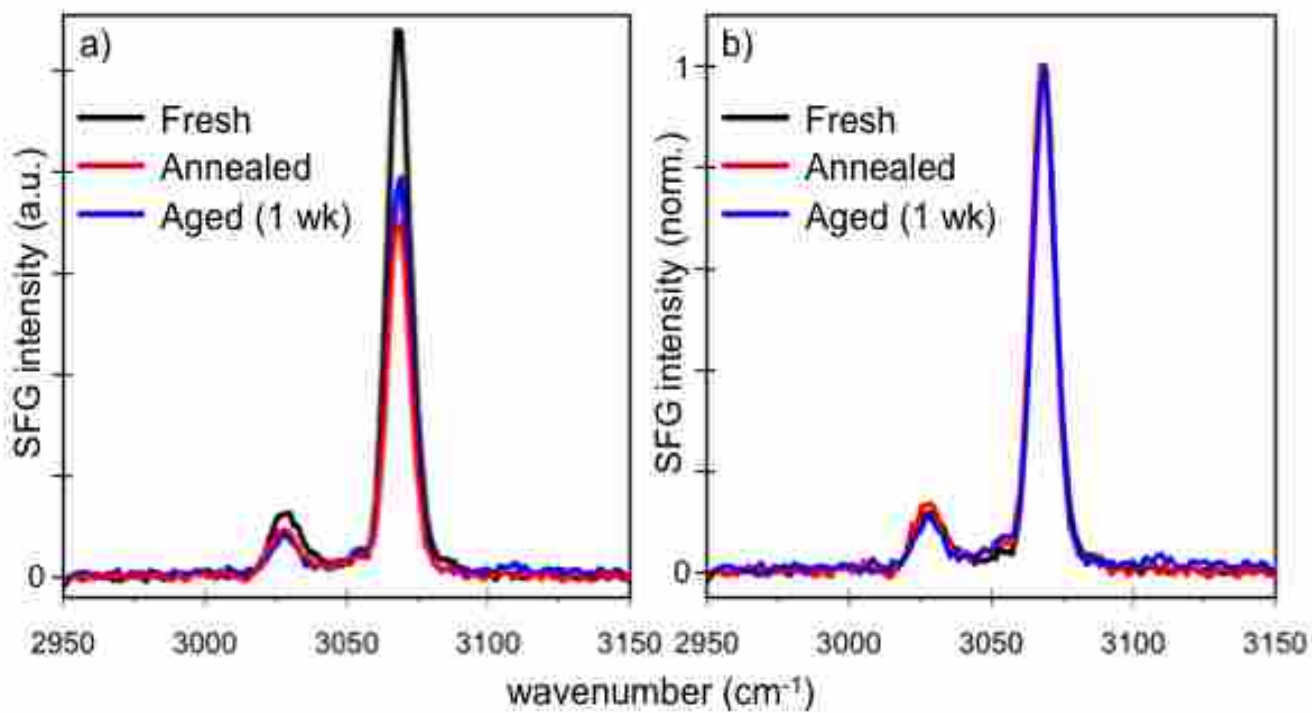
Figure 4-2 VR-SFG spectra of PS on Si with full NR suppression. Samples were either fresh, annealed, or aged for 1 week. a) Signal intensity drops upon annealing and aging. b) The normalized spectra are virtually identical, suggesting the surface structure is unchanged by annealing or aging.
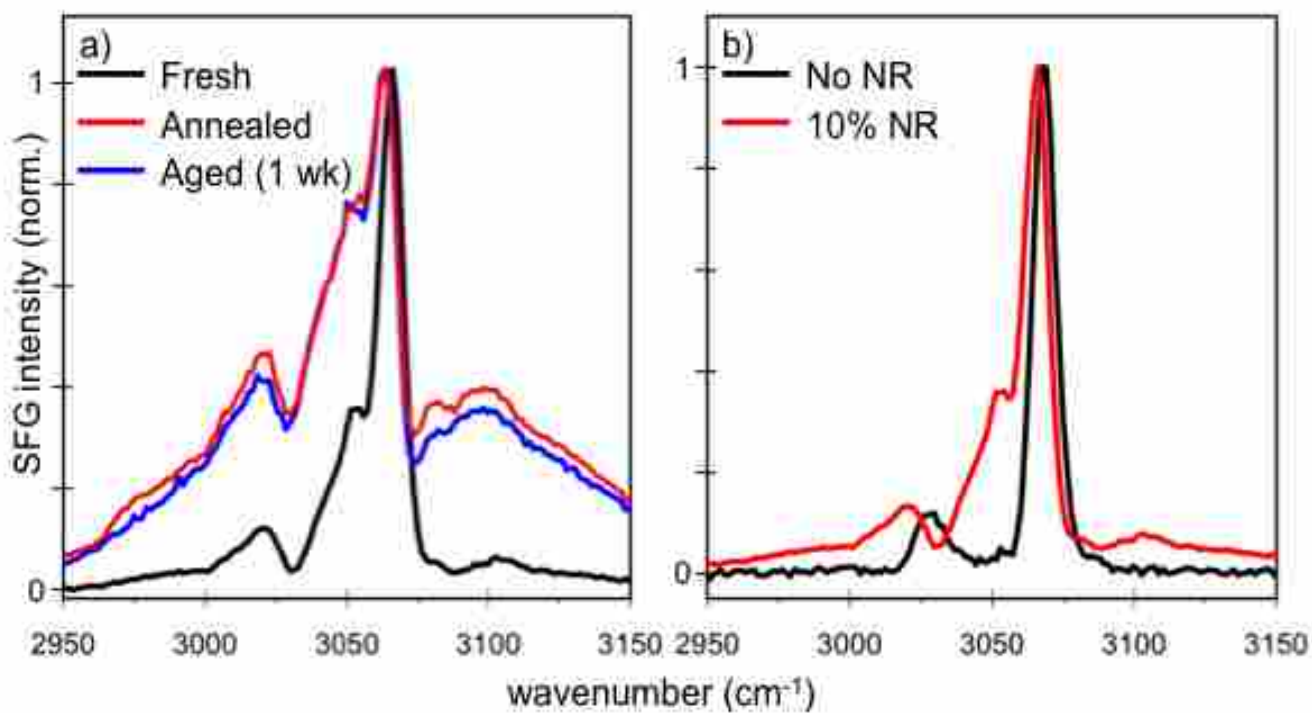
Figure 4-3 a) Normalized spectra of the same samples from Figure 2 with 10% NR contribution.

b) Comparison of the spectra of the fresh sample taken with full NR suppression and 10% NR contribution.

the NR signal is suppressed. If the NR signal is not properly accounted for, peak positions and amplitudes could be improperly determined, leading to erroneous physical interpretations.

To separate resonant and nonresonant effects, we tuned the IR source to ~3300 cm^{-1}, away from the aromatic C-H resonances. Figures 4-4a and 4-4b show nonresonant SFG spectra of Si and Au substrates, respectively, both with and without a layer of PS. The signal from Au is generally much stronger than from Si, but the response upon the addition of PS is very different; on Si the NR-SFG increases significantly, but on Au the NR signal decreases. This result challenges the commonly stated assumption that NR-SFG signal comes solely from the substrate and not the thin film; we clearly observe changes in the NR signal depending on the presence of presumably amorphous material. As shown above, annealing of the PS film further increases the NR signal on Si; the NR signal depends on the processing of the sample and likely indicates changes in the bulk structure of the thin film.

On a dielectric substrate, even though the nonresonant contribution is significantly reduced, it cannot be ignored. As seen in Figure 4-4c, inclusion of NR-SFG significantly affects the spectrum of PS on fused silica. With no PS, however, there is very little NR signal from fused silica. This phenomenon can be understood by Equation (2). When $\left|\chi_{NR}^{(2)}\right|$ is larger than $\left|\chi_{R}^{(2)}\right|$, the cross-term leads to an enhancement of the resonant signal, often with distortion of the resonant line shapes. This phenomenon has been used to great effect, such as with self-assembled monolayers on Au. The same effect can happen in reverse; if $\left|\chi_{NR}^{(2)}\right| << \left|\chi_{R}^{(2)}\right|$, the resonant signal can enhance the nonresonant contribution through the same cross-term and again lead to interference in the spectrum, with resulting changes to line shapes. Thus even on a dielectric
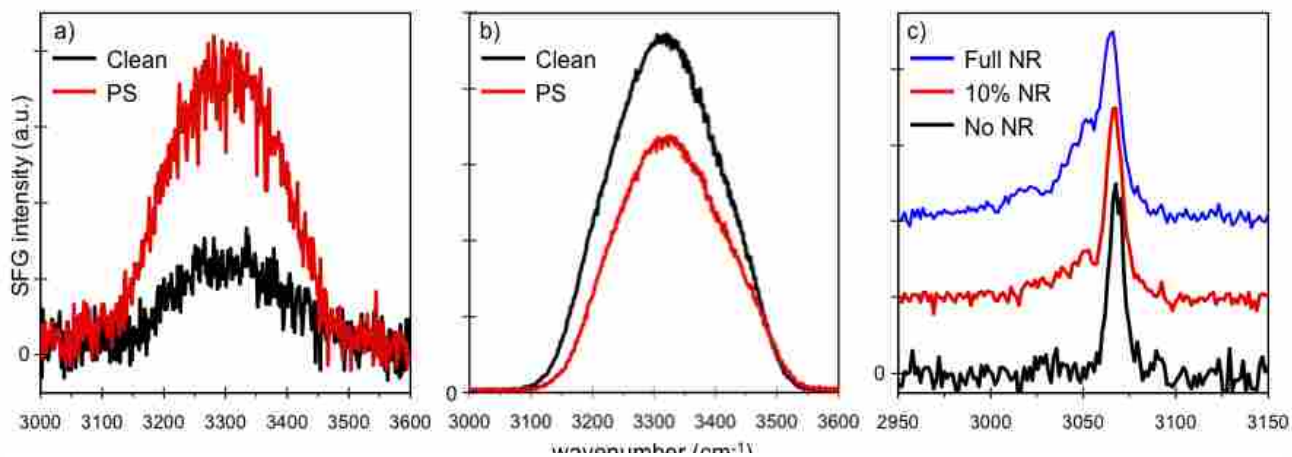
Figure 4-4. Off-resonance spectra of a) Si and b) Au with and without a layer of PS. NR signal increases on Si but decrease on Au. c) VR-SFG spectra of PS on fused silica with different levels of NR contribution. Spectra offset for clarity.

substrate, nonresonant signal must be properly accounted for in the analysis for correct interpretation of the data.

Our work clearly shows that the nonresonant SFG signal is not merely a background that can be removed by post-processing, but contains important physical information about the sample and its history. At this time we are not prepared to speculate on the detailed origin of the nonresonant signal; our investigations into the source are ongoing. It is difficult, if not impossible, to uniquely determine all the parameters of the resonant and nonresonant signal simultaneously from a single spectrum, as demonstrated by Busson and Tadjeddine.[6] Removal of the nonresonant signal by experimental means allows for more unique determination of the resonant parameters. Peak positions, amplitudes and widths are more certain because the line shape is not distorted or inverted by the interference. Once the resonant parameters are controlled, the nonresonant amplitude and phase can also be determined more uniquely. This process overcomes many of the problems in fitting second-order spectra, but challenges may remain due to spectral congestion; overlapping peaks are very difficult to fit uniquely.[20]

We have applied this analysis procedure to our PS spectra. Following the orientational analysis procedures described by Gautam, *et al.*[3] and the hyperpolarizability ratio calculated by Briggman, *et al.*[4], we have made a preliminary determination that the phenyl groups at the surface of our 90 nm PS films are tilted no more than 32° relative to the surface normal, regardless of the substrate. (More details of the fitting and analysis are included in the Supporting Information.) Since Si produces significantly more NR signal than sapphire, it is our opinion that nonresonant interference explains the difference between the previous results.[3,4] Additional work is in progress to further refine and improve our understanding of the surface structure of PS films of varying thickness on a variety of substrates.

SFG spectroscopy is a powerful tool to probe the structure of free and buried interfaces. However, we have shown that some of the assumptions that have commonly been made regarding the nonresonant response may not be fully justified. Experimental suppression of the nonresonant sum-frequency signal reveals the true resonant spectrum and allows for better determination of the resonant parameters. Our results also illustrate possible pitfalls when using complicated data analysis and curve fitting to determine the parameters of the sum-frequency spectrum. A more complete treatment of the surface orientation and a broader discussion of these considerations for analysis of SFG spectra are forthcoming.

Supporting Information Available. The contents of Supporting Information include: detailed experimental procedures, a description of the spectroscopy system, and more details of the analysis procedure. This information is available free of charge via the Internet at http://pubs.acs.org/.

4.3. REFERENCES

(1) Zhu, X. D.; Suhr, H.; Shen, Y. R. *Physical Review B: Condensed Matter and Material Physics* **1987**, *35*, 3047-3050.

(2) Wilson, P. T.; Richter, L. J.; Wallace, W. E.; Briggman, K. A.; Stephenson, J. C. *Chemical Physics Letters* **2002**, *363*, 161-168.

(3) Gautam, K. S.; Schwab, A. D.; Dhinojwala, A.; Zhang, D.; Dougal, S. M.; Yeganeh, M. S. *Physical Review Letters* **2000**, *85*, 3854-3857.

(4) Briggman, K. A.; Stephenson, J. C.; Wallace, W. E.; Richter, L. J. *Journal of Physical Chemistry B* **2001**, *105*, 2785-2791.

(5) Chen, Z.; Shen, Y. R.; Somorjai, G. A. *Annual Review of Physical Chemistry* **2002**, *53*, 437-465.

(6) Busson, B.; Tadjeddine, A. *Journal of Physical Chemistry C* **2009**, *113*, 21895-21902.

(7) Lagutchev, A.; Hambir, S. A.; Dlott, D. D. *Journal of Physical Chemistry C* **2007**, *111*, 13645-13647.

(8) Ishibashi, T.; Onishi, H. *Chemical Physics Letters* **2001**, *346*, 413-418.

(9) Stiopkin, I. V.; Jayathilake, H. D.; Weeraman, C.; Benderskii, A. V. *Journal of Chemical Physics* **2010**, *132*, 234503/1-234503/9.

(10) Lagutchev, A.; Lozano, A.; Mukherjee, P.; Hambir, S. A.; Dlott, D. D. *Spectrochimica Acta, Part A* **2010**, *75A*, 1289-1296.

(11) Shaw, S. K.; Lagutchev, A.; Dlott, D. D.; Gewirth, A. A. *Analytical Chemistry* **2009**, *81*, 1154-1161.

(12) Wei, X.; Shen, Y. R. *Physical Review Letters* **2001**, *86*, 4799-4802.

(13) Hayashi, M.; Shiu, Y.-J.; Liang, K. K.; Lin, S. H.; Shen, Y. R. *Journal of Physical Chemistry A* **2007**, *111*, 9062-9069.

(14) Fourkas, J. T.; Walker, R. A.; Can, S. Z.; Gershgoren, E. *Journal of Physical Chemistry C* **2007**, *111*, 8902-8915.

(15) Rao, Y.; Song, D.; Turro, N. J.; Eisenthal, K. B. *Journal of Physical Chemistry B* **2008**, *112*, 13572-13576.

(16) Nienhuys, H.-K.; Bonn, M. *Journal of Physical Chemistry B* **2009**, *113*, 7564-7573.

(17) Arnolds, H.; Bonn, M. *Surface Science Reports* **2010**, *65*, 45-66.

(18) Wilson, P. T.; Briggman, K. A.; Wallace, W. E.; Stephenson, J. C.; Richter, L. J. *Applied Physics Letters* **2002**, *80*, 3084-3086.

(19) Bain, C. D.; Davies, P. B.; Ong, T. H.; Ward, R. N.; Brown, M. A. *Langmuir* **1991**, *7*, 1563-1566.

(20) Meier, R. J. *Vibrational Spectroscopy* **2005**, *39*, 266-269.

4.4. SUPPORTING INFORMATION:

4.4.1.   Materials and Preparation

Polystyrene (MW 230,000) and Chromasolv water (HPLC grade) was obtained from Sigma-Aldrich. Toluene (spectrograde 99.9%) and hydrogen peroxide (30%) were obtained from Fischer Scientific. All materials were used as received. Rinsing water was obtained from a Millipore Milli-Q RG water system with a resistivity of 18 MΩ-cm. Silicon [100] wafers were obtained from University Wafer and cut into smaller, roughly 1 in^2, samples. Sapphire windows were obtained from Meller Optics and fused silica windows were purchased from Quartz Scientific. The wafers and windows were cleaned with soap and water and immersed in freshly made *piranha* solution (3:1 sulfuric acid and hydrogen peroxide) for one hour. (*Cautionary Note: Piranha* solution is very corrosive and extreme care must be used when handling.) The wafers were then immersed in ~300 mL of HPLC grade water for at least one hour. This cleaning procedure is required to remove any organic contamination that may confuse the spectroscopic measurements.

Immediately before the spin-coating process, samples were removed from water, dried with nitrogen, rinsed with Milli-Q water and dried again. Random samples were scanned on the VR-SFG system to ensure there was no surface contamination. Thickness of the SiO_2 layer was

measured by ellipsometry immediately before spin coating; ~2 nm for a clean sample was typically observed. PS was spin-coated (Laurell Technology, CZ650) at 3,000 rpm from 2% by weight solutions in toluene. The thickness of the PS layer was also measured by ellipsometry and was consistent between samples within about 2 nm. Additional experiments were performed with polystyrene dissolved in chloroform (99.8% from Mallinckrodt) to confirm that SFG signal was coming from polystyrene and not residual toluene solvent. No differences were observed in the spectra, and toluene was used in all the experiments reported in the main text.

4.4.2.   *Set-up & Instrumentation:*

The vibrationally resonant sum-frequency generation (VR-SFG) spectroscopy system is based on an amplified Ti:sapphire laser system (Quantronix, Integra C) that produces 2.7 mJ per pulse at 1 kHz. Pulse duration is ~130 fs. The beam is split, with the majority pumping a broad band IR optical parametric amplifier (Quantronix, TOPAS-C) to produce ~16 µJ of IR light with a bandwidth of ~150 cm^{-1} centered in the aromatic C-H stretch region around 3050 cm^{-1}. Off-resonance scans were centered around 3280 cm^{-1}. A germanium filter removes any remaining visible light from the OPA. The remaining output from the laser passes through two Fabry-Perot étalons to provide the spectrally narrow (~2.5 cm^{-1}) visible pulse at 790 nm. Visible pulse energy after both étalons was 17.5 µJ, with the visible beam defocused sufficiently to prevent damage to the sample.

Polarization control of both the IR and visible beams is accomplished with periscopes. In all experiments, the IR beam was *p*-polarized, and the visible beam was *s*-polarized. This input combination only produces *s*-polarized SFG, which was rotated 90° by a half waveplate for optimal detection by the spectrometer (Andor Shamrock) and CCD (Andor iDus). A short-pass optical filter was placed before the spectrometer to remove any reflected or scattered 790 nm

light. All scans used a front-surface experimental setup with the IR beam incident at approximately 60° to the surface normal; the incidence angle of the visible beam was about 17°.

4.4.3.   *Processing of VR-SFG Signal:*

Because the IR source is broadband, we must properly correct the VR-SFG spectra for the intensity profile of the IR beam. The intensity profile was obtained by collecting a spectrum off a gold mirror; this is an up-converted spectrum of the TOPAS output. Multiple scans of gold were taken over 5 hours to check for possible drift in the intensity profile within a day, but none was observed. Multiple scans of polystyrene samples were also collected for 5 hours to check for possible spectral change from either drift or surface contamination, but no significant changes were observed. We checked the possibility that the azimuthal orientation of the sample affects the SFG signal by rotating the sample. No angular dependence on the SFG signal was observed for bare or coated silicon.

Prior to each experimental run, a reference spectrum from the gold mirror was collected. To correct for the IR intensity profile, each sample spectrum is divided by the gold signal; however, the sample spectra were well centered and narrow enough to produce very little difference after intensity correction. Because correction in this fashion amplifies noise and results in no significant difference in relative intensity of the resonant features, the spectra shown in the main text were not intensity-corrected. Not correcting for the IR profile also makes the nonresonant effects more apparent. For off-resonance scans, a control mirror was used to ensure there were no significant fluctuations that could affect the observed differences in intensity.

Orientational analysis was accomplished following the procedure outlined by Gautam *et al.*[1] For our analysis we used the ν_{20b} and ν_2 modes; this choice differs from both previously published papers on polystyrene orientation.[1,2] Our reason for this selection is that the peak

around 3038 cm^{-1} (ν_{7a}) does not appear to have sufficient oscillator strength in either SFG or diamond ATR-IR (Nicolet 6700) to produce a significant peak in the polystyrene spectrum; we find that the spectrum can be fit equally well without this mode. We used the hyperpolarizability ratio calculated from Briggman *et al.* for the ν_2 mode in our analysis.[2] The fitting parameters are shown in Table 4-S1 and the results of the peak fit are shown in Figure 4-S1. Intensity correction of the IR profile is included in this fitting procedure.

We did attempt to fit the spectrum with five peaks and found the tilt angle decreased further, relative to surface normal. After removal of the nonresonant signal our spectra were best fit with Gaussian peaks, rather than Lorentzian profiles. Ishibashi and Onishi[3] observed a similar phenomenon, with Lorentzian peaks becoming more Gaussian with delay between the pulses. Gaussian peaks suggest some form of inhomogeneous broadening is present in the samples. Fits with Lorentzian peaks resulted in even shallower tilt angles. These considerations, depending on how the spectra are analyzed, support our statement in the text that the tilt angle is no greater than 32°.

Table 4-S1. Results of curve fitting analysis for VR-SFG spectra polystyrene thin films.

Frequency (cm^{-1})	Amplitude (a.u.)	Width (cm^{-1}, FWHM)
3028[a]	0.126 ± 0.001	12.39 ± 0.18
3051[a]	0.043 ± 0.002	9.956 ± 0.31
3068[a]	0.916 ± 0.016	8.879 ± 0.104
3083 ± 1	0.036 ± 0.002	18.95 ± 2.7

[a] The uncertainty of these frequencies is less than 1 cm^{-1}.
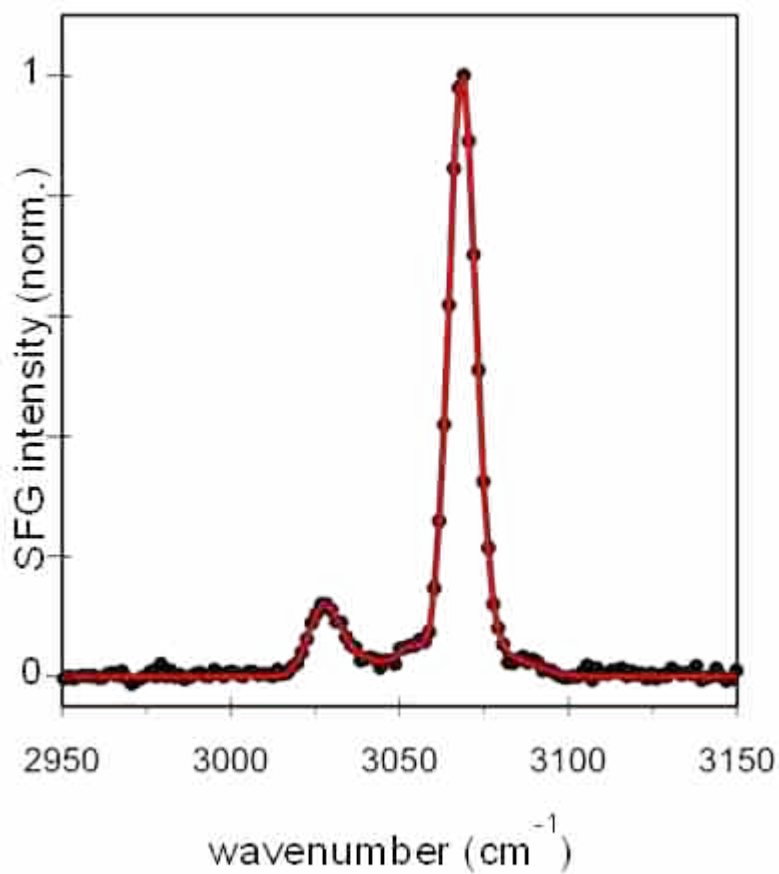
Figure 4-S1. Experimental VR-SFG spectrum (points) of PS on Si with full NR suppression and best-fit line using the parameters in Table S1.

4.4.4.   References

(1) Gautam, K. S.; Schwab, A. D.; Dhinojwala, A.; Zhang, D.; Dougal, S. M.; Yeganeh, M. S. *Phys. Rev. Lett.* **2000**, *85*, 3854-3857.

(2) Briggman, K. A.; Stephenson, J. C.; Wallace, W. E.; Richter, L. J. *J. Phys. Chem. B* **2001**, *105*, 2785-2791.

(3) Ishibashi, T.; Onishi, H. *Chem. Phys. Lett.* **2001**, *346*, 413-418.

4.5. ADDITIONAL DISCUSSION

4.5.1. *Determining the appropriate Gaussian phase*

The fits shown in this paper are from complex gaussian profiles, but the gaussian lineshape does not inherently allow complex interference. Complex interferference of a gaussian lineshape is obtained with the additional factor of e^{iF} added to the profile, synonomous with the factor to allow nonresonant interference. However, the interfering phase should not be arbitrarily determined, so to maintain the same phase innate in the complex form of Lorentzian profiles, the Lorentzian lineshape required some mathematical manipulation to explicitly extract the complex argument. The details of this are shown in appendix B.

4.5.2. *Inability to extract nonresonant parameters*

It was proposed in this paper that details regarding the phase of the nonresonant signal would still be attainable after locking down resonant parameters. Upon direct testing, this philosophy proved to be incorrect. As discussed in the next chapter, there is more to accurately modeling the nonresonant signal than the addition of extra parameters to the fitting equation.

CHAPTER 5:   LIMITATIONS IN THE ANALYSIS OF VIBRATIONAL SUM-FREQUENCY SPECTRA ARISING FROM THE NONRESONANT CONTRIBUTION*

5.1. ABSTRACT

Sum frequency generation (SFG) spectroscopy is a powerful tool for probing the orientations of molecules at surfaces and interfaces, but over-simplification in the treatment of the nonresonant (NR) contribution has obscured some fundamental limitations in the analysis of SFG spectra. These difficulties are demonstrated for the case of polystyrene thin films. The NR signal invariably distorts the spectrum and can cause changes in the spectra even in the absence of actual structural changes. The NR signal originates not only from the substrate but from all materials in the system and should not be modeled as having a frequency-independent amplitude. Because of its complicated nature, NR signal must be isolated experimentally in order to obtain meaningful results. Suppression of NR signal, however, causes a different type of distortion, due to apodization of the resonant signal in the time-domain. Experimental methods need to be refined to take these limitations into account and to obtain unique spectral parameters to be used for orientation determination.

5.2. INTRODUCTION

Sum-frequency generation (SFG) spectroscopy[1] has significantly advanced our understanding of molecules at free surfaces and buried interfaces, as summarized in multiple reviews.[2-6] In particular, SFG spectroscopy provides a method for determining the net orientation of molecules at surfaces with minimal sample preparation, unlike other surface specific

techniques such as electron microscopy. Additionally, under the dipole approximation, no signal is produced from amorphous bulk materials, which sets the technique apart as a non-destructive method that can be used to study buried interfaces *in situ*. Because the probing depth of the technique relies solely upon symmetry arguments, there are, in theory, no thickness limitations; monolayers have routinely been studied with SFG spectroscopy. Like many previous analytical techniques, such as atomic force microscopy (AFM) and surface enhanced Raman spectroscopy (SERS), SFG has opened the door to previously inaccessible knowledge and has inspired understandable enthusiasm in its practitioners.

However, much like its predecessors, SFG has reached a stage where we must step back and reconcile theoretical claims with what is achievable in practice. Practitioners in the fields of SERS and AFM found in the course of developing these techniques that some of the initial claims were exaggerated. Early studies showed that SERS was capable of single molecule detection; however, later research revealed that single molecule detection was only possible with particular molecules because of additional resonant enhancement,[7] or under specific conditions such as localized hot spots.[8] Similarly, AFM has boasted theoretical claims of atomic resolution, but true atomic resolution is not possible for most AFM systems and requires specific experimental conditions, such as contact mode with inert chemical samples or use of frequency-modulation AFM.[9]

Understanding the limitations of these techniques did not hurt the fields of AFM and SERS but instead served to refine them. Further research helped to develop methods to overcome, or better work within, the practical limitations. SFG holds much promise as an interface-specific, analytical method, but in order for it to become a truly analytical technique, we must first identify and acknowledge its limitations. Part of this process includes revisiting

common assumptions, both physical and mathematical, that affect the analysis and interpretation of SFG spectra.

5.2.1. Theoretical Basis of Sum-Frequency Generation

Sum-frequency generation occurs when two laser pulses are overlapped at a surface or interface. In vibrationally resonant SFG (VR-SFG), one pulse is in the visible region of the spectrum and the second is in the infrared region, to be resonant with molecular vibrations. The nonlinear interaction of these pulses at the interface produces both a resonant and a nonresonant (NR) signal, typically modeled as follows:

$$I_{SFG} \propto \left| \chi_{NR}^{(2)} + \chi_{R}^{(2)} \right|^2 = \left| B_{NR} e^{i\Phi} + \sum_R \frac{A_R}{\omega - \omega_R + i\Gamma_R} \right|^2 \tag{1}$$

In this equation, $\chi_{NR}^{(2)}$ and $\chi_{R}^{(2)}$ are the effective nonresonant (NR) and resonant (R) susceptibilities, respectively, B_{NR} is the NR signal amplitude, Φ is the phase difference between the resonant and NR signals, and A_R, ω_R, and Γ_R represent the resonant amplitude, central frequency, and half-width half-max of Lorentzian line-shapes, respectively, of resonant peak R. The amplitude parameters A_R and B_{NR} include local field effects and may be complex, for example in the case of total internal reflection. Generally, nonlinear curve-fitting procedures have been used to determine the NR amplitude and phase in addition to the resonant parameters.

Another way to mathematically represent the SFG signal is as follows:

$$I_{SFG} \propto \left| B_{NR} \right|^2 + \left| \chi_R^{(2)} \right|^2 + \left| B_{NR} \right| \left| \chi_R^{(2)} \right| \cos\left[\Phi - \delta(\omega) \right] \tag{2}$$

where $\delta(\omega)$ is the frequency-dependent phase of the resonant spectrum. The cross-term in this expression leads to interference in the measured spectrum. For systems with a strong nonresonant amplitude, this cross-term can be used to measure weak resonant signals. However, even on substrates with nominally weak nonresonant response, such as fused silica, the cross-

term will amplify this response and distort the resonant spectrum.[10] Once the resonant parameters have been determined, and if the hyperpolarizabilities are known, the molecular orientation can be deduced.[11-12] It must be noted, however, that any analysis of VR-SFG spectra includes assumptions regarding the NR signal, either explicit or implicit. The validity of the determined orientations, if not corroborated by other techniques, is therefore limited by the validity of these assumptions.

A common problem in curve-fitting is that as the complexity of the fit increases, the uniqueness of the fit decreases.[13] An underlying limitation is the unique determination of B_{NR} and Φ, neither of which is measured independently. Busson and Tadjeddine thoroughly discussed the difficulties in obtaining unique fits for SFG spectra.[14] In particular, they showed that there are 2^N equivalent sets of fitting parameters, where N is the number of resonant features in the spectrum. Self-consistency must be sought among these sets of parameters, but even this does not guarantee uniqueness of the results. An inherent drawback in any numerical fitting routine is the fact that the fit parameters are highly dependent on initial guesses due to multiple minima in the parameter space. Even setting this problem aside, the major source of difficulty in analyzing VR-SFG spectra is the complexity caused by NR signal interference, which can lead to apparent shifts in position and amplitude and the creation of ghost peaks.[14]

5.2.2.   *Need to Revisit Assumptions in Analysis of VR-SFG Spectra*

The need for a more critical look at the analysis of VR-SFG spectra is illustrated by two studies on the surface structure of polystyrene thin films by Gautam, et al.[15] and Briggman, et al.[16] (Note that this case is chosen because it is the most relevant to our work, not because it is necessarily the most egregious case of difficulties in analysis of SFG spectra. As we will show in this paper, other results probably also need to be revisited.) Two very different surface

structures of polystyrene were reported; an orientation nearly parallel to the surface normal, with a maximum tilt of 20°,[15] and an orientation with a much greater tilt, around 57°.[16] There are significant differences in the two studies, including the substrate material, film thickness, annealing time, the number of peaks used for fitting, and the analysis methodology. Any one of these differences could potentially explain the discrepancy, but there are also additional factors not so easily apparent, including possible interference between the two interfaces (free surface and buried interface)[17-18] and the handling of the nonresonant signal in the data analysis.[10,14]

Using the method of NR suppression developed by Lagutchev et al.,[19] we have demonstrated that there is no difference in polystyrene thin film surface structure for 90 nm films on three different substrates.[10] Polystyrene films of identical thickness were prepared on silicon, fused silica, and sapphire substrates. Although there appeared to be differences without experimental correction for nonresonant signal, when the NR signal was experimentally suppressed, the spectra were virtually identical. If interfacial interference were occurring, the different Fresnel factors at the buried interfaces would result in different spectra from the different samples. The lack of differences suggests that interference between the free and buried interfaces is not an issue with these samples. In addition, annealing and aging increased the NR response and decreased the resonant signal, but the relative intensities in the resonant response remained unchanged. Given these results, we attribute the discrepancy in the previous results primarily to the NR signal.

5.2.3. *Problems with the NR Signal*

Some of the limitations in the analysis of SFG spectra have been due to the nature of the experimental setup. Two types of laser systems are typically used for VR-SFG spectroscopy. With VR-SFG systems based on nanosecond or picosecond lasers, the IR pulse must be scanned

across the spectral region of interest. This requires constant monitoring of the output to remove experimental artifacts such as power fluctuations. The alternative is a VR-SFG system based on a femtosecond laser that produces a broad-band IR pulse. In broad-band systems, an entire spectrum can be acquired without having to tune the IR frequency, although the spectrum must still be corrected for the intensity profile of the IR source. Broad-band systems have a significant advantage over frequency scanning systems because the two pulses can be delayed relative to each other, resulting in suppression of the nonresonant signal.[19] Such suppression is simply not possible with narrow-band systems. Nonresonant suppression does help to solve many of the problems with the analysis of VR-SFG spectra. Regardless of the type of VR-SFG system, NR signal is a significant factor that must be properly handled if there is to be confidence in the results.

In this paper we illustrate some fundamental limitations of the analysis of VR-SFG spectra in the context of polystyrene thin films. First, we discuss problems imposed by the presence of the NR signal and discuss the validity of specific assumptions regarding this contribution. We then describe how the technique of NR suppression[19] helps to overcome some of these difficulties and show the additional complications that remain, mainly due to apodization of the resonant signal. Lastly, we discuss possible solutions to these issues with the NR signal, including suggested modifications to heterodyne-detected SFG.[20]

5.3. EXPERIMENTAL

The procedures for substrate cleaning, creation of polystyrene thin films, and our experimental setup are identical to that published previously.[10] Briefly, the VR-SFG system is based on an amplified femtosecond laser (Quantronix Integra C) with a broadband OPA (Quantronix TOPAS-C). Frequency narrowing of the visible pulse is accomplished with a pair of

Fabry-Perot étalons. Whenever Fourier transforms were incorporated in data analysis, the experimental data were interpolated to an evenly spaced frequency axis using Matlab's *interp1* command. To maintain the same spectral shape, the number of data points was doubled in this interpolation process.

5.4. RESULTS AND DISCUSSION

5.4.1. *Assumptions Regarding the NR Signal*

Any procedure for analyzing VR-SFG spectra must, of necessity, include some assumptions for handling the nonresonant contribution. In particular, we have experimentally investigated the validity of the following: NR signal originates solely from the substrate and can be described by a single amplitude term; the amplitude of the NR signal is independent of frequency; the NR signal can be described by a single relative phase term; the NR signal is primarily due to fast effects that decay more quickly than the resonant signal; if there is negligible NR signal from a bare substrate, it can be ignored in further analysis. We leave it to the reader to determine which of these assumptions, if any, are relevant to their analysis procedures and to identify other assumptions that we have not considered here. We also point out that these physical assumptions have mathematical analogs; care must be taken to ensure that all mathematical assumptions are in agreement with the desired physical interpretation.

i. SOURCE OF THE NR SIGNAL

The simplest assumption one can make about the source of the NR signal is that it arises primarily from the substrate. Our earlier work, however, shows that this assumption is an over-simplification. The differences in the amplitude of NR signal on bare and coated substrates have been described in our previous paper and are reproduced here in Figure 5-1.[10] Although uncoated metallic and semi-conductor substrates produce significant nonresonant signal, the total NR
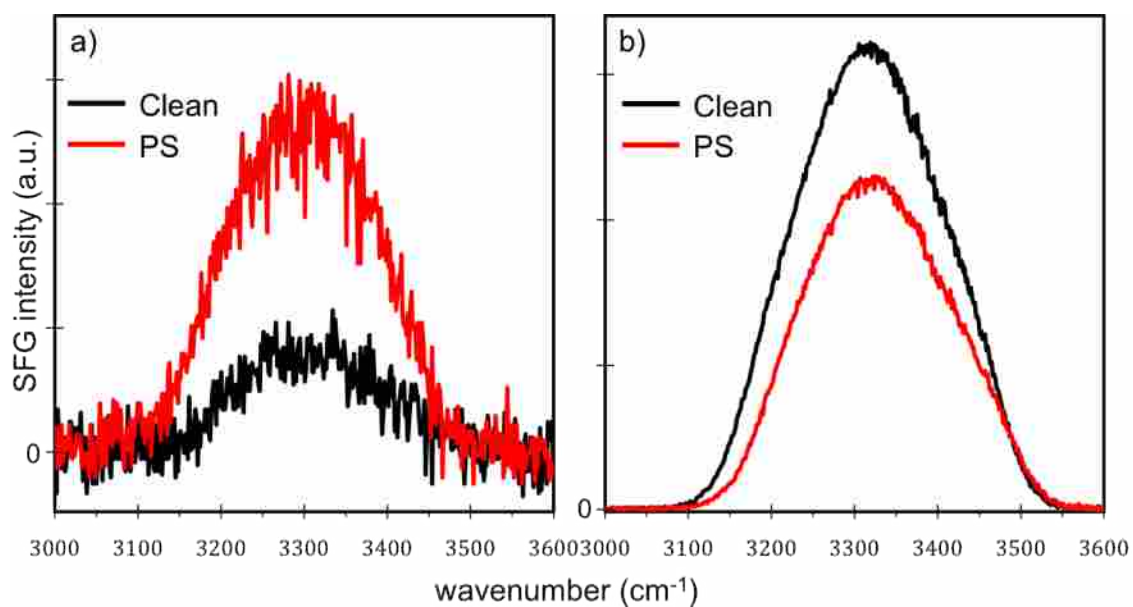
Figure 5-1. Off-resonance spectra of (a) Si and (b) Au with and without a layer of PS. NR signal increases on Si but decreases on Au. Reproduced from Reference 10.

signal is also affected by the presence of the PS thin film. Interestingly, different substrates show a different response with the presence of the PS film; on Si, the NR amplitude increases but on Au it decreases. These changes may be due to substrate-molecule interactions[21] or an optical artifact caused by thin film interference, as we discuss below. We also showed that the NR signal amplitude changes with the handling of the sample. When PS films were annealed or aged, the magnitude of the NR signal increased, but the relative intensities of the resonant features were unchanged.[10]

These results cause us to revisit how we mathematically model the NR contribution to the VR-SFG signal. In Equation (1), the NR signal is represented by an amplitude and a phase, B_{NR} and Φ, respectively. Our results show that the presence of the PS layer changes the NR amplitude, therefore it is inappropriate to simply measure B_{NR} from a bare substrate and use that value in Equation (1). Determining B_{NR} from an uncoated substrate is, in fact, the mathematical equivalent of assuming the nonresonant signal is due solely to the substrate with no contribution from the thin film. Neither assumption is borne out by the experimental results. Relaxing the assumption that NR signal is only produced by the substrate complicates the analysis because B_{NR} can no longer be measured separately from the resonant parameters.

ii. FREQUENCY INDEPENDENCE OF THE NR AMPLITUDE

A second mathematical assumption is typically made about the nonresonant amplitude: B_{NR} is a single constant and completely independent of frequency. Consider the situation of a free-standing polystyrene film (Mattson Instruments, Inc.) that is placed in the path of the IR beam when acquiring a spectrum from gold. A nonresonant spectrum is measured, but with resonant portions removed from this NR signal, as seen in Figure 5-2. This exact procedure is commonly done to calibrate the detection system, but this exercise is much more significant than
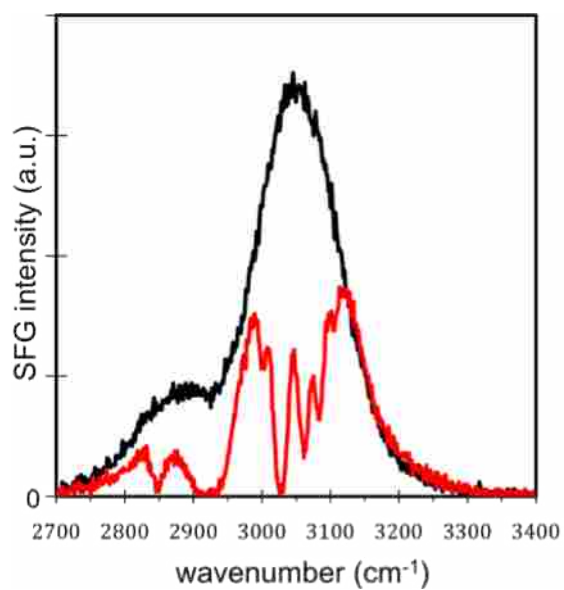
Figure 5-2. Nonresonant profile from bare Au without (black) and with (red) a polystyrene film placed in the path of the IR beam. The spectrum from bare Au corresponds to the output of the OPA. Absorbance in the PS film attenuates the NR SFG signal.

it would appear. First, this effect shows that the NR signal will be attenuated by any IR absorbance in the path, such as a polymer thin film on any substrate. The magnitude of this effect at the sample is unknown and is possibly small for some systems, but must be considered. Second, based on conservation of energy arguments, it logically follows that the production of resonant signal from the sample should attenuate the NR signal in those frequency regions. This results in an inverse relationship between resonant amplitudes and NR amplitudes. Larger resonant peaks will not experience the addition of as much NR signal as smaller resonant peaks, which will lead to nonlinear distortions of the measured amplitude and line shape.

The SFG signal, both resonant and NR portions, depends on the intensity of both the IR and the visible fields at the sample. Generation of resonant signal at the free surface perturbs the fields that enter the bulk and arrive at the buried interface. Because neither individual field is bound by the surface specific selection rules of the SFG process, the input fields can change without affecting the resonant signal from the free surface, but still alter the NR signal. These interactions may explain why the NR signal can change with bulk material changes, as occurs in aging and annealing, without affecting the relative resonant signal.[10] This also greatly complicates the ability to accurately correct the measured spectrum for NR interference, because the NR spectral profile is not identical to that measured on a bare substrate. Even attempting to mimic the sample, e.g. with full or partial deuteration, does not enable an independent measurement of NR amplitude, because the interactions between the fields and the mimic are different from those with the actual sample.

Previous arguments about the difficulties of obtaining unique fits with interfering NR signal still assumed frequency independence,[14] thus the frequency dependence of B_{NR} complicates the analysis even more. Accurate correction for the NR signal cannot be

accomplished by a single amplitude factor. Additionally, because it is unknown how to measure exactly what the resonant attenuation is at the sample, it may be impossible to correct for this interference in any way other than removing the NR signal experimentally.

iii. PHASE OF THE NONRESONANT SIGNAL

The last parameter of the NR signal that needs to be discussed is the phase, Φ in Equation 1. Unless efforts are made to measure the phase directly, a VR-SFG spectrum does not contain the phase information and the value of Φ must be inferred. For samples with constrained geometry, such as self-assembled monolayers on metal substrates or surfactant molecules at a liquid surface, relationships have been observed between the resonant and NR phases.[4] Inversion of this phase relationship has been used to argue for molecules flipping over.[22] However, this situation is complicated if the geometry is not physically constrained. As with the amplitude parameter, B_{NR}, it may not be appropriate to determine the phase parameter Φ independently from a bare substrate; the presence of the thin film affects this value as well. Even with independent knowledge of molecular hyperpolarizabilities, the connection of the resonant/NR phase relationship to molecular orientation is not clear.

We have observed an additional effect that further complicates using the phase difference between the resonant and NR contributions in determining molecular orientations. We prepared samples with various thicknesses of PS on Si. With changing thickness, we observed interference between the resonant and NR signal, as shown in Figure 5-3. As thickness changes, the interference changes from constructive to destructive, however when the NR signal is experimentally suppressed, all the normalized spectra appear identical. This is similar to what we observed for 90 nm films on three different substrates; the surface structure appears to be
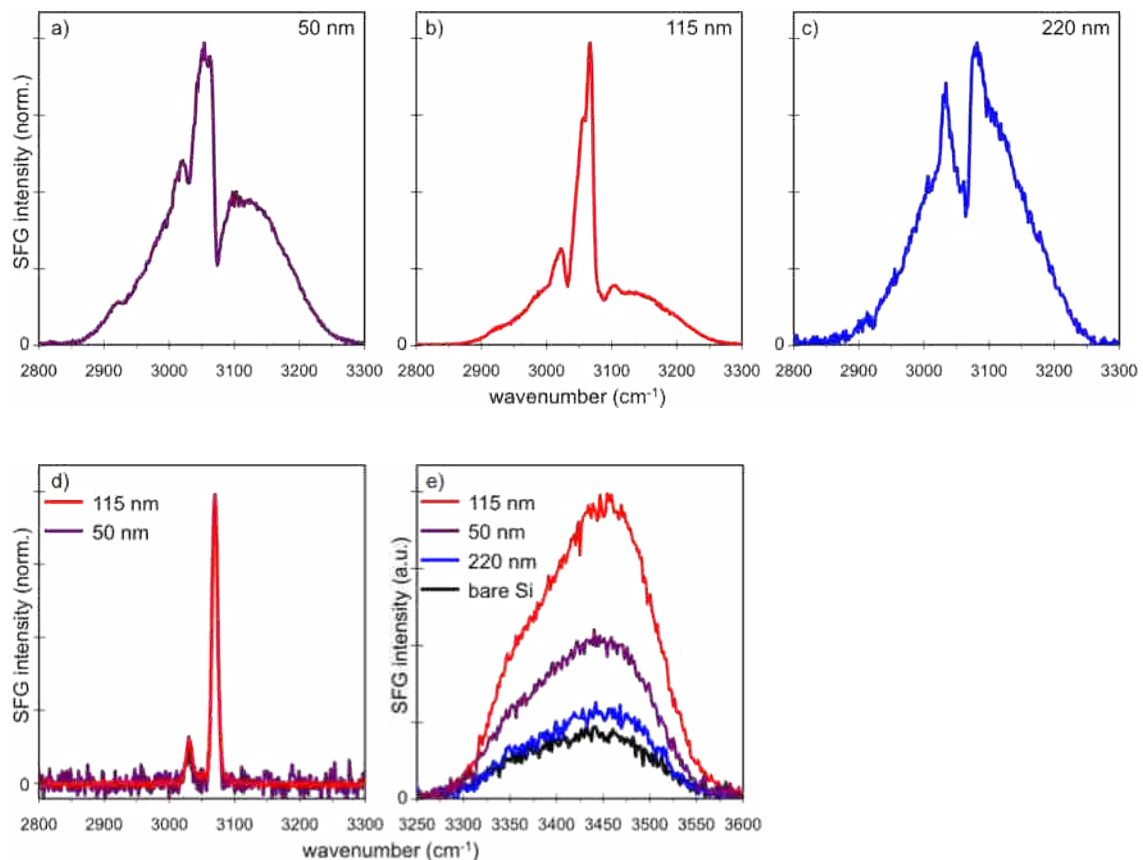
Figure 5-3. VR-SFG spectra of PS on Si. Thickness of PS was a) 50 nm, b) 115 nm, and c) 220 nm.

Spectra were not corrected for the IR profile to make the NR contribution more apparent. d) 50 and 115

nm PS films with fully suppressed NR. e) Off resonance scans of the same films and a bare Si substrate.

independent of substrate and film thickness. (There are changes in the absolute intensities, and this is discussed further in the Supporting Information.)

We also tuned the IR source away from the resonant features to investigate the NR response alone. As seen in Figure 5-3e, we observed a periodic trend in the overall intensity of the NR signal. The dependence of both the resonant and NR signals with PS film thickness is consistent with a simple model of thin film interference, described more fully in the Supporting Information. In this model, resonant signal is generated only from the free surface, but NR signal is generated from both the free and buried interfaces. (This differs significantly from the thin film model previously proposed that allowed for resonant signal from the buried interface as well.[17-18,23]) As the film thickness changes, the interference between the NR signal generated at the free and buried interfaces changes, matching the observed trends. This model also explains the interference between the resonant and NR contributions. This type of interference probably also explains some of the differences that have been observed with different experimental geometries;[24] as the angles of the beams change, the effective thickness of the layer also changes, resulting in different degrees of interference. Additionally, the observed decrease in NR intensity on a Au mirror (Figure 5 - 1b) may be due to the ~150 nm thick protective coating present on commercial mirrors. The broader point of this discussion is that the phase relationship between the resonant and NR signals is not adequately described by a single parameter.

iv.   TIME SCALE OF RESONANT AND NONRESONANT SFG

With a broad-band VR-SFG system, the temporal delay between the visible and IR pulses is an additional experimental parameter that can be adjusted. Varying this delay has been shown to have significant effects on lineshapes in VR-SFG spectra.[25-26] These papers assume that the NR signal maximum occurs earlier than the resonant signal because the NR signal is assumed to

arise from electronic effects in the substrate that relax faster than the vibrational free induction decay. This is, however, one more assumption that must be validated experimentally.

We directly measured the signal intensity as a function of delay between the visible and IR pulses on three different substrates: Au, PS on fused silica, and bare Si/SiO_2. As seen in Figure 5-4, the time delay corresponding to the maximum NR signal changes with the system. In fact, for polystyrene on fused silica, which is assumed to have little NR contribution, the signal reaches its maximum before the purely NR signal from bare silicon/SiO_2. Because both the resonant and NR signals depend on the IR and visible fields, the time response of both the resonant and NR signal will change with the sample system; the sample perturbs both fields, and hence the measured VR-SFG response. This makes it unclear how to define time-zero, or how to optimize the IR-visible delay for broad-band VR-SFG measurements.[25]

<h3>v. Insignificant NR Signal from the Substrate</h3>

The final assumption that we treat here is negligible NR signal from the substrate. As shown in Equation (2), even if B_{NR} is small compared to $\chi_R^{(2)}$, the cross-term will serve to amplify the NR signal, leading to spectral distortion of the resonant features. We reported this effect previously for PS on fused silica with different degrees of NR suppression.[10] As discussed above, it is improper to measure the NR amplitude on a bare substrate and simply use this value in determining the resonant parameters.

5.4.2. Problems Arising from the Nonresonant Signal

It is well established that the NR signal distorts the resonant features of the VR-SFG spectrum. The presence of NR signal can also lead to confusion in setting the correct number of resonant peaks to be used in nonlinear curve fitting. In the two previously published structures of polystyrene, different numbers of resonant peaks were used in the fitting; 5 peaks were used in
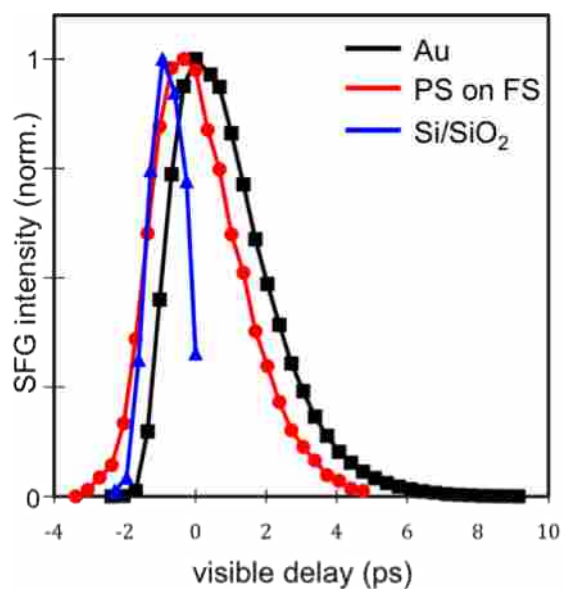
Figure 5-4. Time response of signal intensity for Au, PS on fused silica, and bare Si/SiO$_2$, with $t = 0$ as the maximum nonresonant signal from Au. The time at which the maximum signal occurs depends on the sample.

the first,[14] whereas the second group fit with 7.[16] There are 5 peaks theoretically calculated for the phenyl group of polystyrene, but the IR data obtained by the second group showed two additional combination bands. However, to obtain reliable information from a fit, the parameters must be unique, which can only be obtained by fitting with the minimum number of peaks. Fitting with too many peaks will inevitably influence the fitting parameters because the extra peaks will mathematically withdraw amplitude and width from the true peaks, while appearing to give a better fit.[13]

To better determine the correct number of peaks that should be used, we acquired ATR-IR spectra of PS. In our analysis, one of the 5 theoretically calculated peaks (around 3035 cm^{-1}) is not apparent, which agrees with IR results previously reported for polystyrene.[16] Neither of the previous groups observed this peak, but both fit a dip in that region of the VR-SFG spectrum as a negative peak. Moreover, the parameters of this negative peak were used in both group's orientation analysis. With nonresonant suppression, phase changes can cause dips to become peaks[19] but in our spectra, no peak ever appeared in the region of the purported dip, even after full suppression. The absence of this peak indicates that the given vibrational mode does not have sufficient IR and/or Raman activity to appear in the VR-SFG spectrum. (A vibrational mode must be both Raman and IR active to appear in the spectrum.) Use of this peak in orientation analysis is therefore problematic. Additionally, the NR signal may cause the appearance of the two combination bands; Busson and Tadjeddine discussed such "ghost peaks" in their work.[14] With full NR suppression, we do not observe either of these peaks; there are only 4 apparent peaks. Even with significant NR contribution, we obtained a good fit for a polystyrene sample, using the model given by Equation 1, with just 4 peaks as shown in Figure 5-5.
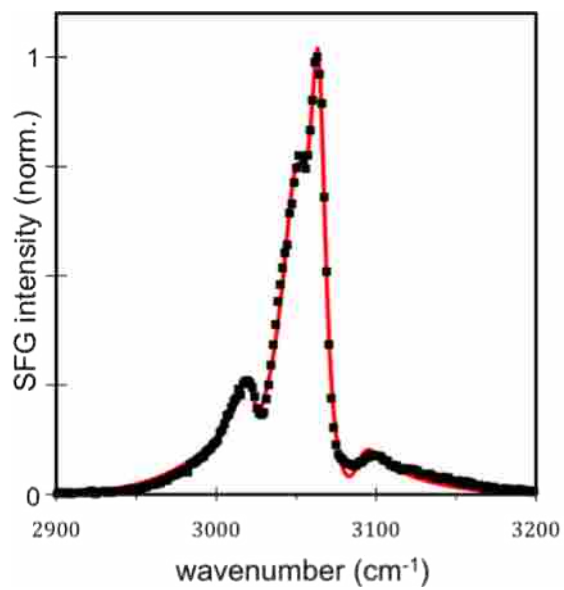
Figure 5-5. Fit to PS spectrum with full NR contribution with only four Lorentzian profiles.

5.4.3. *Consequences of NR Suppression*

Given the difficulties caused by the presence of the NR signal, the most viable approach appears to be to eliminate it experimentally. This is accomplished by changing the time delay between the broad-band IR and narrow-band visible pulses.[19] Because our visible pulse is produced by étalons, the profile in time is asymmetric, allowing the NR response to decay but preserving the interaction of the visible pulse with the resonant free induction decay (FID). However, delaying the visible pulse does more than just suppress the NR signal. This delay also modifies the sampling of the beginning of the resonant FID, resulting in apodization of the resonant signal. This apodization has both positive and negative effects that we will now discuss.

i. APODIZATION OF RESONANT FEATURES

It has been previously reported that delaying the visible pulse relative to the IR causes a change in the peak shapes from Lorentzian to Gaussian and increases peak resolution.[25-26] Both of these changes result from signal apodization, many examples of which are found in NMR spectroscopy.[27-28] Figure 5-6 illustrates the transformations that result from the delay of the visible pulse. In Figure 5-6a, a simulated polystyrene resonant spectrum in the frequency domain is shown, with 5-6b showing the corresponding FID in the time domain. The apodization function is the measured time profile of our visible beam, also shown in Figure 5-6b with a fit line overlay. The apodized FID, shown in 5-6d, is no longer a pure exponential decay, but develops a Gaussian leading edge. The Fourier transform of this Gaussian-like profile in time becomes a Gaussian profile in the frequency domain upon detection; the line shapes are now Gaussian as seen in Figure 5-6c.

Because the latter portion of the FID is primarily responsible for resolution, selective sampling of the latter part of the FID by NR suppression results in increased spectral resolution.
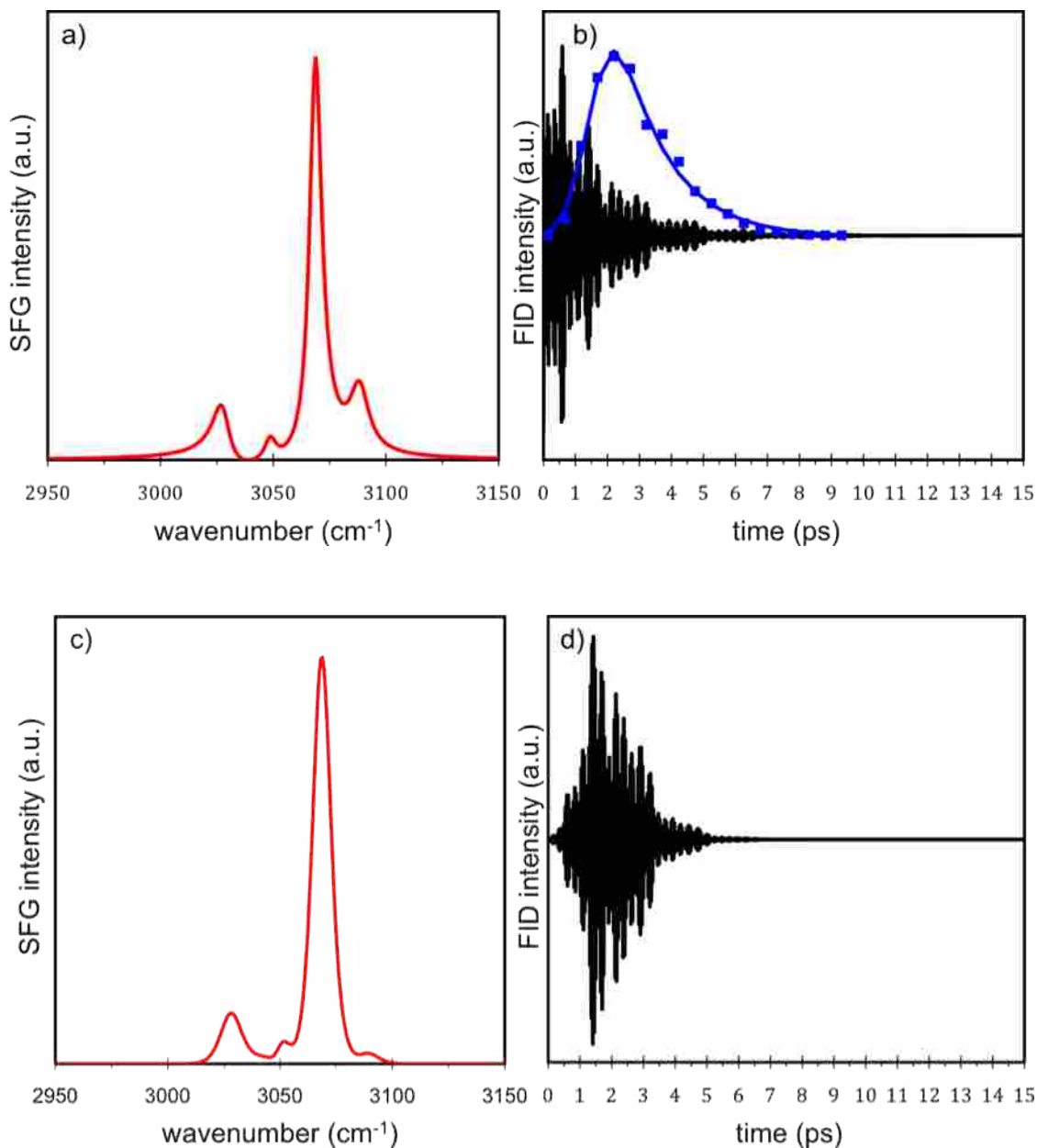
Figure 5-6. Simulation of the effects of NR suppression. (a) Simulated resonant PS spectrum with four Lorentzian peaks. (b) Corresponding free induction decay and measured time profile of the narrow-band visible pulse delayed by 2.2 ps. (c) Apodized spectrum and (d) free induction decay, showing changes in relative intensity and line shape.

This approach is routinely used in NMR spectroscopy.[27-28] However, this process has the negative effect of distorting the peak areas because of the attenuation of the first several points of the time domain signal. Again, this problem is frequently encountered in solid state NMR where probe and filter ringing often corrupt the first few points of the time domain signal.[28-29] This effect is easily illustrated by looking at the mathematics of the Fourier transform. The Fourier transform, generalized without normalization factors, is written as follows:

$$\int_{-\infty}^{\infty} F(\omega) e^{i\omega t} d\omega \tag{3}$$

At the first time point, $t = 0$, the exponential term goes to 1 and we are left with the integration of the frequency-domain signal, which is equivalent to the peak area. Any degree of suppression modifies the sampling of the initial time points, which distorts the observed peak areas. This is readily seen by the changes in relative amplitudes in the simulated spectra in Figure 5-6.

As long as all peaks have the same width, the peak heights maintain proportionality to the true peak areas. However, vibrational modes with different T_2 times have different peak widths, thus the proportionality of amplitudes is often lost. Specifically, broad peaks are affected more than narrow peaks because they are short-lived in the time domain; delaying the visible pulse has a greater effect on these peaks. Because all samples will be convolved with the same apodization function, this distortion does not remove all meaningful information, and qualitative comparison between samples is still possible. In fact, spectral changes can be seen more accurately with the removal of the interfering NR signal because of the improved spectral resolution, despite the changes in peak amplitude. Caution must still be exercised in determining absolute peak parameters because the spectra are distorted.

In NMR spectroscopy, reference deconvolution allows one to obtain the apodization function, which is then used to reconstruct the time-domain signal for other samples. It is therefore theoretically possible to reconstruct the resonant VR-SFG signal with knowledge of the apodization function, but VR-SFG is a frequency-domain technique and that complicates this process. We can, however, determine the shape of the apodization function by measuring the time profile of the visible beam. For systems that use an étalon to narrow the visible beam, the apodization function is described by a convolution of the Gaussian time profile of the entering pulse with the exponential decay imposed by the etalon.[19] Our system uses two étalons, requiring a second exponential decay; the fit of our visible beam to this function is shown in Figure 5-6b. By measuring the relative time delay of our pulses, we can move the function to the correct time delay relative to the FID. We then fit the experimental data with a set of resonant Lorentzians convolved with this apodization function. The only unknowns are then from the set of Lorentzian parameters. A fit to our data using this method is shown in Figure 5-7.

Because we are measuring in the frequency domain, we require additional deconvolution steps that are not required in NMR, which forces us to adopt additional assumptions. These assumptions deal primarily with our ability to accurately model the signal in the time domain. Additionally, it should be remembered that although this approach may give a good fit, the best fit is not necessarily the most correct one.[13] Reconstructing resonant Lorentzians does not yield a unique solution. A similarly good fit can be obtained by using 4 complex Gaussians, as we have shown previously.[10] In fact, Gaussian fitting may give the most meaningful results due to uniqueness arguments, even though such a model does not attempt to exactly reconstruct the
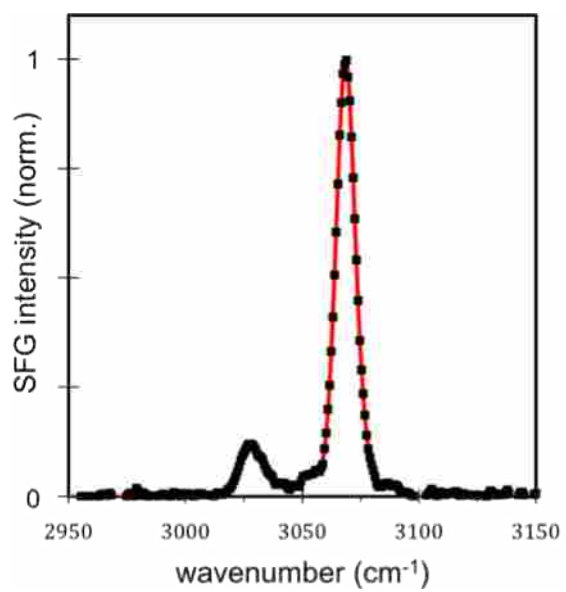
Figure 5-7. Fit to experimental spectrum with NR suppression accounting for apodization effects.

original signal; accurate relative comparisons can still be made to understand changing conditions, even though absolute determinations of structure would be suspect.

iii. Inclusion of Different Levels of NR Signal

One other point should be made regarding the three analyses of the polystyrene surface structure. In the previous two studies, no suppression of the NR signal took place. In our analysis, the NR signal was fully suppressed. To improve the accuracy and confidence of fit parameters, simultaneous fitting with different degrees of NR signal could be used. Within a single polarization there is no difference in the resonant parameters once apodization is accounted for, so amplitude, frequency, and width should all be consistent. Simultaneous determination with multiple spectra should allow us to obtain an accurate and unique set of parameters.

We tried just such an analysis, using the conventional model of the NR signal $\left(\chi_{NR}^{(2)} = B_{NR}e^{i\Phi}\right)$, but our results were unsatisfactory (see Figure 5-8). We also tried to find consistency among the 2^4 sets of possible parameters, as suggested in ref 14, but this was unsuccessful. This is not surprising given the previous discussion regarding the NR signal, especially considering that the resonant portions attenuate the NR signal. In other words, the model of $\chi_{NR}^{(2)}$ consisting of a constant amplitude and constant phase is inadequate. A different model could be used, but altering the model for the more complicated nature of the NR signal would require additional unknown parameters, making a unique and meaningful solution unobtainable.
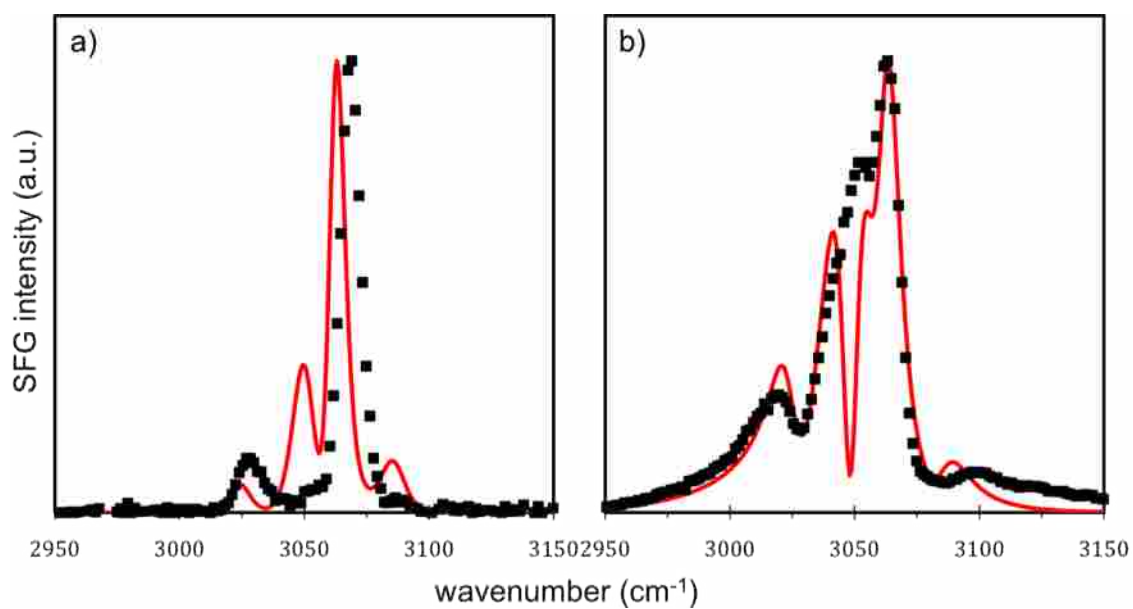
Figure 5-8. Attempt to simultaneously fit multiple spectra acquired with different levels of NR suppression. (Additional spectra not shown.) Because of the simple model of the NR signal, this approach is unsuccessful.

We did, however, perform a simultaneous fit of multiple spectra acquired at different time delays with the NR contribution fully suppressed. Two representative spectra from the full set of five are shown in Figure 5-9. The quality of the fit is dramatically improved, but there is still considerable uncertainty in the amplitudes, due to the time-domain effects; we still do not have the initial time points that are primarily responsible for peak areas. We are currently working to resolve this problem by implementing a time-domain measurement.[30]

Other un-validated assumptions related to signal reconstruction also complicate this analysis. One assumption we have made is that our visible pulse can be modeled as a Gaussian pulse convolved by the exponential decays imposed by the étalons, but we know that our entering pulse is not purely Gaussian. Because very small changes in the time domain can result in fairly significant changes in the frequency domain, the inaccuracy introduced by the visible fit in Figure 5-6 may be too great to correctly model the resonant signal. We also assumed that our measurement accuracy of time delay is good enough to adequately reconstruct the unapodized signal, which may not be true. In particular, determination of time-zero is problematic. Even without these extra difficulties, accounting for the frequency dependence of the NR signal is still insurmountable. For these reasons, it is probably better to simply use a more unique Gaussian fit to compare sets of NR suppressed data to detect relative changes.

5.4.4. *Potential Solutions for Proper Analysis*

One of the most important points to make here is that sum-frequency spectra are never free of some type of distortion. Without suppression, the NR signal affects the spectrum in a very complex fashion which inevitably causes errors in analysis as described above, including ghost peaks[14] and uncertainty in peak amplitudes and widths. With NR suppression, apodization effects distort the amplitudes and widths, which, if not properly reconstructed, will lead to uncertainty in
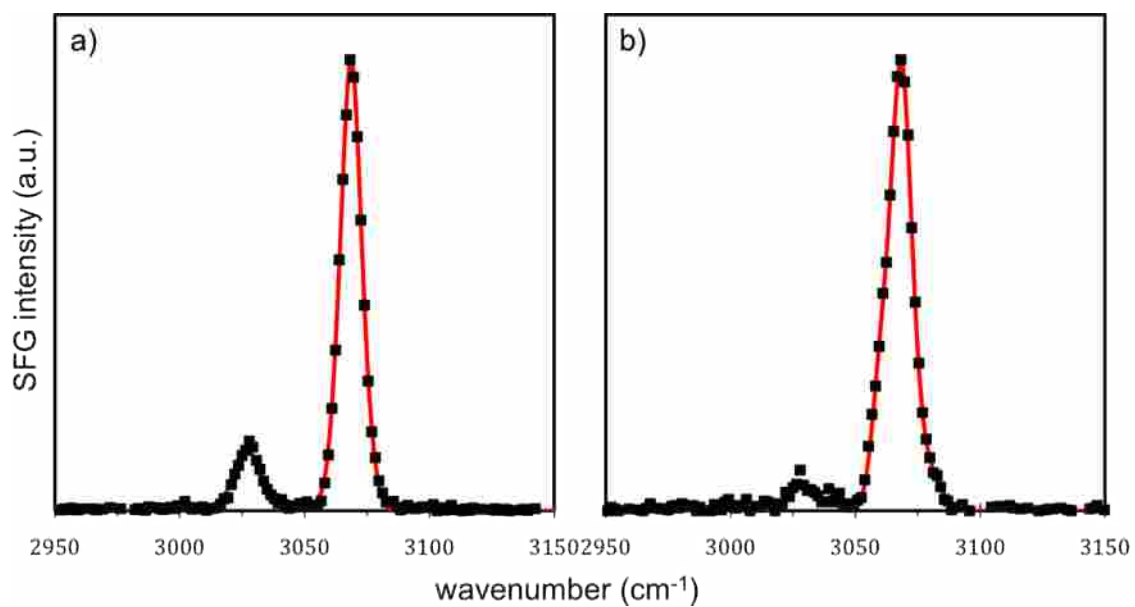
Figure 5-9. Simultaneous fit to multiple spectra acquired at different IR-visible delay times separated by 0.6 ps, but with full NR suppression. Only the first and last spectra from the full set of five delay times are shown.

determining molecular orientations. Without some definitively known peak parameters, unique reconstruction cannot occur. With NR suppression, all spectra will be affected in the same way, allowing for accurate relative comparisons. Even relative comparisons are suspect when NR signal is present, because of the complex nature of the interaction with the resonant signal.

Various numerical methods have been used to deal with the difficulties caused by the NR contribution. These approaches include techniques such as Kramers-Kronig analysis and the maximum entropy method (MEM).[31] These methods are used to determine the relative phase and/or correction of single valued amplitude of the NR signal for absolute orientation determination. However, all numerical analysis techniques must be used with caution, because they are of necessity based on underlying assumptions that must also be validated.[32] As we have shown, the NR amplitude is not single-valued and the NR signal has significant contributions aside from the substrate. The fundamental problem is that a single VR-SFG spectrum is an underdetermined system, and there is no way to determine a unique set of parameters without additional constraints. Knowledge of the NR signal must be determined experimentally if we are to have confidence in the resonant parameters.

Because of these difficulties, real progress must be made on the experimental front. One potential solution is phase-sensitive SFG, which can be accomplished using heterodyne methods.[20,33] However, conventional heterodyne methods do not actually assist in NR phase determination. Because the NR signal is not localized to the substrate and can be comparable in amplitude to the resonant signal, a heterodyne-detected method will amplify both the NR and resonant signal, and the same complications in separating the two signals remain. This can be seen by looking at the mathematics behind the amplification effect, which has been modeled by the following relation[20]:

$$I_{HDSFG} = \left| E_{SFG} + E_{LO} \right|^2 = \left| E_{SFG} \right|^2 + \left| E_{LO} \right|^2 + 2\,\mathrm{Re}[E_{SFG}E_{LO}^*]\,(4)$$

where I_{HDSFG} is the intensity of the heterodyne SFG signal, E_{SFG} is the SFG optical field and E_{LO} is the local oscillator field. Because the LO can be independently measured, accurate correction for it can be made, and because E_{SFG} is so much weaker, $\left| E_{SFG} \right|^2$ is effectively 0. The necessary information is contained and enhanced primarily in the cross-term. It must be remembered, though, that E_{SFG} is a combination of both the resonant and NR signal. Because the NR signal does not originate solely from the substrate, what remains should be modeled as

$$2\,\mathrm{Re}[(B_{NR}e^{i\Phi} + \sum \frac{A_R}{\omega - \omega_R + i\Gamma_R})E_{LO}^*] \qquad\qquad (5)$$

which still contains all of the difficulties associated with NR interference, including the unknown NR phase.

What is actually needed for absolute orientation determination by phase considerations is not the phase difference between resonant and NR signals, but between the sample and substrate signals. One possible approach would be to determine the phase of the substrate relative to the LO by measuring a bare substrate with no NR suppression. Then, by measuring the sample with the NR signal suppressed, the phase difference between the resonant sample signal and the LO is measured, and the phase difference between the sample and the substrate can be inferred. This method still requires that there are no substrate-molecule interactions that could be altering the phase of either the substrate or sample and caution must be taken to verify the validity of this assumption for an accurate analysis. Although apodization problems will still exist in the resonant signal, the needed phase difference for absolute orientation determination could be determined. This approach still needs to be demonstrated experimentally, and we are pursuing

this effort. A recently demonstrated heterodyne detected time-domain SFG technique also holds much promise, but it remains to be seen how it performs on a variety of systems.[30]

5.4.5. *Consequences for Other Systems*

We have demonstrated significant problems in the analysis of VR-SFG spectra of thin films of polystyrene caused by the NR signal. If this contribution to the spectrum is not handled correctly, differences in spectra can lead to incorrect conclusions regarding differences in structure; the same surface gives apparently different spectra on different substrates or with different film thickness. We have seen similar problems in our investigations of model chromatography systems. Spectral changes that we initially attributed to differences in structure are actually due to changes in the optical properties of the interface, as we will discuss in detail in a forthcoming publication. It remains to be determined how significant the effects of the NR contribution are for other systems.

We have also shown that, even with removal of the NR contribution, absolute determinations are still problematic without additional information. This does not prevent the detection and proper interpretation of *relative* changes, either from sample to sample or for the same sample under different conditions. For example, changes in relative methyl/methylene intensity still have meaning, even if absolute tilt angles are not determined. To the extent that other physical changes, such as fast reorientation,[34-35] manifest themselves in the resonant portion, they should also be detectable once the NR contribution has been removed. Ultimately, experimental suppression of the NR signal, or corroboration with other techniques, is required before definitive statements can be made.

5.5. CONCLUSIONS

We have discussed the difficulties in the analysis of VR-SFG spectra caused by NR signal interference, as well as the complications introduced by experimental suppression of the NR signal. Although the spectra are distorted in both cases, the NR signal corrupts the results in a complicated manner that varies with any changes to the system, including non-structural changes. Additionally, the difficulty of the inverse relation between resonant and NR amplitude makes correction for the NR signal extremely difficult if not impossible. The apodization effects observed with suppression of the NR signal, however, are consistent and actually improve relative comparisons. NR suppression ensures that observed changes seen in SFG spectra are actually the changes of interest (e.g. orientation changes) as opposed to changes solely in the NR signal.

Although absolute orientation cannot be determined unambiguously when NR signal is present, and additional problems arise with NR suppression, VR-SFG is still one of the very few techniques that can probe buried interfaces in a non-destructive fashion. VR-SFG is still ideally suited for monitoring relative changes at interfaces, but suppression of the NR signal is necessary to determine unique parameters. These comparative abilities alone are still of great use for science and engineering applications, but we must understand the fundamental limitations of this technique to improve it even further.

Supporting Information Available: More detailed discussion of the thin film interference model and the changes of the resonant and nonresonant SFG signal observed with different film thickness. This material is available free of charge via the Internet at http://pubs.acs.org.

5.6. REFERENCES

(1) Zhu, X. D.; Suhr, H.; Shen, Y. R. *Physical Review B* **1987**, *35*, 3047-3050.

(2) Williams, C. T.; Beattie, D. A. *Surface Science* **2002**, *500*, 545-576.

(3) Buck, M.; Himmelhaus, M. *Journal of Vacuum Science and Technolology, A* **2001**, *19*, 2717-2736.

(4) Bain, C. D. *Journal of the Chemical Society, Faraday Transactions* **1995**, *91*, 1281-1296.

(5) Chen, Z. *Polymer International* **2007**, *56*, 577-587.

(6) Shen, Y. R. *Pure and Applied Chemistry* **2001**, *73*, 1589-1598.

(7) Moskovits, M.; Tay, L.-L.; Yang, J.; Haslett, T. In *Optical Properties of Nanostructured Random Media*, Vol. 82; Shalaev, V., Ed.; Springer Berlin / Heidelberg, 2002.

(8) Stranahan, S. M.; Willets, K. A. *Nano Letters* **2010**, *10*, 3777-3784.

(9) Giessibl, F. J. *Materials Today* **2005**, *8*, 32-41.

(10) Curtis, A. D.; Reynolds, S. B.; Calchera, A. R.; Patterson, J. E. *Journal of Physical Chemistry Letters* **2010**, *1*, 2435-2439.

(11) Hirose, C.; Naotoshi, A.; Kazunari, D. *Journal of Chemical Physics* **1992**, *96*, 997-1004.

(12) Hirose, C.; Naotoshi, A.; Kazunari, D. *Applied Spectroscopy* **1992**, *46*, 1051-1072.

(13) Meier, R. J. *Vibrational Spectroscopy* **2005**, *39*, 266-269.

(14) Busson, B.; Tadjeddine, A. *J. Phys. Chem. C* **2009**, *113*, 21895-21902.

(15) Gautam, K. S.; Schwab, A. D.; Dhinojwala, A.; Zhang, D.; Dougal, S. M.; Yeganeh, M. S. *Physical Review Letters* **2000**, *85*, 3854-3857.

(16) Briggman, K. A.; Stephenson, J. C.; Wallace, W. E.; Richter, L. J. *Journal of Physical Chemistry B* **2001**, *105*, 2785-2791.

(17) Wilson, P. T.; Briggman, K. A.; Wallace, W. E.; Stephenson, J. C.; Richter, L. J. *Applied Physics Letters* **2002**, *80*, 3084-3086.

(18) Lambert, A. G.; Neivandt, D. J.; Briggs, A. M.; Usadi, E. W.; Davies, P. B. *Journal of Physical Chemistry B* **2002**, *106*, 5461-5469.

(19) Lagutchev, A.; Hambir, S. A.; Dlott, D. D. *Journal of Physical Chemistry C* **2007**, *111*, 13645-13647.

(20) Stiopkin, I. V.; Jayathilake, H. D.; Bordenyuk, A. N.; Benderskii, A. V. *Journal of the American Chemical Society* **2008**, *130*, 2271-2275.

(21) Superfine, R.; Guyot-Sionnest, P.; Hunt, J. H.; Kao, C. T.; Shen, Y. R. *Surface Science* **1988**, *200*, L445-L450.

(22) Ward, R. N.; Davies, P. B.; Bain, C. D. *Journal of Physical Chemistry* **1993**, *97*, 7141-7143.

(23) McGall, S. J.; Davies, P. B.; Neivandt, D. J. *Journal of Physical Chemistry B* **2004**, *108*, 16030-16039.

(24) Gan, W.; Wu, B.-H.; Zhang, Z.; Guo, Y.; Wang, H.-F. *Journal of Physical Chemistry C* **2007**, *111*, 8716-8725.

(25) Stiopkin, I. V.; Jayathilake, H. D.; Weeraman, C.; Benderskii, A. V. *Journal of Chemical Physics* **2010**, *132*, 234503/1-234503/9.

(26) Ishibashi, T.-a.; Onishi, H. *Chemical Physics Letters* **2001**, *346*, 413-418.

(27) Ernst, R.R., Bodenhausen, G., Wokaun, A., *Principles of Nuclear Magnetic Resonance in One and Two Dimensions*, Oxford University Press, New York, NY, 1987.

(28) Cavanagh, J., Fairbrother, W.J., Palmer, A.G.,III, Skelton, N.J. *Protein NMR Spectroscopy*; Academic Press, San Diego, CA, 1996.

(29) Hoult, D. I.; Chen, C. N.; Eden, H.; Eden, M. *J. Magn. Reson. (1969)* **1983**, *51*, 110-117.

(30) Laaser, J. E.; Xiong, W.; Zanni, M. T. *Journal of Physical Chemistry B* **2011**, *115*, 2536-2546.

(31) Sovago, M.; Vartiainen, E.; Bonn, M. *Journal of Physical Chemistry C* **2009**, *113*, 6100-6106.

(32) Press, W. H. *Numerical Recipes in C : The Art of Scientific Computing*; Cambridge University Press: Cambridge, U.K., 1988.

(33) Ji, N.; Ostroverkhov, V.; Chen, C.-Y.; Shen, Y.-R. *Journal of the American Chemical Society* **2007**, *129*, 10056-10057.

(34) Wei, X.; Shen, Y. R. *Physical Review Letters* **2001**, *86*, 4799-4802.

(35) Fourkas, J. T.; Walker, R. A.; Can, S. Z.; Gershgoren, E. *Journal of Physical Chemistry C* **2007**, *111*, 8902-8915.

5.7.1.   *Thin-Film Interference of NR Signal*

The behavior of both the resonant and NR VR-SFG signals from polystyrene films of different thicknesses can be understood with a very simple thin-film interference model. In this model, the resonant signal originates only from the free surface and can propagate in two directions: away from the sample or into the thin film followed by reflection from the substrate. The NR signal originates both at the free and buried interfaces. This is notably different from the previous model of thin-film interference, where resonant signal is also taken to originate from both the free and buried interfaces.[1]

We first consider the behavior of the NR signal that originates at the free surface. Upon reflection from the substrate, the forward propagating signal undergoes a 180° phase change relative to the beam traveling away from the sample. Constructive interference will result when:

$$2nd = (m + \frac{1}{2}) \lambda \tag{S1}$$

Here n is the index of refraction, d is the thickness of the sample material, λ is the wavelength of the SFG light, and m is any integer. The quantity $2nd$ represents the effective path length traveled by the SFG beam through the film, assuming normal incidence. Similarly, destructive interference occurs according to the following relation:

$$2nd = m\lambda \tag{S2}$$

For our system, λ is approximately 640 nm and the index of refraction (n) will lie somewhere between that of bulk PS, and the average of bulk PS and air; as films get thinner the index of refraction approaches the average between the two interfacial media.[2] Because we are uncertain of the exact index of refraction for a particular thickness, we can bound the problem between the two possible values: 1.59 (the bulk index of refraction at this wavelength), and 1.30 (the average

between bulk PS and air). For our experimental geometry, no correction is needed for the small angle offset of the path length of the beam; the greatest uncertainty is in the index of refraction. The equations above allow us to calculate the type of interference expected for a given film thickness. For 640 nm light, constructive interference occurs at an effective path length 2nd of 320 nm while destructive interference occurs at 640 nm. The effective path length varies with film thicknesses as shown below. (The range is from uncertainty in the index of refraction.)

Table 5-S1. Effective path length for polystyrene thin films

Film thickness (d) / nm	Effective path length (2$nd)$ / nm
50	130 – 159
115	299 – 366
220	570 – 700

This simple model predicts that 115 nm films will exhibit constructive interference, 220 nm films will exhibit destructive interference, and 50 nm films will have partial interference. This matches the observations of NR signal intensity seen in Figure 3e, showing the plausibility of the model. Note that for the 220 nm film, the signal is comparable to that of an uncoated substrate; the only NR signal observed is from the buried interface.

This model also explains the observations in Figures 5-3a-c. The resonant signal propagating away from the sample can interfere with each of the other beams: transmitted resonant signal, free-surface NR signal traveling both into and away from the sample, and NR signal from the buried interface. Similar to what was observed with the NR signal, the 115 nm film shows constructive interference between the resonant and NR signals, whereas the 220 nm film shows destructive interference between them. The overall intensity of the measured spectra

also follows the same pattern; the 220 nm film has a weaker spectrum than the 115 nm film. This simple optical model accounts for all the experimental observations.

5.7.2.   *References*

(1) Wilson, P. T.; Briggman, K. A.; Wallace, W. E.; Stephenson, J. C.; Richter, L. J. *Applied Physics Letters* **2002**, *80*, 3084-3086.

(2) Simpson, G. J.; Daily, C. A.; Plocinik, R. M.; Moad, A. J.; Polizzi, M. A.; Everly, R. M. *Analytical Chemistry* **2004,** *77* (1), 215-224.

5.8. ADDITIONAL INFORMATION

This paper ended with the implication that absolute parameters may not be available, and there is large uncertainty in paramters from multiple time delay fits. Absolute parameters are not currently available when trying to include data that contains a nonresonant response; however, as indicated in this chapter, simultaneous fits can be accomplished to data at different time delays that are free of the nonresonant interference. Defining a single amplitude can also provide the absolute ratios of peak amplitudes. By exploiting these facts, data that differs in frequency and time can be used to constrain fit parameters and effectively reconstruct the unapodized resonant response with accompanying parameters. This process is detailed in the next chapter.

CHAPTER 6: USE OF VARIABLE TIME-DELAY SUM-FREQUENCY GENERATION FOR IMPROVED SPECTROSCOPIC ANALYSIS*

6.1. ABSTRACT

The interpretation of vibrationally resonant sum-frequency generation (VR-SFG) spectra is often complicated by two factors: spectral congestion and the presence of nonresonant signal. With broadband VR-SFG systems, the spectra are further distorted because of incomplete sampling, or apodization, of the resonant free induction decay (FID) in the time domain. An experimental method is presented that takes advantage of these time-domain effects to obtain more accurate parameters than can be achieved by fitting a single VR-SFG spectrum. VR-SFG spectra are acquired at multiple delay times of the visible pulse with full suppression of the nonresonant signal and then simultaneously fit to determine a single set of spectral parameters. The multiple, independent spectra serve to constrain the results of the fitting. This variable time-delay approach allows for improved determination of the parameters of the resonant spectrum, including the proper number of peaks in the spectrum, and is demonstrated for thin films of polystyrene and surface-bound octadecylsilane. An additional advantage of the technique is that it can be implemented with minimal modification to an operational broadband VR-SFG system.

6.2. INTRODUCTION

The proper analysis of highly congested spectra can be a difficult undertaking, and any deficiencies or problems in the analysis will affect the physical interpretation of the data. Two main strategies have been employed to address this issue. The first is to utilize advanced non-linear curve fitting procedures to provide reasonable values for peak positions, widths, and

amplitudes. This can be problematic, however, due to an inherent paradox in curve-fitting; nonlinear curve-fitting does not generally yield unique results unless most of the parameters are already known.[1] Without sufficient constraints on the analysis, multiple solutions are attainable that yield an equally good fit, but with different determined parameters, which in turn affects the interpretation of the spectra. The second strategy is to obtain more experimental information, which can be accomplished in various ways. One approach is to controllably vary aspects of the sample, e.g. through isotopic labeling and other perturbations, to obtain more information. Another is to obtain more data through higher-order or multidimensional spectroscopic techniques. What we present in this article is an experimental methodology for analyzing congested vibrationally resonant sum-frequency generation (VR-SFG) spectra that does not perturb the system and provides additional information through a hybrid time- and frequency-domain approach. This method can be employed with existing broadband VR-SFG systems and avoids the costs of isotopic labeling and other perturbative approaches.

In addition to the general problems of analyzing congested spectra, VR-SFG spectra present the investigator with two other challenges. First, because VR-SFG is inherently sensitive to surfaces and interfaces, spectral parameters from the literature cannot always be used to constrain the fits. This is because known bulk parameters, such as line widths or even center frequencies, may change due to the different environment at the interface. For example, previous studies on polystyrene, a material often used for calibration purposes, have suggested that central frequencies can shift up to 9 cm^{-1} from reported measurements of bulk samples.[2-4] (These changes are not seen in linear surface-sensitive techniques such as ATR-IR due to a greater probing depth that results in the sampling of more material in a bulk-like environment.) This inability to use literature data makes it difficult to properly constrain the fits.

A second complication inherent in VR-SFG, and other nonlinear techniques, is interference from a nonresonant signal. This nonresonant signal can distort the apparent peak positions and even give rise to "ghost peaks" that will affect spectral fitting.[5,6] The VR-SFG spectrum is typically represented mathematically as:

$$I_{SFG} = \left| B_{NR}e^{i\Phi} + \sum_R \frac{\Gamma_R A_R}{\omega - \omega_R + i\Gamma_R} \right|^2 \tag{1}$$

Here, B_{NR} represents the nonresonant amplitude, Φ represents the phase of the nonresonant signal, and A_R, ω_R, and Γ_R represent the amplitude, central frequency, and Lorentzian half-width at half-max (HWHM), respectively, of the resonant vibrational modes. Both terms in equation (1) are complex, which leads to the possibility of interference. This is better illustrated by looking at an expanded version of equation (1):

$$I_{SFG} = \left| B_{NR}e^{i\Phi} + L(\omega) \right|^2 = \left| B_{NR} \right|^2 + \left| L(\omega) \right|^2 + 2\left| B_{NR} \right|\left| L(\omega) \right|\cos(\Phi - \delta(\omega)) \tag{2}$$

In equation (2), we have substituted $L(\omega)$ to represent the summation of resonant Lorentzian peaks from equation (1) and $\delta(\omega)$ is the frequency-dependent phase of the resonant spectrum. Because of the cross-term, the nonresonant signal is not isolated but directly affects the observed resonant signal.

Generally, we are most interested in the resonant signal, since it contains the structural information about the interface. Unfortunately, it is often the case that none of the resonant parameters, from either of the above equations, are known *a priori*. In linear algebra, in order to solve a problem with N parameters, N linearly independent relations, or data points, are required. In a typical spectrum, there are M data points, where M is much greater than N, the number of spectral parameters. However, most of the points in the spectrum are not independent of the other points. In other words, there is no guarantee that N points are linearly independent, particularly

with spectral congestion. This leads to multiple solutions, or multiple local minima in the parameter-space. Without sufficient constraints, it is difficult to determine which of these possible solutions is correct and physically meaningful. What is needed to accurately determine the system of N parameters is additional linearly independent data points.

A common approach to obtain more information is to acquire VR-SFG data in multiple polarization combinations, which often results in dramatically different spectra. These differences are due to a combination of local field effects and molecular orientation. Accounting for these influences requires the introduction of additional variable parameters, thus resulting in minimal constraint of the spectral parameters in equation (1). Additionally, interference from the nonresonant signal can complicate this type of analysis further by introducing different degrees of distortion into the individual spectra. Another experimental approach that varies another independent parameter can provide the necessary information for the full analysis of congested spectra, even for a single polarization combination.

Some additional aspects of equation (2) merit further discussion. In cases where the resonant signal is much weaker than the nonresonant signal, it is often through the cross-term that information is obtained about the resonant response. This is seen in the case of self-assembled monolayers (SAM's) on metals, such as Au or Ag.[7] The resonant features appear on top of the strong nonresonant signal, and the lineshape is indicative of the phase difference between the resonant and nonresonant responses. The reverse situation can also occur, with the resonant response being much stronger than the nonresonant response. It must be noted, however, that just because the nonresonant response is small does not mean it can be ignored. The same cross-term that allows the resonant features to be observed in the presence of a strong nonresonant signal allows a weak nonresonant signal to be observed in the presence of a stronger

resonant response. The consequences of this enhancement are different in that the resonant signal strength varies with frequency. Thus, the nonresonant signal will be amplified more in regions of stronger resonant signal than it will be off-resonance. This amplification results in distortion of the resonant spectrum, even though it may appear that only negligible nonresonant signal is present; i.e. no elevated baseline. Later in this paper we illustrate an example of a small nonresonant response distorting resonant features.

While it is tempting to treat the nonresonant signal merely as a background, that is not always appropriate. Unfortunately, the underlying nature of the nonresonant signal is not fully understood, and our recent work has called into question some of the commonly made assumptions regarding it.[4,6] We have shown that, in the case of polystyrene thin films, the intensity of the nonresonant signal changes with the history of the sample; i.e., the nonresonant signal increases with aging or annealing of the polymer thin film.[4] We have also shown that the nonresonant signal does not arise solely from the substrate material. Furthermore, our work questions the appropriateness of modeling the nonresonant signal with only two parameters, B_{NR} and Φ.[6] In short, the nonresonant signal is a complicated response that carries additional information about the sample, but it is unclear how to properly deal with it.

Correcting for the nonresonant signal with numerical post-processing methods, such as the maximum entropy method (MEM),[8-10] can be problematic, because of assumptions about the nonresonant signal that are inherent in these methods.[6] Furthermore, MEM is known to suffer from problems such as overestimation of the number of peaks[11] and has been shown to not always be accurate in phase determination.[12] All numerical methods should be used with caution and, where possible, additional constraints should be obtained experimentally.

The nonresonant signal can readily be removed experimentally by changing the delay between the visible and IR pulses used to generate the sum-frequency spectrum.[13] This process, however, leads to distortions of the resonant spectrum because of effects in the time-domain.[6] In VR-SFG, the IR pulse excites vibrational resonances that are upconverted by the visible pulse. Depending on the length of the visible and IR pulses, the production of the SFG signal occurs differently in the time-domain, which will affect what is observed in the frequency-domain spectra. As we show in this paper, when these time-domain effects are properly handled, the differences in the measured spectra help solve the problem of uniquely determining the resonant parameters. This approach requires us to explicitly consider effects in the time domain.

In frequency scanning VR-SFG systems, both the IR and the visible pulses are of nanosecond duration.[14] The nanosecond visible upconversion pulse provides high spectral resolution, and the narrow-band IR pulse is scanned across many frequencies to collect a full spectrum. However, because the long IR pulse is continually driving both responses, the nonresonant signal is inseparably connected with the resonant signal. Spectral congestion can also be a problem, depending on the sample. At the other extreme, femtosecond visible and IR pulses can be used for time-domain SFG measurements.[15] The short IR pulse initiates a vibrational free induction decay (FID) that persists for a few picoseconds. The visible upconversion pulse, also very short in time, is scanned over many time points to build the full time-domain response, which is then Fourier transformed to yield a spectrum with high frequency resolution. This process also involves full upconversion of the nonresonant signal, although some discrimination may be possible with heterodyne detection if there is a phase difference between the resonant and nonresonant responses.[15] Even with full time-resolved data,

however, peak overlap can still cause difficulties in analyzing congested frequency-domain spectra.

Conventional broadband VR-SFG involves combining short IR pulses (often 100-200 femtoseconds) with longer visible pulses (up to a few picoseconds);[16,17] the spectral resolution is dependent on the length and shape of the visible pulse.[15] With sufficient time delay of the visible pulse relative to the IR pulse, the nonresonant signal, which decays more quickly than the resonant FID, can be suppressed and effectively removed.[13] This is not without consequence on the measured spectrum, however, because the upconverting pulse is neither long nor short compared to the few-picosecond lifetime of the vibrational FID, but rather of similar duration. Therefore, with the delay needed to nonresonant suppression, the initial portion of the resonant FID is not upconverted. This truncation, or apodization, in the time domain causes some distortion of the measured resonant spectrum.[6,15]

In fact, any broadband VR-SFG measurement is subject to this apodization effect, and effects on the lineshape with delay of the visible have been observed.[6,18,19] Even disregarding the nonresonant signal, the upconversion process will either preferentially sample the beginning portion of the FID, which is primarily responsible for peak areas, or the latter portion, primarily responsible for resolution. Adjusting the visible time delay to provide maximum signal will preferentially sample the leading portion of the FID, but undersample the latter portion. Apodization of the tail of the FID will broaden the peaks in the frequency-domain spectrum beyond what would be anticipated from the bandwidth of the visible pulse. Thus, any broadband VR-SFG is distorted to some extent but, as we will show, these effects can be used to our advantage.

Recently, heterodyne detection (HD) and other phase sensitive techniques have been applied to VR-SFG spectroscopy.[20,21] In the HD-SFG approach, the weak VR-SFG signal is combined with a much stronger (>100 times) local oscillator (LO) that is generated in a separate nonlinear crystal. The two beams are combined and detected either through spectral interferometry[20] or balanced heterodyne detection.[15] Heterodyne detection allows for three main advantages: improved detection limits due to increases in signal-to-noise, linear scaling of the VR-SFG signal with surface concentration, and determination of the phase as well as the amplitude of the VR-SFG signal.[20] The measured signal intensity is written as

$$I_{HD-SFG} \propto |E_{SFG} + E_{LO}|^2 = |E_{SFG}|^2 + |E_{LO}|^2 + 2Re[E_{LO}^* E_{SFG}]$$ (3)

where E_{SFG} denotes the sample signal and E_{LO} denotes the local oscillator. The relative intensity of the two signals is chosen such that $|E_{SFG}|^2$ is effectively zero. The $|E_{LO}|^2$ can be removed either by Fourier filtering or direct subtraction. The desired information is found in the cross term, which still contains phase information about the sample. Another advantage of this approach is that it provides the real and imaginary spectra, which can be used as additional constraints for fitting.

Note the similarity between equation (3) and equation (2); in many ways, the conventional VR-SFG experiment with nonresonant signal present is a self-heterodyne measurement between the resonant and nonresonant signals. In fact, unless the nonresonant signal is suppressed, E_{SFG} in equation (3) contains both resonant and nonresonant contributions, which must be properly accounted for in the analysis. It has been argued that the nonresonant signal can be properly removed from the HD-SFG data because of a difference in phase between it and the nonresonant signal, assuming an instantaneous response of the nonresonant signal.[15,20] While this may be true for monolayers, we have reservations about making this assumption when

investigating thin films. The nonresonant signal that propagates through the thickness of the film, and reflects off the substrate, is not necessarily in phase with the nonresonant signal that propagates directly away from the film. We have shown such an effect in the amplitude of the nonresonant signal with film thickness.[6] We have also reported different onset times of the nonresonant signal, depending on the sample; we observed a lag in the maximum nonresonant signal on a Si/SiO_2 compared to a Au surface.[6] Thus the assumption that the nonresonant signal has no phase lag should be checked experimentally for each new sample to be studied. It seems that the only way to be absolutely certain the nonresonant contribution is not affecting the results is to experimentally suppress it and properly account for the resulting apodization effects. Our methodology will therefore enhance the results obtained from phase-sensitive experiments.

6.3. BASIS FOR THE VARIABLE TIME-DELAY SUM-FREQUENCY GENERATION APPROACH

Although the observed spectrum changes with the delay of the visible pulse, the underlying resonant FID remains unchanged. The problem is then how to determine the resonant parameters from the distorted spectra. The solution is to acquire spectra at multiple time delays after full experimental removal of the nonresonant signal, each of which will appear different because of different sampling of the FID. The full set of spectra is then simultaneously fit to accurately obtain all of the resonant parameters. It should also be noted that the sample itself is not altered or perturbed in any way during this procedure.

This method is similar to the linear algebra approach of using multiple linearly independent equations to determine a set of multiple unknowns, where the minimum number of equations needed is equal to the number of unknowns to be determined. In spectroscopy, however, a single peak is described by three parameters (amplitude, width, and position) that can

all be simultaneously determined if there is no interference from neighboring peaks. When overlapping peaks are present, the ability to determine these parameters is compromised unless additional constraints are known. Analogous to having additional linearly independent equations, the frequency-domain spectra acquired at different visible delay times provide the information that is necessary for a complete analysis.

To better understand this approach, it is helpful to look at the mathematical representation of the physical generation of the signal, as shown in the equation below:

$$I_{SFG} = |L(\omega) \otimes V(\omega)|^2 \qquad (4)$$

In this equation, $L(\omega)$ and $V(\omega)$ represent the resonant signal and visible pulse, respectively, and $\otimes$ denotes convolution. ($L(\omega)$ is again the sum of resonant Lorentzian profiles from equation (1).) The nonresonant term is not included in equation (4) because it has been removed experimentally. Because the visible pulse is variably delayed in time, it is more useful to rewrite the previous equation as follows:

$$I_{SFG} = \left| ft\left[ift(L(\omega)) \times ift(V(\omega)) \right] \right|^2 = \left| ft\left[ift(L(\omega)) \times V(t) \right] \right|^2 \qquad (5)$$

Here ft and ift represent a Fourier transform and inverse Fourier transform, respectively, and $V(t)$ represents our visible pulse in time. With variable delay, $V(t)$ changes position in time, but not shape, and causes a change in I_{SFG}. $L(\omega)$, however, remains constant because the resonant FID is not changing. Multiple spectra, each with different delay times, are acquired and then simultaneously fit to determine $L(\omega)$. In this fashion, all the time-domain distortions are corrected and the true resonant signal is extracted.

6.4. EXPERIMENTAL METHODS

6.4.1. *VR-SFG Spectroscopy System and Sample Preparation*

The details of our SFG system have been described previously.[4] In short, a portion of the output of a femtosecond laser pumps a broadband OPA to produce femtosecond IR pulses. The remaining visible light is stretched by two etalons to produce time-asymmetric Lorentzian pulses[13] with approximately 2.5 cm^{-1} HWHM bandwidth. All spectra were acquired with *s*-polarized SFG, *s*-polarized visible and *p*-polarized IR pulses. We measured the time-domain profile of our visible pulse by cross-correlation of the pulse before and after the etalons. The time profile of our visible pulse has also been shown previously.[6] The delay between the visible and IR pulses was adjusted with a manual delay stage. Care was taken to only use spectra acquired at the points indicated by the tick marks on the micrometer to ensure better reproducibility in setting the time delay.

Polystyrene samples were prepared following the procedures of Reference 4. Briefly, polystyrene (average molecular weight 230,000 g mol^{-1}) was spin-cast from toluene solution (2% by weight). We used approximately 100 nm thick polystyrene films to take advantage of constructive interference of the transmitted and reflected surface signals, as described previously.[6] The spin-cast films were not annealed prior to characterization. As we have previously shown, annealing does not change the shape of the resonant spectrum, although overall amplitude decreases slightly, but annealing does significantly increase the amplitude of the nonresonant signal.[4]

Fused silica discs (1" round by 1/8" thick, Quartz Scientific) were functionalized with octadecyltrichlorosilane (OTS, $Cl_3SiC_{18}H_{37}$), using the following procedure, based on literature precedents.[22] The discs were first cleaned by sonicating them in $CHCl_3$ for ~5 minutes followed

by immersion in 100+ °C *piranha* solution for 1 to 2 hours. *(Caution: Piranha solution, 3:1*

concentrated H_2SO_4:30% H_2O_2, is highly corrosive and should be handled with extreme care.)

The cleaned discs were then rinsed with copious amounts of ultrapure water from a 18 MΩ

Millipore system, followed by acetone, chloroform, methylene chloride, and finally immersed in

100 mL of methylene chloride. (Once the discs were cleaned in *piranha*, they were never

allowed to dry out to minimize the possibility of surface contamination.) All solvents were

HPLC grade unless otherwise noted. Roughly 1 mL of $Cl_3SiC_{18}H_{37}$ reagent (Gelest) was added

to the methylene chloride and allowed to react on a shaker table for 24 hours. Following the

reaction, the discs were again rinsed with copious amounts of methylene chloride, chloroform,

acetone, water, acetone, chloroform and sonicated in chloroform to remove any unreacted

material. The discs were then stored in ultrapure water until they were characterized.

6.4.2.   Data Analysis

The spectra acquired with different time sampling of the FID were simultaneously fit to

determine the underlying resonant parameters. Because Fourier transforms are involved as part

of the fitting process, all data sets were interpolated to an evenly spaced axis. The number of data

points resulting from interpolation was double the number of actual data points to preserve

spectral integrity. The gold spectrum was also fit to a single Gaussian to provide noiseless

intensity correction.

The fitting process was accomplished by the following procedure. As described in

equation 4, a set of Lorentzian peaks were created from initial guesses, inverse Fourier

transformed into the time domain, and multiplied by the apodization function (time profile of the

visible beam) centered at the various experimental time delays. The apodized signals in the time

domain were then Fourier transformed back into the frequency domain. The squared modulus

was computed and multiplied by the profile of the IR pulse (obtained from the gold spectrum). The theoretical peaks were then mathematically checked against the original interpolated data by calculation of absolute error. The fitting parameters of amplitude, central frequency, and width, were varied and the process was iterated until a good fit was obtained. As part of the routine, the residuals and Jacobian matrix are calculated and used to determine the 95% confidence intervals for each fitting parameter. As the final check, the fit functions were plotted against the raw, uninterpolated data for visual verification of a good fit. If this visual characterization was unsatisfactory, the initial guesses were changed and the processes repeated.

6.5. Results and Discussion

6.5.1. *Variable Time-Delay Approach for Polystyrene*

Polystyrene has well-characterized bulk properties (it is often used as a calibration reference), but uncertainty remains in its surface characterization. Specifically, there is significant disagreement in the spectral assignments, and hence in the surface structure.[2-4,23] We acquired VR-SFG spectra of the free surface of polystyrene on silicon at various visible delay times, shown in Figure 1. The time indicated in each panel is the delay between the visible and IR pulses, with time zero set to the maximum nonresonant signal from a Au reference. Note the change in relative intensity of the two large features at 3069 and 3027 cm^{-1} at the various delay times. Note also the emergence of a small feature at ~3045 cm^{-1} that is not observable at early delay times. The peaks also appear to broaden somewhat and adopt a more Gaussian lineshape, due to the incomplete sampling in the time domain.[6,18,19]

The solid lines in Figure 6-1 are from the simultaneous fit performed in accordance with equation (5). These curves include the distortions caused by the time delay and apodization effects, and are, in fact, calculated from the single set of fit parameters shown in Table 6-1. It
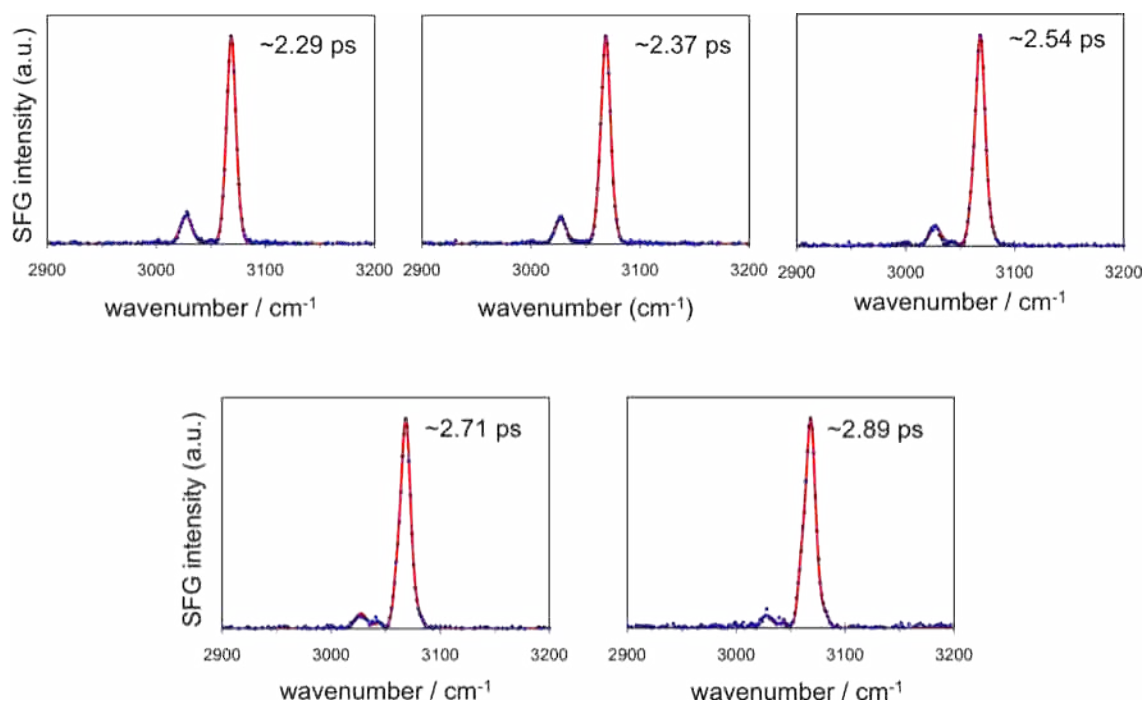
Figure 6-1. Polystyrene spectra collected at various visible beam time delays and simultaneously fit according to equation (5).

Table 6-1: The extracted parameters for the simultaneous fit of polystyrene with 5 different spectra at different visible delays.

ω_R	95% Confidence Interval	% uncertainty	A_R	95% Confidence Interval	% uncertainty	Γ_R	95% Confidence Interval	% uncertainty
3026.98	(3026.85, 3027.10)	0.004%	0.43	(0.39,0.48)	10%	7.31	(7.06,7.56)	3.39%
3044.86	(3044.58, 3045.13)	0.009%	-0.013	(-0.022,-0.003)	76%	0.86	(0.20,1.52)	76.59%
3057.52	(3057.46, 3057.58)	0.002%	0.064	(0.30,0.34)	6.2%	2.13	(1.96,2.31)	8.05%
3068.80	(3068.78, 3068.82)	0.001%	1.00	(fixed)	(fixed)	3.85	(3.80,3.90)	1.41%
3084.67	(3084.45, 3084.88)	0.007%	-0.016	(-0.018,-0.014)	12%	2.56	(2.0,3.12)	21.97%

should be noted that amplitudes have been normalized because suppression of the nonresonant signal, though needed for accurate analysis, removes the t_0 information needed for absolute amplitude determination. Reference deconvolution techniques could be used to reconstruct the t_0 information if a suitable reference peak were available, but is not possible in this case. Additionally, assignments of positive and negative peaks are relative to our arbitrarily fixed positive amplitude for the 3068.80 cm^{-1} peak; absolute phase determination requires measurement with an independent phase standard, as can be accomplished with HD-SFG or other phase sensitive methods.[20,21]

This analysis also assists in determining the correct number of peaks that should be used in fitting the resonant spectrum, which has not always been clear *a priori*. Previous analyses of polystyrene have used 3, 5, or 7 peaks.[2,3,23-25] In our previous work with the nonresonant signal removed, we used only 4 peaks.[4,6] With our variable time-delay method, we have been able to resolve and quantify 5 peaks, but with some differences from previously reported parameters. Other than slight differences in position and width, the features at 3026.98, 3057.52, and 3068.80 cm^{-1} are similar to the previous studies. Our peak at 3084.67 cm^{-1} differs from Briggman *et al.*[2] (in their report, two peaks were included above 3075 cm^{-1}, which could account for the difference), but is very similar to Gautam, *et al.*[3], except our analysis assigns a negative amplitude to this peak. The most significant difference in our analysis is the lack of a feature at ~3035 cm^{-1}. The prior studies included a negative peak at this position; in Briggman *et al.* this peak was much broader than any other feature in the spectrum.[2] What was previously fit as a dip we simply attribute to the lack of a peak. The presence of nonresonant signal in the two previous studies probably confused this issue further. Our analysis, instead, shows a weak and very narrow peak, also with negative amplitude, at 3044.86 cm^{-1}.

As stated by Meier,[1] nonlinear curve fitting methods can produce multiple solutions with equally good values of χ^2, the sum of squared errors, but that does not guarantee a physically meaningful result. For instance, if more functions are added to the fitting procedure, the value of χ^2 may decrease, but some of the resultant parameters will be very uncertain and hence provide minimal physical insight. Without appropriate constraints, there is no guarantee of obtaining a physically meaningful outcome. A better discriminator is the relative uncertainty of the fit parameters; the majority of our parameters have a relative uncertainty of less than 10%, with greater uncertainty in the smaller features. One key advantage of this method is that all the peaks used in the fit are visibly discernible in at least one of the variable time-delay spectra, and are thus justified in the fitting routine. This method is not guaranteed to produce the smallest values of χ^2, but we have more confidence in the determined parameters.

The detection of this narrow peak at 3044.86 cm^{-1} further illustrates the power of the variable time-delay approach. In conventional VR-SFG measurements, this peak is not resolved because of the neighboring peak at 3057.52 cm^{-1}, but is detectable with the variable time-delay approach because of the effects of apodization. As the visible pulse is delayed, all the peaks are broadened. Futhermore, the natively broad peaks (with short lifetimes) are diminished in amplitude allowing the narrower peaks, which are now broadened, to be resolved because of decreased congestion. The broadening effect is simulated in Figure 6-2. The natural linewidth of the 3044.86 cm^{-1} peak is shown in blue. At a 2.54 picosecond delay (the time at which the peak starts to appear) this peak broadens to about 3.87 cm^{-1} HWHM (shown in red), which is within the resolution limit of our system. By simultaneously fitting various spectra acquired at different time points along the FID, the effective FID can be reconstructed within an arbitrary amplitude scaling factor. This process allows the variable time-delay method to determine the natural line-
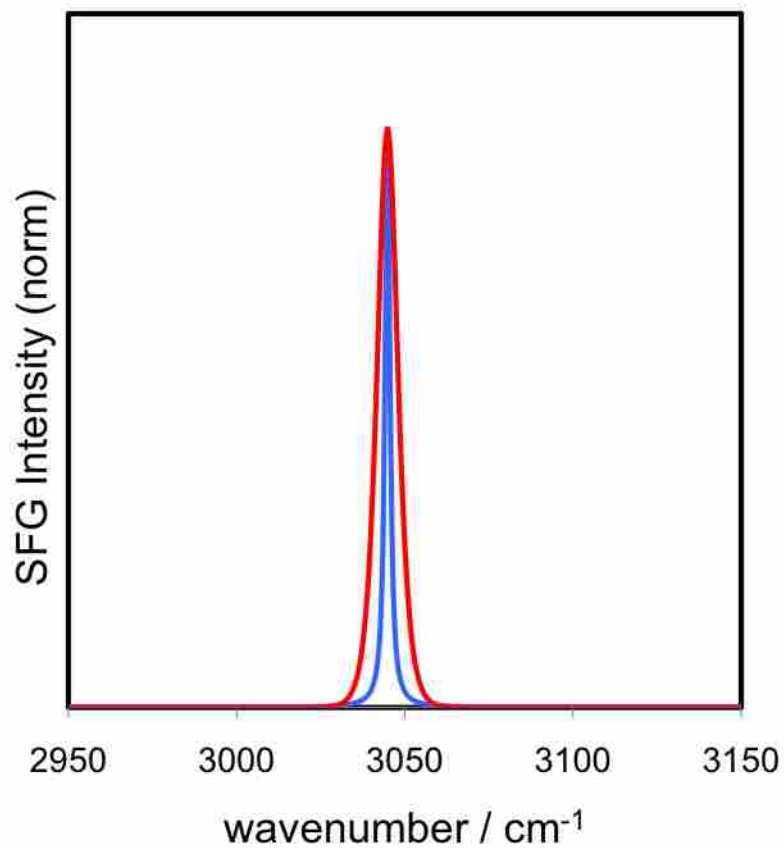
Figure 6-2. The natural width of the 3045 cm^{-1} peak (blue) is beyond the resolution capabilities of our system. With a time-delayed visible pulse, apodization effects broaden the peak (red), making it detectable.

width of narrow features, even if they would otherwise be beyond the resolution of the spectroscopic system. A peak this narrow can easily be missed even in high resolution experiments due to two constraints: the resolution provided by the pulse (determined by pulse length) and the number of data points acquired in a given frequency region. Furthermore, independent of experimental resolution, there must also be minimal overlap from neighboring peaks. Considering the relative uncertainty in the amplitude and width of this peak, which is a direct result of its small relative strength, quantifying anything other than its existence and position is impractical. In conventional VR-SFG measurements, this peak is effectively absent, as it was in our previous studies.[4,6]

6.5.2. *Surface-Bound Octadecylsilane*

Another system that we have investigated with the variable time-delay technique is octadecyltrichlorosilane (OTS) attached to fused silica, a model system for investigating the structure of the liquid chromatography interface.[26-28] In previous studies, the amplitude of the nonresonant signal has often been considered negligible, but our results show that to be a faulty assumption. When the solvent environment of OTS on fused silica is changed from methanol to water, changes in the VR-SFG spectra are observed over 2 hrs, suggesting a structural change in response to the new solvent (See Figure 6-3a). However, when the same sample is probed with the nonresonant signal fully suppressed, the spectra look virtually identical between the two environments, as shown in Figure 6-3b. Something has changed in the new solvent environment, but it is not clear that the change is solely structural.[29] Changes that could be attributed to changes in the structure of the interface in various solvents are no longer observed once the nonresonant signal is fully suppressed, as discussed more fully in a forthcoming manuscript. For
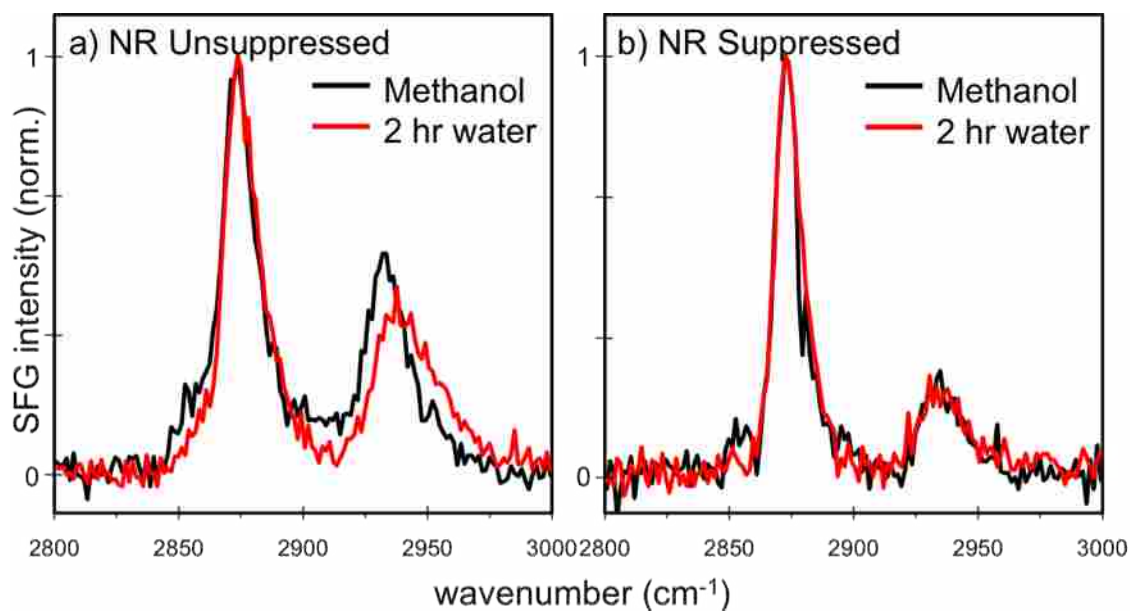
Figure 6-3. VR-SFG spectra of surface-bound octadecyltrichlorosilane (OTS) obtained with a) no suppression of the nonresonant signal and b) full suppression of the nonresonant signal. The sample was previously stored in methanol, then exposed to water for a period of 2 hrs. Apparent differences in the spectra after the change in solvent environment are not observed with suppression of the nonresonant signal.

purposes of this discussion, it is sufficient to state that so long as nonresonant signal is present, extreme caution must be exercised in interpreting VR-SFG spectra.

Applying the variable time-delay approach to surface-bound OTS on fused silica provides the spectra shown in Figure 6-4. The initial spectrum, which includes some degree of nonresonant signal, contains two prominent features. Note that both peaks exhibit derivative lineshapes, indicative of the nonresonant interference. When the nonresonant signal is fully suppressed, the peaks are generally much more symmetric. The peak at 2880 cm^{-1}, assigned as the methyl symmetric stretch, appears to shift slightly in the first time-delayed spectrum, but this is due to the nonresonant interference; even the small amount of nonresonant signal from fused silica is amplified by the cross-term in equation (2), giving the derivative lineshape. That peak maintains it shape and frequency position during the rest of the series, which is indicative of no interference from neighboring resonant features. This is contrary to what was recently reported for this system, based on computational modeling, where an additional peak was proposed.[30] The variable time-delay approach also reveals that the feature at about 2945 cm^{-1} is not, in fact, a single peak, but is made up of at least two contributions. These are assigned as the antisymmetric methylene stretch at 2920-2930 cm^{-1}, and a Fermi resonance between the methyl symmetric bend and symmetric stretch at 2945 cm^{-1}; the methyl antisymmetric stretch, expected at 2965 cm^{-1}, is very weak in this sample, presumably due to the orientation of the alkyl chains.[31]

Use of the variable time-delay technique allows for more definite assignment and interpretation of the spectra of the surface-bound OTS, but full quantification is made difficult by the presence of the Fermi resonance at 2945 cm^{-1}. Note that the relative intensity of this peak changes considerably with delay; it weakens much more than other modes with delay of the visible pulse. This likely happens because the Fermi resonance arises from two separate
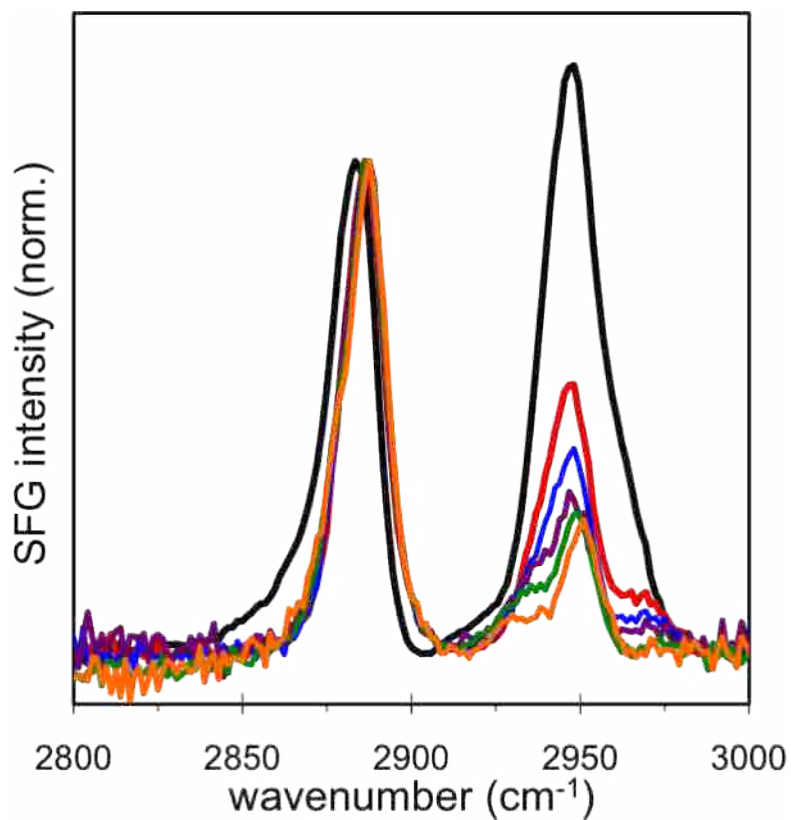
Figure 6-4. VR-SFG spectra of surface-bound OTS on fused silica with various delay times for the visible pulse. Delay times were: (Black) 0 ps; (Red) 1.86 ps; (Blue) 2.04 ps; (Purple) 2.20 ps; (Green) 2.40 ps; (Orange) 2.54 ps. All spectra normalized to the peak at 2880 cm^{-1}.

vibrational modes, a stretch and the overtone of a bend, and thus dephases much more quickly than the other individual modes; Fermi resonances have been shown to have shorter lifetimes than would be anticipated from the peak width.[32] The analytical approach we have developed assumes well-behaved Lorentzian profiles, thus further modification will be needed to better account for Fermi resonances. We can, however, identify Fermi resonances with this approach by their anomalous behavior, which has its own merit.

6.5.3. *Inclusion of Spectra with Nonresonant Signal*

The question naturally arises if more can be learned by including spectra with nonresonant signal in the simultaneous fitting approach that we have demonstrated here. In our previous report, we attempted to simultaneously fit multiple spectra with different degrees of nonresonant signal, but this was not successful.[6] Although nonresonant interference follows the same mathematical model of heterodyne detection, we lack the independent knowledge and control of the nonresonant signal that is present with the LO signal. Because the nonresonant signal is generated with the resonant signal, this creates additional interferences that affect the shape and relative phase of the nonresonant signal, and it is not known how to correct for these factors. Because it is not clear how the nonresonant signal should be modeled, or what constraints should be used, the spectra still cannot be analyzed uniquely. The broader question that still needs to be addressed is the physical origin of the nonresonant signal. While it is true that the nonresonant signal can tell us interesting things about the sample by measuring its relative strength, it must be fully suppressed in order to accurately determine the resonant parameters.

This method has been presented primarily in the context of overcoming spectral congestion, but the presence of nonresonant interference creates difficulties in the analysis of

even well-separated peaks. Nonresonant signal affects the apparent peak position, as seen for OTS (Figure 4), and its suppression distorts the spectrum, affecting line widths and relative amplitudes.[4,6] Note that the full variable time-delay approach is not always required. If all that is desired is a measurement of relative changes in the resonant signal, no additional work is needed beyond suppression of the nonresonant signal. The nonresonant signal should still be suppressed to be sure that the observed changes are in fact taking place in the resonant signal, as we have seen with OTS (Figure 3). However, for determining absolute parameters of the resonant spectrum, the distortions caused by apodization in the time-domain must be properly handled, which requires the full variable time-delay approach with full suppression of the nonresonant signal.

6.5.4.   General Considerations

The general use of this variable time-delay technique involves three experimental steps:

1.   Measure the time profile of the visible pulse.

2.   Determine the delay time required for full suppression of the nonresonant signal.

3.   Acquire multiple spectra at delay times beyond the point of full suppression.

The time profile of the visible pulse is readily determined by autocorrelation or cross-correlation. It is important that the temporal profile of the visible pulse be asymmetric, with a sharp leading edge. Thus, étalons are well suited for producing the spectrally narrow visible pulse.[13] The minimum delay time needed for full suppression of the nonresonant signal is given by the rise-time of the front of the asymmetric visible pulse, and the steepness of the rise will depend on how the narrow-band visible pulse is produced. Delaying past this time should remove most of the nonresonant signal, but this should be verified experimentally, particularly if the IR pulse is longer than this rise time.

The number of spectra and specific delay times that are required will vary depending on the sample. As the visible delay is increased, the spectrum may change in several ways. If the only change is a decrease in absolute intensity, then all peak widths are the same and fewer spectra are required. However, if changes in relative intensity are observed, then the vibrational modes have different lifetimes, requiring more spectra at different delay times. Another change that may be observed is the growth or disappearance of peaks, as was seen with polystyrene. This is an indicator of how many peaks must be present in the fit. Though we cannot mathematically prove this, it is reasonable to use the same number of spectra as there are resonant peaks. Using too few spectra does not ensure an accurate analysis. (An example of an incomplete analysis with too few spectra is shown in the Supporting Information.) The main consideration in collecting the experimental data is that the spectra must be different enough for the analysis to uniquely determine all of the parameters.

The number of peaks used in the fitting analysis is also critical. Use of too few peaks will never result in a good fit, however, there should be experimental verification for adding more fit functions to the analysis routine.[1] This verification may be achieved by acquiring additional spectra at different delay times and watching for the growth of new features. Additionally, if too many peaks are used, many of the parameters will be highly uncertain. In general, it is preferable to perform more experiments rather than make adjustments in post-processing or fitting.

6.6. CONCLUSIONS

We have demonstrated an experimental approach that overcomes both the problems of interference from the nonresonant SFG signal and spectral congestion in the resonant signal. This is done by acquiring multiple spectra at variable delays of the visible pulse relative to the IR pulse and simultaneously fitting all the spectra to determine the parameters of the resonant

spectrum. This approach has been demonstrated for polystyrene and surface-bound octadecyltrichlorosilane. In addition to providing accurate determinations of the position, linewidth, and relative amplitude of the resonant features, this approach also provides an improved determination of the number of fit functions that should be used in modeling the resonant spectrum. Another advantage of this technique is that it can be implemented in existing broadband VR-SFG systems with minimal modification and cost. This technique will supplement heterodyne detection and other phase-sensitive techniques.

Although this fitting method is more complicated and time-consuming than traditional fitting routines, once it has been performed, the information that is gained can be used for accurate analysis with simpler methods of analysis. With definitive peak positions, widths, and relative amplitudes, one can accurately observe and quantify observed spectral changes at a single time delay that fully suppresses the nonresonant signal. With accurate hyperpolarizabilities (which can be difficult to obtain[33,34]) absolute orientations can also be determined. Similar experimental data must be acquired for any new systems to be studied, but once a sufficient library is built with definitive parameters, there should no longer be any significant hindrance for using SFG spectroscopy as a general analytical tool.

Supporting Information Available: Additional discussion of how to determine the correct number of peaks to use in the fit function and the consequences of fitting with too few peaks. This material is available free of charge via the Internet at http://pubs.acs.org.

6.7. REFERENCES

(1) Meier, R. J. *Vibrational Spectroscopy* **2005**, *39*, 266-269.

(2) Briggman, K. A.; Stephenson, J. C.; Wallace, W. E.; Richter, L. J. *Journal of Physical Chemistry B* **2001**, *105*, 2785-2791.

(3) Gautam, K. S.; Schwab, A. D.; Dhinojwala, A.; Zhang, D.; Dougal, S. M.; Yeganeh, M. S. *Physical Review Letters* **2000**, *85*, 3854-3857.

(4) Curtis, A. D.; Reynolds, S. B.; Calchera, A. R.; Patterson, J. E. *Journal of Physical Chemistry Letters* **2010**, *1*, 2435-2439.

(5) Busson, B.; Tadjeddine, A. *Journal of Physical Chemistry C* **2009**, *113*, 21895-21902.

(6) Curtis, A. D.; Burt, S. R.; Calchera, A. R.; Patterson, J. E. *J. Phys. Chem. C* **2011**, *115*, 11550-11559.

(7) Bain, C. D. *Journal of the Chemical Society, Faraday Transactions* **1995**, *91*, 1281-1296.

(8) Yang, P.-K.; Huang, J. Y. *Journal of the Optical Society of America B* **1997**, *14*, 2443-2448.

(9) Yang, P.-K.; Huang, J. Y. *Journal of the Optical Society of America B* **2000**, *17*, 1216-1222.

(10) Sovago, M.; Vartiainen, E.; Bonn, M. *Journal of Physical Chemistry C* **2009**, *113*, 6100-6106.

(11) Press, W. H. *Numerical Recipes in C: the art of scientific computing*; Cambridge Unversity Press: Cambridge, U.K., 1988.

(12) Chen, X.; Hua, W.; Huang, Z.; Allen, H. C. *Journal of the American Chemical Society* **2010**, *132*, 11336-11342.

(13) Lagutchev, A.; Hambir, S. A.; Dlott, D. D. *Journal of Physical Chemistry C* **2007**, *111*, 13645-13647.

(14) Zhu, X. D.; Suhr, H.; Shen, Y. R. *Physical Review B: Condensed Matter* **1987**, *35*, 3047-3050.

(15) Laaser, J. E.; Xiong, W.; Zanni, M. T. *Journal of Physical Chemistry B* **2011**, *115*, 2536-2546.

(16) Van Der Ham, E. W. M.; Vrehen, Q. H. F.; Eliel, E. R. *Opt. Lett.* **1996**, *21*, 1448-1450.

(17) Richter, L. J.; Petralli-Mallow, T. P.; Stephenson, J. C. *Optics Letters* **1998**, *23*, 1594-1596.

(18) Ishibashi, T. a.; Onishi, H. *Chemical Physics Letters* **2001**, *346*, 413-418.

(19) Stiopkin, I. V.; Jayathilake, H. D.; Weeraman, C.; Benderskii, A. V. *Journal of Chemical Physics* **2010**, *132*, 234503/1-234503/9.

(20) Stiopkin, I. V.; Jayathilake, H. D.; Bordenyuk, A. N.; Benderskii, A. V. *Journal of the American Chemical Society* **2008**, *130*, 2271-2275.

(21) Ji, N.; Ostroverkhov, V.; Chen, C.-Y.; Shen, Y.-R. *Journal of the American Chemical Society* **2007**, *129*, 10056-10057.

(22) Liu, Y.; Wolf, L. K.; Messmer, M. C. *Langmuir* **2001**, *17*, 4329-4335.

(23) Zhang, D.; Dougal, S. M.; Yeganeh, M. S. *Langmuir* **2000**, *16*, 4528-4532.

(24) Wilson, P. T.; Richter, L. J.; Wallace, W. E.; Briggman, K. A.; Stephenson, J. C. *Chemical Physics Letters* **2002**, *363*, 161-168.

(25) Yang, C. S. C.; Wilson, P. T.; Richter, L. J. *Macromolecules* **2004**, *37*, 7742-7746.

(26) Pizzolatto, R. L.; Yang, Y. J.; Wolf, L. K.; Messmer, M. C. *Analytica Chimica Acta* **1999**, *397*, 81-92.

(27) Li, X.-Q.; Messmer, M. C. *Journal of Chromatogrophy A* **2003**, *984*, 19-28.

(28) Henry, M. C.; Wolf, L. K.; Messmer, M. C. *Journal of Physical Chemistry B* **2003**, *107*, 2765-2770.

(29) Quast, A. D. *Thesis - Investigating a Model Reversed-Phase Liquid Chromatography Stationary Phase with Vibrationally Resonant Sum Frequency Generation Spectroscopy*; Brigham Young University: Provo, UT, 2011.

(30) Nihonyanagi, S.; Eftekhari-Bafrooei, A.; Borguet, E. *Journal of Chemical Physics* **2011**, *134*, 084701/1-084701/7.

(31) Quast, A. D.; Wilde, N. C.; Matthew, S. S.; Maughan, S. T.; Castle, S. L.; Patterson, J. E. *Vibrational Spectroscopy* **2011**, **DOI:** 10.1016/j.vibspec.2012.03.003.

(32) Fendt, A.; Fischer, S. F.; Kaiser, W. *Chemical Physics* **1981**, *57*, 55-64.

(33) Bell, G. R.; Li, Z. X.; Bain, C. D.; Fischer, P.; Duffy, D. C. *Journal of Physical Chemistry B* **1998**, *102*, 9461-9472.

(34) Buck, M.; Himmelhaus, M. *Journal of Vacuum Science and Technology, A* **2001**, *19*, 2717-2736.

Determining the Correct Number of Spectra and Peaks for Variable Time-Delay Analysis

In our analysis, we ultimately used five spectra for determination of the five resonant peaks. Use of too few spectra does not yield the same results. This is demonstrated by attempting a simultaneous fit with only the first and last spectra in the set. In this case, we obtained a good fit with only 4 resonant peaks, as shown in Figure 6-S1 and Table 6-S1. Note that some of the amplitudes and widths obtained here (especially in the 3086 cm^{-1} peak) differ significantly from what is obtained from the five-peak fit reported in the main text.
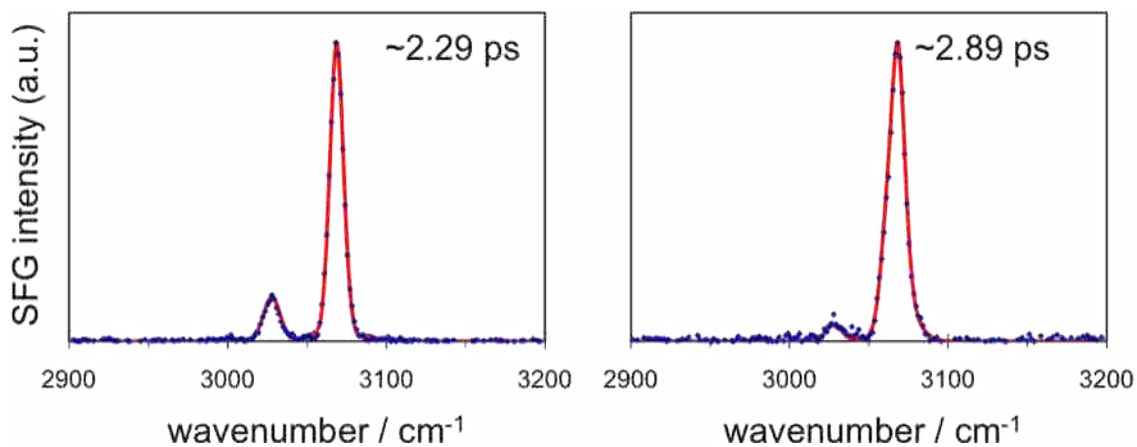
Figure 6-S1. Simultaneous fitting of only two spectra requires only four fit functions.

149

Table 6-S1. The parameters obtained from the simultaneous fit of the two spectra in Figure 6-S2.

ω_R	95% Confidence Interval	% uncertainty	A_R	95% Confidence Interval	% uncertainty	Γ_R	95% Confidence Interval	% uncertainty
3027.83	(3027.65, 3028.02)	0.006%	0.44	(0.39, 0.49)	12.2%	7.98	(7.64, 8.32)	4.24%
3057.70	(3057.60, 3057.79)	0.003%	0.09	(0.08, 0.10)	7.2%	3.40	(3.09, 3.71)	30.6%
3068.84	(3068.79, 3068.89)	0.002%	1.00	(fixed)	(fixed)	4.50	(4.36, 4.64)	3.03%
3086.15	(3085.77, 3086.53)	0.012%	−0.11	(−0.15, −0.07)	35%	7.89	(6.94, 8.83)	12.0%

Furthermore, it is possible to pick sets of five spectra that do not definitively show the small peak at 3045 cm^{-1} and obtain good fits with only 4 peaks. The additional peak is not really present in either of the two spectra shown in Figure 6-S1, though there are some data points that are easily passed off as noise where this peak should be. We know that it is not solely noise because we clearly see the 3045 cm^{-1} peak in other spectra before that time delay, as can be seen in the 2.54 and 2.71 ps delays shown in the main text. We also collected additional spectra that were not used in the fitting analysis due to greater uncertainty in the delay time (they were between the marks on our manual delay stage). Those spectra served as further verification of the number of peaks we used. Accurate simultaneous fitting necessitates incorporation of some of the spectra that more clearly show the additional peak. When choosing how many spectra and what time delays must be employed, the researcher must obtain enough spectra that are sufficiently different to properly identify all the features of the spectrum.

6.9. ADDITIONAL INFORMATION

The greatest difficulty to the methodology outlined in this chapter is obtaining the simultaneous fit to all data for two reasons. First, the number of acceptable fit solutions has greatly decreased, ideally down to only a single working solution. This complicates the fitting process because computers have no innate intelligence with which to reason. The computer is only provided with starting points, ranges to search within, and a given number of iterations before it gives up and provides whatever the minimum error it found happened to be within those iterations. This process requires much closer initial guesses to the absolute minimum to aid the computer into finding the single solution as opposed to the significantly easier task of providing arbitrary parameters to guide into one of the many local minima that exist when working with multiple solutions from underdetermined systems.

Second, the Fourier Transform process is very sensitive to noise, so fitting should not transform the raw data. This is overcome by only subjecting the theoretical fit, which contains no noise, to the Fourier Transform process. In the routine used, as will be shown in Appendix 2, the data is imported into the program and interpolated for the theoretical fit because Fourier transforms require evenly spaced points, but our raw data does not contain evenly spaced points. The theoretical fit contains the initial guesses in the frequency domain that are transformed to the time domain, apodized by the various overlaps with the visible pulse in time, and transformed back into the frequency domain to compare the multiple apodized spectra from the experimental data before reiterating. In this way, Fourier artifacts cannot occur, maintaining accuracy of analysis.

CHAPTER 7:   IMPROVED MODE ASSIGNMENTS FOR POLYSTYRENE

IN VIBRATIONAL SUM-FREQUENCY GENERATION SPECTRA*

7.1. ABSTRACT

The assignment of the aromatic C-H stretching modes observed in the vibrationally-resonant sum frequency generation (VR-SFG) spectra of polystyrene surfaces has been difficult due to two fundamental aspects of the technique. First, not all modes observed in bulk spectroscopic techniques, such as IR and Raman, are necessarily present in VR-SFG spectra. Second, VR-SFG can detect responses from molecules in multiple environments. In addition to thin films of polystyrene, we have collected VR-SFG spectra of dimethylphenyl silane, layered polystyrene and poly(methyl methacrylate) (PMMA), and plasma-treated polystyrene to aid our mode assignments. Based on these experimental data, we have determined that not all the expected modes are present in the VR-SFG spectrum of polystyrene. We have also found that one particular mode, the ν_2 symmetric stretch, accounts for two of the observed peaks because of a VR-SFG signal that is generated from a subsurface layer within the polymer thin film. After properly reconciling theory and experiment, the mode assignments are simplified and map well from bulk spectroscopies. With these experimentally validated mode assignments, VR-SFG spectra in the aromatic C-H stretching region can be interpreted more reliably.

7.2. INTRODUCTION

One of the more powerful applications of vibrationally resonant sum-frequency generation (VR-SFG) is the ability to determine the orientation of molecules at surfaces and interfaces. As the orientation changes, so do the relative intensities of the peaks in VR-SFG

spectra. Such an analysis presupposes that the mode assignments are correct; to the extent that the vibrational mode assignments are inaccurate, the results of any orientation analysis are compromised. Unfortunately, because the surface is a different environment than the bulk, the mode assignments of molecules do not necessarily map directly from Raman or infrared spectroscopy to VR-SFG spectra. In this paper, we report a comprehensive determination of the assignments for the aromatic C-H stretching modes of polystyrene as observed in VR-SFG spectra. Perhaps the most striking result of our analysis is that one of the peaks is due to phenyl groups in a sub-surface layer with bulk density and does not arise from molecules at the free surface.

The structure of polystyrene and a typical VR-SFG spectrum of a polystyrene thin film are shown in Figure 7-1a. (This spectrum was acquired with suppression of the nonresonant SFG contribution, as discussed further below.) Figure 7-1b shows an ATR-IR spectrum of the same polystyrene thin films. The VR-SFG spectrum clearly has two strong features, the strongest occurring at ~3069 cm^{-1} with a weaker peak at ~3027 cm^{-1}. There are also small shoulder peaks on either side of the 3069 cm^{-1} feature. The ATR-IR spectrum is dominated by a peak at ~3025 cm^{-1} with a noticeable peak at about 3060 cm^{-1}. Also shown in Figure 7-1 are the five normal vibrational modes for monosubstituted phenyl rings, traditionally labeled ν_2, ν_{7a}, ν_{7b}, ν_{20a}, and ν_{20b}.[1] The challenge is to assign these individual modes to the features in the VR-SFG spectrum.

Table 7-1 summarizes prior mode assignments of the aromatic C-H stretch modes for VR-SFG spectra of polystyrene thin films, and it is readily seen that there are significant differences in these assignments. Also included are the generally accepted assignments from FTIR and Raman measurements. Gautam et al.[2] were the first to investigate the molecular surface structure
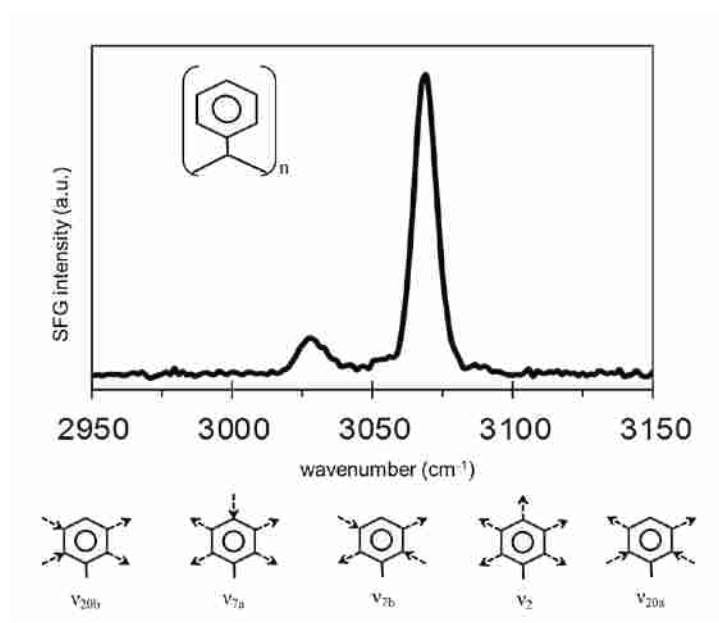
Figure 7- 1. Typical VR-SFG spectrum of polystyrene with the structure of the monomer. Below are the motions characteristic of the C-H stretch modes for a monosubstituted phenyl ring.

Table 7-1. Summary of prior PS mode assignments.

Mode	Bulk Studies[1,3]	Gautam et al.[2]	Briggman et al.[3]	Zhang et al.[5]
		Vibrational Frequency / cm^{-1}		
ν_{20b}	3027 (IR)	3027	3078.2	unassigned
ν_{7a}	3034 (Raman)	3038	3035	3053
ν_{7b}	3050 (Raman)	3058	3054.5	3027
ν_2	3060 (IR & Raman)	3069	3066.7	3068
ν_{20a}	3083 (IR)	3082	3024.2	unassigned

of native polystyrene with VR-SFG spectroscopy and assigned five modes in the aromatic C-H stretching region. The strongest peak was assigned as ν_2, the fully symmetric stretching motion. This mode is the only one that appears in both Raman and IR spectra, and as the nonlinear susceptibility includes a product of IR and Raman susceptibilities, the ν_2 mode is expected to be the strongest in the VR-SFG spectrum. This assignment does require a 9 cm^{-1} shift from the bulk frequency; however, this is reasonable considering the different environment at the surface relative to the bulk. We infer that the remaining features were assigned in the same order as they are observed in IR and Raman spectra. This model results in excellent agreement for the ν_{20b}, ν_{7a}, and ν_{20a} modes between the VR-SFG spectral assignments and the IR and Raman data, but there is an unexplained 8 cm^{-1} shift for the ν_{7b} mode. Such a shift is still less than what is determined for ν_2, and therefore can be easily overlooked.

Shortly after this study, Briggman et al.[3] reported a somewhat different molecular structure of the polystyrene surface as determined from VR-SFG spectroscopy; they also reported different mode assignments. These assignments were based on the calculated IR spectrum, which, as they claimed at the time, did not agree with the frequency ordering previously provided by Varsanyi.[1] They appear to have made the same assumption that all peaks are present and maintain the same frequency ordering as observed in IR spectra, but with a switch of the ν_{20a} and ν_{20b} modes as well as the ν_{7a} and ν_{7b} assignments. (It should be noted, however, that in a later publication from this group[4] they reverted back to the more conventional ordering.) They also included two additional modes in their fitting analysis that they labeled as combination bands, presumably because they had observed two additional peaks in their IR spectra. These combination bands are not included in Table 7-1 because they are unique to this study.

Previous to either publication on the structure of the native polystyrene surface, Zhang et al.[5] employed another set of mode assignments during studies of the response of polystyrene to plasma treatment. Their paper did not comment on the assignments of all 5 modes, but what they did explicitly state is included in Table 7-1. These assignments do not have the same frequency ordering as observed in IR and Raman spectra, but were based on the results of curve fitting with the theoretical requirement shown by Duffy et al.[6] that the ν_{7b} mode should be opposite in phase from the ν_2 mode. Although this requirement was determined for a di-substituted phenyl ring, it is based on symmetry arguments that do not change for the monosubstituted phenyl rings of polystyrene. Because they fit the 3027 cm^{-1} peak as a negative peak, they argued for the location of the ν_{7b} mode at that frequency. In the other two assignments, the ν_{7b} mode was assigned to the 3058 cm^{-1} peak, which had a positive amplitude and therefore does not satisfy this phase requirement.

Given the discrepancy in the mode assignments of polystyrene surface spectra, it is clear that this issue needs to be revisited. The mapping of mode assignments from linear spectroscopic techniques to VR-SFG spectra is complicated for two reasons. First, the surface or interface is typically a very different environment from the bulk, which can cause frequency shifts from what is observed in IR or Raman spectroscopy, both of which probe the bulk. Second, because the SFG signal involves both IR and Raman processes, if either the IR transition dipole moment or the change in Raman polarizability is zero, that mode cannot be seen in a VR-SFG spectrum. Thus, when assigning modes in VR-SFG spectra, these aspects of the technique may preclude the use of literature precedent and can frustrate what would otherwise be a straightforward process. Standard curve-fitting approaches for congested spectra can often be misleading because multiple solutions exist that appear to fit the data equally well.[7]

These problems are exacerbated by the presence of the nonresonant signal.[8] Given our recent work on the complexity of the nonresonant signal, and the distortions it causes,[9] it is not surprising that the previous mode assignments need to be re-evaluated; the various measurements cited above all included different amounts of nonresonant signal, and nonresonant interference irreparably distorts the desired resonant response. These factors severely limit our ability to use curve-fitting to determine the frequencies of the vibrational modes and can additionally complicate the determination of which modes are present or absent. The choice of how many peaks to use is an input parameter for the analysis; therefore the curve-fitting results will always match the proposed model. The curve-fitting model must be validated by direct experimental evidence. Furthermore, the relative phases of peaks in VR-SFG spectra are often arbitrary without additional experimental constraints, such as phase-sensitive detection[10–13] or an approach such as the variable time-delay method.[14]

To illustrate these problems, we now consider the spectral feature near 3035 cm^{-1}. In all the VR-SFG spectra of polystyrene with a peak around 3035 cm^{-1}, that peak was fit with a negative amplitude. A peak in that area has never been experimentally resolved, and its existence has been inferred solely from the fitting models. As we have previously shown, removing the nonresonant signal and acquiring spectra at differing temporal overlaps of the upconverting visible pulse provides additional experimental verification of how many peaks are actually present. Even with this approach, no peak at ~3035 cm^{-1} is observed.[9,14] Fitting the dip in the nonresonant signal as a negative peak appears to be an inaccurate model of the spectroscopic response. The absence of this peak in VR-SFG spectra is consistent with its lack of IR activity, as shown in the study by Briggman et al.,[3] and confirmed by our own ATR-IR experiments, and

indicates that a direct mapping of both IR and Raman assignments to VR-SFG spectra is not always valid.

In fact, the absence of the 3035 cm^{-1} peak is not surprising, given the lack of an experimentally observed peak in IR spectra. The selection rules of VR-SFG require that modes be both IR- and Raman-active, but this can lead to apparent contradictions between experimental and theoretical considerations. In IR and Raman experiments, as previously shown by Briggman et al.,[3] the only aromatic peak that exhibits a response in both techniques is the peak around 3060 cm^{-1}, assigned to ν_2. Thus, only the ν_2 mode should be present in VR-SFG spectra, yet there are at least 4 observable aromatic peaks in the VR-SFG spectrum of polystyrene. Assuming local C_{2v} symmetry of the phenyl groups, all the C-H stretch modes should be both IR- and Raman-active, but they are not all observed in either technique or in VR-SFG, again leading to an apparent contradiction. The VR-SFG spectrum of polystyrene has too many peaks, based on experimental predictions from IR and Raman spectra, and too few, based on a theoretical symmetry analysis. Additional considerations and direct experimental data are necessary to identify the vibrational modes that are present at the surface.

The uncertainty in the available mode assignments of polystyrene surface spectra has caused us to re-evaluate them based on additional experimental data, complemented by density functional theory calculations. In our investigations of polystyrene with VR-SFG, we have applied additional experimental constraints, including suppression of the nonresonant signal,[15] acquisition of multiple spectra with variable delay times between the visible and IR pulses,[14] investigation of phenylsilane monolayers, and modification of the polystyrene surface with plasma treatment. We have found that our experimental observations cannot be reconciled to any of the previous mode assignments. We attribute the confusion in the previous assignments to two

main factors. The first is an over-reliance on curve fitting to extract information from the congested spectra of polystyrene. The second factor addresses a more general problem of VR-SFG that is often overlooked; the probing depth of the technique is not always known, but it is generally assumed that signal only arises from the free surface and/or buried interface. Our results raise new possibilities for what can be probed with VR-SFG by showing that this assumption is not always valid.

7.3. EXPERIMENTAL METHODS

7.3.1. *VR-SFG Spectroscopy System and Sample Preparation*

The details of our VR-SFG system have been described previously.[16] In short, a portion of the output of a femtosecond laser (Quantronix Integra-C) pumps a broadband OPA (Light Conversion via Quantronix TOPAS-C) to produce femtosecond IR pulses. The remaining visible light is frequency-narrowed by two étalons to produce time-asymmetric Lorentzian pulses with approximately 2.5 cm^{-1} HWHM bandwidth. Nonresonant signal was suppressed with the technique developed by Lagutchev et al.[15] whereby the visible pulse is delayed relative to the IR probe pulse. All spectra were acquired with *s*-polarized SFG, *s*-polarized visible and *p*-polarized IR. The *ssp* combination is chosen because it produces sufficiently strong signal while probing only a single element of $\chi^{(2)}$. (Additional justification for only using *ssp* spectra is given in the Results and Discussion section.)

The variable time-delay technique[14] is used to identify the number of peaks and their positions. The different delay times of the visible pulse provide spectra with varying levels of interference that allow for a more conclusive determination of which peaks are present or absent. Because the phenyl rings of polystyrene generate a highly congested spectrum, this technique also allows more definitive constraints to be applied in a fitting analysis because all peak

parameters can be fully constrained, including amplitudes that must remain unconstrained using other data collection methods. These constraints arise because the optical fields remain constant without significantly impacting the signal-to-noise level; therefore, the underlying resonant parameters remain constant for all the different spectra collected as the visible upconverting pulse is delayed in time.

7.3.2. *Sample Preparation*

Polystyrene samples were prepared following the procedures of Reference 16. Briefly, polystyrene (average molecular weight 230,000 g mol^{-1}) was spin-cast from toluene solution (2% by weight). We used approximately 100 nm thick polystyrene films to take advantage of constructive interference of the transmitted and reflected surface signals, as described previously.[9] The spin-cast films were not annealed prior to characterization. As we have previously shown, annealing does not change the shape of the resonant spectrum, although overall amplitude decreases slightly, but annealing does significantly increase the amplitude of the nonresonant signal.[16]

The layered samples involved the same coating procedure on a stainless steel substrate. Stainless steel was chosen because the resulting spectra on that substrate provided the highest signal-to-noise level for the layered samples. The layered samples included an additional layer of approximately 150 nm of PMMA on top of polystyrene. PMMA was dissolved in nitromethane, which does not measurably dissolve the polystyrene film, and spin-cast onto the polystyrene-coated substrates. The plasma-treated samples were exposed for approximately 1s at 18 W inside a PDC-32G radio frequency plasma cleaner from Harrick Plasma.

Phenylsilane samples were prepared with chloro(dimethyl)phenylsilane (98% from Sigma-Aldrich) on silicon substrates with a 100 nm thermal oxide layer, based on literature protocols.[17]

We have previously prepared phenylsilane samples on various oxide thicknesses, but due to constructive thin film interference, the signal-to-noise is highest with a 100 nm oxide film. Similar results can also be obtained by attaching phenylsilane to fused silica substrates. Samples were prepared by rinsing silicon substrates with solvents (HPLC grade) in the following order: acetone, CH_2Cl_2, $CHCl_3$, acetone, H_2O (18 M Ω), $CHCl_3$. Rinsed samples were then immersed in 100°C piranha solution for 1 hour, rinsed with H_2O and then sonicated in $CHCl_3$ for approximately 10 minutes. (*Caution*: Piranha solution, 3:1 concentrated H_2SO_4:30% H_2O_2 is extremely corrosive and must be handled with extreme care. Avoid contact with all organic compounds.) The silicon was then rinsed with H_2O and the surface was hydrolyzed by dipping in 90°C NaOH (50%) for approximately 10 seconds, rinsed with H_2O, followed by dipping in HNO_3. The samples were then rinsed with H_2O and dried with a stream of nitrogen. A drop of phenylsilane was applied to the dried surface, and another silicon substrate that had been through the same cleaning process was placed on top. The substrate sandwich was placed on a hot plate preheated to 50°C for 10-15 minutes, after which the samples were removed, given another round of solvent rinses as described above, sonicated in $CHCl_3$ for 10 minutes, received another solvent rinsing cycle followed by a rinse with H_2O, and then dried off with a stream of nitrogen.

7.3.3. *Computational Methods*

We have also performed theoretical calculations of the vibrational modes of the phenyl rings of polystyrene using DFT with the B3LYP functional and 6-311G basis set; all calculations were performed using the NWChem 6.0 software package.[18] Small oligomers of polystyrene, trimer and pentamer, were modeled. The vibrational frequencies that are reported are for the phenyl ring in the middle of the oligomer. We also modeled a toluene molecule for direct comparison to previous calculations.[1,19] No significant variation in the calculated frequencies or

amplitudes between toluene and either of the oligomers was seen, showing that a direct comparison between them is valid.

7.4. RESULTS AND DISCUSSION

The VR-SFG spectrum of polystyrene, shown in Figure 7-1a, contains two dominant features: a peak at ~3027 cm^{-1} and a strong feature centered around 3069 cm^{-1}. As we have previously shown, there are in fact five discernible peaks in the VR-SFG spectrum. The weakest of these is only seen in variable time-delay experiments at long delay times. It is tempting to simply assign the observed peaks to the five expected modes; however, these assignments must be verified before such an approach is applied. We now consider each assignment, and each observed peak in the spectrum, in turn.

7.4.1. Assignment of v_2

The first mode we consider in the VR-SFG spectrum of polystyrene is the v_2 mode, the fully symmetric stretch. This mode should have the greatest intensity due to its high activity in both IR and Raman spectra. Based on prior assignments, it also appears to experience the largest shift relative to the bulk spectra. In particular, there is considerable variability in the reported frequency for this mode at buried interfaces; reported frequencies range from 3053 to 3069 cm^{-1}.[2,20–22] Unfortunately, no consistent justification for these shifts has been put forward.

Ringwald and Pemberton[23] showed that the v_2 mode of benzene and toluene shifts with packing density. Specifically, higher packing densities caused shifts to ~2 cm^{-1} lower than what is typically observed in bulk samples, whereas a decrease in the packing density resulted in shifts to higher energy by up to 13 cm^{-1}. At the surface of polystyrene, the density of packing for the phenyl rings is less than in the bulk, which is consistent with the 9 cm^{-1} shift to higher energy. Thus, we concur with the assignment of the dominant peak at 3069 cm^{-1} as v_2.

However, one consideration that must be made in assigning modes in VR-SFG spectra is that signal can be generated from all areas of broken symmetry, not just the topmost surface layer or the buried interface layer. As previously shown, polystyrene does not natively order at the buried interface,[16] showing that the duplicate peak present in the spectra of unperturbed polystyrene cannot result from interference with the buried interface. Even at depths of a few molecular thicknesses, there may be some anisotropy that occurs before reaching an isotropic bulk, but these molecules are now packed with higher density. We therefore propose that the peak around 3058 cm^{-1} is actually a duplicate ν_2 mode, but originating from a separate, more densely packed environment. The VR-SFG spectrum of polystyrene is dominated by the surface species, but the strong intensity of this mode allows us to detect a response from more densely packed phenyl rings in subsurface regions where complete cancellation in the isotropic bulk has not yet been achieved.

Further evidence for the existence of two separate ν_2 modes was obtained by comparing spectra of polystyrene with those of phenylsilane monolayers and polymer bilayers, and by observing the effects of plasma treatment on the polystyrene surface. These results are summarized in Figure 7-2. For dimethylphenylsilane, the ν_2 mode is also readily identified as the strongest peak, but it occurs around 3058 cm^{-1}, close to the frequency for bulk polystyrene. We expect that the phenyl rings for the monolayer are packed more tightly than on the surface of polystyrene because of additional hindrance from connection to the rest of the polymer, and this result is consistent with that model.

Investigation of a multilayered sample involving polystyrene also indicates that the 3058 cm^{-1} peak belongs to the ν_2 mode. As seen in Figure 7-2b, when looking at layered samples of polystyrene underneath PMMA, there is only one observable peak at approximately 3058 cm^{-1}.
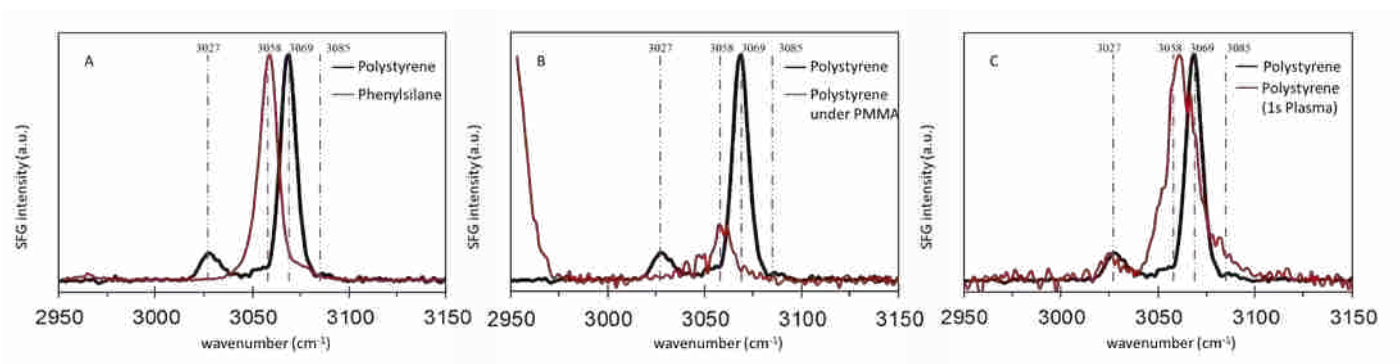
Figure 7-2. a) VR-SFG spectra (*ssp* polarization combination) of polystyrene and dimethylphenylsilane. The predominant mode in both cases is v_2 with the shift from 3069 to ~3060 cm^{-1} caused by the different local density of the phenyl groups. b) VR-SFG spectra (*ssp*) of both free and buried polystyrene. The v_2 mode in the buried polystyrene is again at lower energy, reflecting the higher local density. The large peak centered below 2950 cm^{-1} is due to PMMA. c) VR-SFG spectra (*ssp*) of polystyrene before and after plasma treatment. Following plasma treatment, a strong peak is observed at 3058 cm^{-1}, again indicative of higher local density. In all three cases, a small peak is seen in the unperturbed polystyrene at this location.

Based on the same arguments used to identify the ν_2 mode at the surface, this feature is assigned ν_2; it is the strongest feature in the spectrum. The buried polystyrene is in a denser environment; therefore the frequency has shifted relative to what is observed at the free surface. No peak is observed at 3069 cm^{-1} because this sample has no exposed polystyrene surface.

The appearance of a duplicate ν_2 mode is also confirmed by exposing polystyrene surfaces on silicon substrates to low-temperature plasma. Plasma treatment is commonly employed for surface modification and destroys the topmost surface layers. After plasma treatment, the intensity of the 3069 cm^{-1} peak decreases, but treatment also induces an order in previously isotropic bulk material, causing the much smaller peak around 3058 cm^{-1} to increase in intensity, shown in Figure 7-2c. We acknowledge that these results contradict what has been previously claimed with plasma treatment,[5,24] however, previous studies used fused silica substrates instead of the silicon we have used here. More details about the effects of plasma treatment, including the role of the substrate material, are presented in a separate manuscript.[25] For purposes of this discussion, the results of the previous two experiments confirm the proposal that we do, in fact, observe a duplication of the ν_2 mode in the VR-SFG spectrum of polystyrene arising from two different environments.

7.4.2.   Assignment of ν_{20b}

With the discovery of the duplicate ν_2 mode, three additional peaks remain in the spectrum that must be assigned. However, there are still four candidates: ν_{7a}, ν_{7b}, ν_{20a} and ν_{20b}. As we will show, for the phenyl rings of polystyrene, the strongest modes that are typically observed in VR-SFG spectra are those that are observed in IR spectra. The strongest mode seen in the IR spectrum of polystyrene occurs at 3027 cm^{-1}. Considering the previous assignments of Varsanyi, coupled with our DFT calculations (shown in Table 7-2) for Raman, IR, and relative

hyperpolarizability (which can be estimated by the product of IR and Raman intensities), this allows the 3027 cm^{-1} peak to be assigned as ν_{20b}. This statement maintains the assignment from IR spectra and is consistent with Gautam[2] and the revised Briggman[4] assignments.
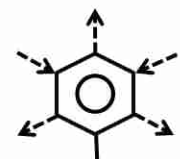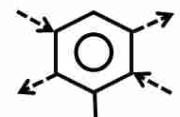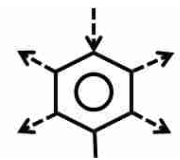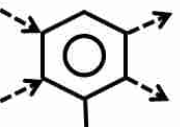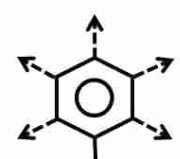
7.4.3. *Considerations in Assigning the Remaining Modes*

We have assigned three of the features in the VR-SFG spectrum of polystyrene, but we have only used two of the five candidate vibrational modes. We must now assign the last two spectral features to the three remaining candidates and determine which of these candidates is not observed in the VR-SFG spectrum. Before making these assignments, we will briefly reconsider some of the aspects of the current IR and Raman assignments.

As previously stated, if we consider the IR and Raman spectra, we should only observe the ν_2 peaks at 3069 and 3058 cm^{-1}; the ν_2 mode is the only one that is strong in both IR and Raman spectra. However, a symmetry analysis assuming a local C_{2v} point group for the phenyl rings of polystyrene indicates that all modes are both IR- and Raman-active. This suggests we should see all four remaining modes, giving six observable peaks. This discrepancy between theoretical predictions and experimental observation leads us to further evaluate the requirement that all modes be both IR- and Raman-active. While this requirement is strictly true, its predictive power is somewhat limited by the actual IR and Raman susceptibilities, which are not always known.

For an idealized case, if either the IR or Raman activity is zero, then the product of the two is zero, causing an absence of the feature in the VR-SFG spectrum. In reality, however, susceptibility is rarely identically zero, but rather so small that the response is undetectable. Symmetry considerations can be used to argue for zero susceptibility, but the simple classification of point groups is only valid under very strict conditions, including the harmonic approximation for the vibrations and the dipole limit for the light. In addition, it only holds

Table 7-2. DFT Calculations for the phenyl modes

mode	stretch	Frequency (cm^{-1})	IR Intensity (a.u.)	Raman Intensity (a.u.)	Hyperpolarizability product
ν_{20a}		3153	9.60	10.33	99.17
ν_{7b}		3157	0.91	93.98	85.52
ν_{7a}		3169	17.47	89.55	1564.44
ν_{20b}		3177	56.38	41.23	2324.55
ν_2		3193	31.40	287.27	9020.28

completely true in the case of isolated molecules and may not reflect what is actually observed in experiment, especially in solids.[26] The non-isolated nature of the phenyl groups in the polymer chains can greatly compromise a theoretical determination of IR or Raman activity by point group approximations; the point group is strictly C_s, though as we will show, the C_{2v} assumption still works for many practical applications. On the other hand, a mode may have a nonzero susceptibility but still not be observed experimentally in either IR or Raman spectroscopy simply because it is extremely weak. Such a weak mode may not be seen in VR-SFG either.

Because VR-SFG is sensitive to the product of the IR and Raman susceptibilities, the stronger susceptibility can amplify the weaker response, allowing modes to be observed in VR-SFG spectra that are not observed in either the IR or Raman spectrum. When the absolute magnitude of the IR dipole moment is much greater than the associated Raman polarizability (which may appear to be zero), this mode can be weakened by the Raman activity, but maintain sufficient susceptibility to be detectable with VR-SFG. However, if the magnitude of an insufficiently strong Raman polarizability (that is still detectable in Raman experiments) is coupled with an even weaker IR dipole moment, the VR-SFG susceptibility will become too weak for that mode to be detected; the susceptibility in this case is effectively zero.

Because of the difficulties involved in predicting true VR-SFG susceptibilities, mode assignments are best determined through direct experimental observation with the aid of theoretical models rather than relying on curve-fitting alone. Identifying unresolved peaks through fitting procedures often does not provide physically meaningful information for two reasons. First, the lack of a sufficient number of constraints results in non-unique solutions that have little to no physical meaning.[7] Second, the model might include additional peaks that are predicted theoretically but may not be present in reality. Inclusion of spurious peaks not only

corrupts the determination of the true peak parameters, but also creates difficulties in making mode assignments. This can be seen in the previous assignments of the 3035 cm^{-1} peak, the inclusion of combination bands, and the assignment of ν_{7b} to the peak at 3058 cm^{-1}, which we have now shown to be a duplicate of ν_2.

DFT calculations can aid in making mode assignments, but they also have their limitations; we cannot expect accuracy better than a few percent. Because the absolute frequencies of the vibrational modes are around 3000 cm^{-1}, this means the uncertainty in frequency is on the order of 30-60 cm^{-1}. Unfortunately, all the modes in question are within about 60 cm^{-1} of each other. For this reason, we do not rely on absolute frequencies to assign the remaining modes. Instead, we focus on the intensity calculations because they provide a larger range of values with which to make these discriminations.

One other factor that needs to be discussed at this point is the use of multiple polarization combinations. Our analysis has been based on VR-SFG spectra acquired in the *ssp* polarization combination, *s*-polarized VR-SFG output, *s*-polarized visible probe, and *p*-polarized IR probe. Although *sps* and/or *ppp* spectra are commonly included in this type of study, the *sps* and *ppp* spectra do not provide any additional information in this case. This is in part because the *sps* signal is significantly weaker than *ssp,* causing very poor signal to noise. The *ppp* spectrum is problematic because that polarization combination probes all the non-zero elements of $\chi^{(2)}$ and includes redundancies with both *ssp* and *sps*. Furthermore, after removal of the interfering nonresonant signal, *ppp* spectra look very similar to *ssp* spectra with no additional discernible peaks. (More details on this issue are available in the Supporting Information.) In experiments using the *sps* combination for polystyrene, there are typically no resolvable features outside of the nonresonant response. However, in the previous study by Zhang et al.[5] one peak was

definitively resolvable from the nonresonant interference, but it was the peak at 3027 cm^{-1}, which we have already assigned to ν_{20b} and their data are consistent with our assignment.

This inability to use additional polarization combinations is not a serious issue, however, because of the symmetry of the system in question. Assuming local C_{2v} symmetry for the phenyl groups, all vibrational modes are either of A_1 or B_1 symmetry. The IR transition dipole moment vectors for A_1 and B_1 modes are orthogonal, and this allows for determination of tilt angle with Equation 1.

$$R = \left| \frac{A_{B1}}{A_{A1}} \right| = \left| \left(\frac{\beta_{caa,B1}}{\beta_{aac,A1}} \right) \left(\frac{2(<\cos 3\theta> - <\cos \theta>)}{(7+2r)<\cos \theta> + (1-2r)<\cos 3\theta>} \right) \right| \qquad (1)$$

In this equation, A_{A1} and A_{B1} represent the amplitudes of the peaks corresponding to modes of A_1 and B_1 symmetry, respectively. $\beta_{aac,A1}$ and $\beta_{caa,B1}$ represent the respective hyperpolarizabilities of the same two modes, and r is the ratio of β_{ccc}/β_{aac} for the A_1 mode. In actual fact, we already have sufficient information to investigate tilt angles because the ν_2 mode is of A_1 symmetry and ν_{20b} is of B_1 symmetry. In addition, ν_2 and ν_{20b} are the most prominent features in the spectrum, so it is not necessary to use the other modes. For the sake of completeness, however, we now propose assignments for the remaining features in the VR-SFG spectrum of polystyrene.

7.4.4.   Assignment of ν_{7a}, ν_{7b} and ν_{20a}

Thus far, we have assigned three of the features of the VR-SFG spectrum of polystyrene, but we have only utilized two of the five normal mode candidates. The remaining features are much weaker, and will therefore be more difficult to assign. Because the selection rules of VR-SFG require IR and Raman activity, it is useful to review what is seen with those techniques. The only mode common to both is ν_2, which we have assigned to two features because of the different environments at and just below the surface. The other two modes assigned in IR spectra

are ν_{20b}, already assigned at 3027 cm^{-1}, and ν_{20a}. The two remaining modes assigned in Raman spectra are ν_{7a} and ν_{7b}. With three candidates, but only two features remaining, it appears that one of these modes is simply not observed in the VR-SFG of polystyrene. Further evidence suggesting the actual absence of one of the modes can be seen in previous studies for monosubstituted benzene compounds using both IR and Raman techniques. As discussed by Varsanyi,[1] neither of the two ν_7 modes are observed with either technique, so it is not surprising that not all 5 modes are seen with VR-SFG.

Our results suggest that the VR-SFG signal for polystyrene is primarily dominated by the IR activity once modes with strong IR and Raman activity have been accounted for. In previous assignments, the remaining IR peak around 3083 cm^{-1} was assigned to ν_{20a};[1,2] however, our DFT calculations for both the IR intensity and relative hyperpolarizability do not agree with such an assignment. Rather, according to our DFT calculations, the remaining peak at 3085 cm^{-1} should be assigned to ν_{7a} as it possesses a significantly stronger hyperpolarizability than the remaining two modes, ν_{7b} and ν_{20a}. This assignment does conflict with prior determinations, but it is justified by our data. We now have two candidates, ν_{7b} and ν_{20a}, for the remaining feature at ~3045 cm^{-1} that is only resolvable (see Figure 7-3) after selectively upconverting later portions of the vibrational free-induction decay.[14]

We have already discussed the absence of the 3035 cm^{-1} peak that is normally associated with ν_{7b}, which may indicate that this Raman-active mode is VR-SFG inactive. The peak we observe at ~3045 cm^{-1} likely corresponds to the Raman peak at 3050 cm^{-1}. However, the choice of which vibrational mode belongs to the observed peak and which mode is completely absent is not clear. Briggman et al.[3] explicitly stated that they reversed the assignments of ν_{7a} and ν_{7b}, and the assignments of Gautam et al.[2] implicitly show the same reversal. If the modes are in the order
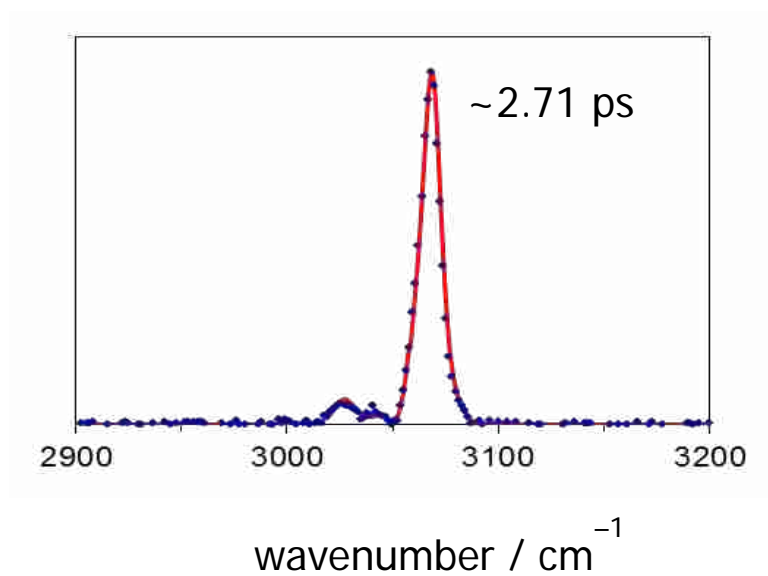
Figure 7-3. As latter portions of the vibrational response are selectively sampled, peak interferences are altered to more definitively resolve which peaks are present. After an approximately 2.71 ps delay with our system, a fifth peak in polystyrene is definitively resolvable as the interference from the other peaks is diminished. The data points are shown in blue, and the red line is the fit to the data that was performed simultaneously with the full set of five spectra of differing delays in our previous publication. Reproduced from Reference 14.

of both Gautam and Briggman, the ν_{7a} mode should be absent, but if the reversal of modes applied is inaccurate, the ν_{7b} mode is absent. Additionally, considering the susceptibility arguments provided by our DFT calculations, the ν_{7a} mode should belong to the peak at 3085 cm^{-1}, with the remaining peak assigned to either ν_{7b} or ν_{20a}.

Based on symmetry arguments, the *sps* spectrum should be able to aid in making this assignment, but as we have previously discussed, it does not. This polarization should be more sensitive to a mode of B_1 symmetry, which would be ν_{7b}. If the peak were definitively present it may suggest that it belongs to ν_{7b}; if the peak were definitively absent in the *sps* spectrum, it could be concluded that the mode is ν_{20a}, but it is difficult to prove the presence or absence of that spectral feature with the signal-to-noise levels that have been published. The 3045 cm^{-1} peak in *sps* spectra has not been observable, but that may be due in part to the overall weaker response provided by that polarization combination. The negligible *sps* response is further confirmed by the similarity of our *ppp* data to our *ssp* data (see Supporting Information). Because the response in *sps* polarization is so weak, it is difficult to tell whether the 3045 cm^{-1} peak is absent or just undetectable.

With the tools currently available, it is not possible to unambiguously determine which vibrational mode should be assigned to the small peak around 3045 cm^{-1}. The DFT calculations report relative hyperpolarizabilities and frequencies that are nearly identical for both candidate modes. It is possible that this remaining peak is an overlap of both the ν_{7b} and ν_{20a} modes. Considering the extremely weak response of both modes in VR-SFG, it may be the overlap of both responses that makes this peak detectable at all. However, if this peak is due to two overlapping modes, they must possess the same linewidth because, as the variable time delay approach shows, this peak does maintain the same dephasing behavior as for a single peak.[14]

Because no discrimination between these two possibilities can be made, this weak feature cannot be unambiguously assigned with current methods.

7.4.5. *Summary of Mode Assignments*

With a combination of experimental investigation and computational modeling, we are able to make new assignments for the aromatic C-H stretching modes of polystyrene, shown in Table 7-3. As we have shown in our experiments, there are 5 peaks in the VR-SFG spectrum of polystyrene assigned to only 4 resolvable modes; the ν_2 mode appears in two different environments, which provides the fifth peak. Under standard experimental conditions, the observed polystyrene modes are the IR-active ones, resulting in 4 peaks at approximately 3027, 3058, 3069, and 3085 cm^{-1}. These modes map well to the standard IR assignments, after consideration of the ν_2 mode in the two separate environments. Although the 3085 peak likely belongs to the ν_{7a} mode instead of the traditional ν_{20a} assignment, the direct correlation between IR and VR-SFG spectra is maintained because this assignment also applies to IR spectra. The appearance of the second ν_2 mode, which results from probing deeper into the interface than the topmost layer, is likely due to its much stronger VR-SFG susceptibility, allowing it to be detected in the second environment. There is no Raman-active peak at 3035 cm^{-1} in VR-SFG spectra, either because it does not produce sufficient amplitude when coupled with the weak IR response, or because it is shifted to ~3045 cm^{-1}. This fifth peak at ~3045 cm^{-1} can be resolved with use of variable time delay detection,[14] but this mode cannot be unambiguously assigned with currently known methods; in fact, this feature is not resolvable in standard experiments.

Once all pertinent factors have been considered, the assignments actually do maintain excellent agreement with previously determined IR and Raman assignments, as may be expected because the same material is being probed. The most significant difference in our assignments

Table 7-3. Revised PS mode assignments.

mode	VR-SFG peak / cm^{-1}
ν_{20b}	3027
ν_{20a}	Inactive/3045
ν_{7b}	Inactive/3045
$\nu_{2 \text{ (free)}}$	3069
$\nu_{2 \text{ (buried)}}$	3058
ν_{7a}	3085

compared to previous attempts is the observation of a duplicate ν_2 mode in a subsurface region. One other aspect of these assignments that should be mentioned is that they do not contain any anomalies that require further explanation, such as overtones or combination bands.

7.4.6.   *Practical Considerations*

It should be noted that, despite the ambiguity of some of the modes, the assignments of ν_2 and ν_{20b}, which are now unambiguously determined, are all that is required in many practical applications. As discussed above, these modes are of different symmetry type, assuming local C_{2v} symmetry, and can be used to determine molecular orientation. In fact, the other modes should not be used for this determination because of their weak response; orientations determined with these modes will be very uncertain.

Because the IR transition dipole moment of the ν_{20b} mode is orthogonal to that of the other modes, modifications to the sample that cause phenyl rings to stand more upright or lie down provide confirmation of these assignments, as shown in Figure 7-4. The phenylsilane samples contain phenyl rings that are primarily straight up because of the direct molecular attachment of the phenyl rings to the substrate. This upright orientation results in an absence of the 3027 cm^{-1} peak in the VR-SFG spectrum, as is predicted because the transition dipole moment is orthogonal to the surface normal, i.e. parallel to the surface. Likewise, when polystyrene is subjected to plasma treatment on insulating substrates, the surface phenyl rings that are sticking up are selectively destroyed, leaving only the 3027 cm^{-1} peak, indicating that the remaining phenyl groups are preferentially lying down.[25] The definitive assignment of these two modes provides the required information to identify a full range of behavior for the phenyl rings in polystyrene. Although we can provide relative orientations of the phenyl ring, we note that absolute orientations cannot be determined with currently available information; most
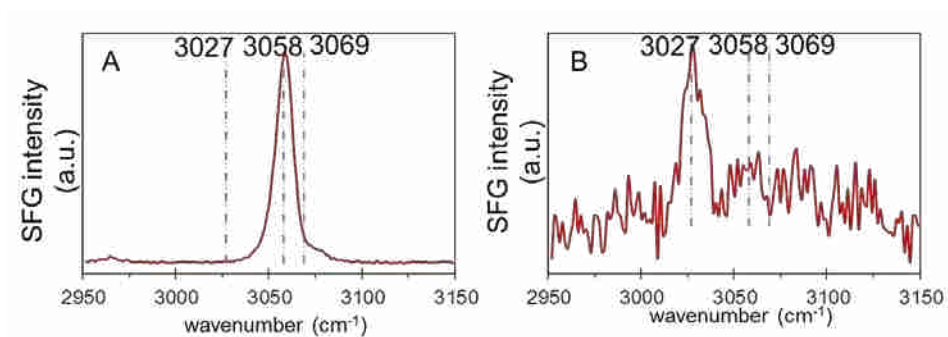
Figure 7- 4. When the orientation of phenyl rings are changes, the relative intensities of the orthogonal modes found at 3027 and 3058/3069 cm^{-1} changes. **A**) Direct molecular attachment of our phenylsilane samples forces a phenyl ring orientation that is straight up, causing the v_{20b} peak at 3027 cm^{-1} to be absent. B) After polystyrene has been exposed to plasma on fused silica, the phenyl rings that were sticking up are destroyed, leaving behind the phenyl rings that are lying down. This orientation allows only the 3027 cm^{-1} peak to be present with all remaining modes absent due to orthogonal vibrations.

importantly there are deficiencies in the available hyperpolarizabilities, as discussed in the Supporting Information.

7.5. Conclusions

With a combination of experimental investigation and computational modeling, we have put forth new assignments for the aromatic C-H stretches of polystyrene. Our work has shown that the mode assignments for polystyrene spectra do map well with assignments from bulk techniques once full consideration is given to all the rules governing VR-SFG susceptibility. First, it is possible to observe multiple peaks from a single mode in different environments, and this consideration should not be neglected, particularly in assigning surface spectra. Additionally, the ability to observe a particular mode depends on the mathematical product of the IR and Raman susceptibilities; however, this product can be difficult to predict. For this reason, not all peaks that appear in either IR or Raman spectra will necessarily be present in VR-SFG spectra, just as not all peaks mathematically calculated as having some IR or Raman activity are necessarily present in an IR or Raman spectrum. Direct experimental observation should be used to determine which modes are present in a VR-SFG spectrum.

Our mode assignments differ somewhat from those put forth previously, and other systems might need to be revisited to ensure proper interpretation of VR-SFG spectra. For example, the susceptibility rules that allow different environments to be detected likely affect the spectra of other polymer surfaces. This seems especially likely when an unusually strong mode, such as ν_2 in polystyrene, is present; it could arise from multiple environments. Additionally, not all the modes that are observed in both IR and Raman spectroscopies are necessarily present in VR-SFG spectra. Forcing a fit to include all the IR and Raman peaks can be problematic. Further

experimental confirmation is needed to identify what modes are actually present in the VR-SFG spectrum.

Although this study focused specifically on the mode assignments for polystyrene, this investigation has highlighted some interesting aspects of VR-SFG spectroscopy. The most significant result we report is the observation of VR-SFG signal from a sub-surface layer of higher density that the free surface. This observation shows that, under the right conditions, VR-SFG is not exclusively a surface-sensitive technique. Rather than limiting the scope of VR-SFG, however, this observation should be thought of as broadening its power because changes from surface ordering to bulk ordering can be monitored.

7.6. REFERENCES

(1) Varsanyi, G. *Vibrational Spectra of Benzene Derivatives*; Academic Press: New York, 1969.

(2) Gautam, K. S.; Schwab, A. D.; Dhinojwala, A.; Zhang, D.; Dougal, S. M.; Yeganeh, M. S. *Physical Review Letters* **2000**, *85*, 3854–3857.

(3) Briggman, K. A.; Stephenson, J. C.; Wallace, W. E.; Richter, L. J. *Journal of Physical Chemistry B* **2001**, *105*, 2785–2791.

(4) Wilson, P. T.; Richter, L. J.; Wallace, W. E.; Briggman, K. A.; Stephenson, J. C. *Chemical Physics Letters* **2002**, *363*, 161–168.

(5) Zhang, D.; Dougal, S. M.; Yeganeh, M. S. *Langmuir* **2000**, *16*, 4528–4532.

(6) Duffy, D. C.; Davies, P. B.; Bain, C. D. *Journal of Physical Chemistry* **1995**, *99*, 15241–15246.

(7) Meier, R. J. *Vibrational Spectroscopy* 2005, *39*, 266–269.

(8) Busson, B.; Tadjeddine, A. *Journal of Physical Chemistry C* **2009**, *113*, 21895–21902.

(9) Curtis, A. D.; Burt, S. R.; Calchera, A. R.; Patterson, J. E. *Journal of Physical Chemistry C* **2011**, *115*, 11550–11559.

(10) Ji, N.; Ostroverkhov, V.; Chen, C.-Y.; Shen, Y.-R. *Journal of the American Chemical Society* **2007**, *129*, 10056–10057.

(11) Stiopkin, I. V.; Jayathilake, H. D.; Bordenyuk, A. N.; Benderskii, A. V. *Journal of the American Chemical Society* **2008**, *130*, 2271–2275.

(12) Yamaguchi, S.; Tahara, T. *Journal of Chemical Physics* **2008**, *129*, 101102–101102–4.

(13) Pool, R. E.; Versluis, J.; Backus, E. H. G.; Bonn, M. *Journal of Physical Chemistry B* **2011**, *115*, 15362–15369.

(14) Curtis, A. D.; Asplund, M. C.; Patterson, J. E. *Journal of Physical Chemistry C* **2011**, *115*, 19303–19310.

(15) Lagutchev, A.; Hambir, S. A.; Dlott, D. D. *Journal of Physical Chemistry C* **2007**, *111*, 13645–13647.

(16) Curtis, A. D.; Reynolds, S. B.; Calchera, A. R.; Patterson, J. E. *Journal of Physical Chemistry Letters* **2010**, *1*, 2435–2439.

(17) Husseini, G. A.; Linford, M. R.; Asplund, M. C.; Peacock, J.; Sevy, E. T. *Surface Science Spectra* **2001**, *8*, 291–296.

(18) Valiev, M.; Bylaska, E. J.; Govind, N.; Kowalski, K.; Straatsma, T. P.; Van Dam, H. J. J.; Wang, D.; Nieplocha, J.; Apra, E.; Windus, T. L.; de Jong, W. A. *Computer Physics Communications* **2010**, *181*, 1477–1489.

(19) Varsanyi, G. *Assignments for Vibrational Spectra of Seven Hundred Benzene Derivatives*; Halsted Press: New York, 1974; Vol. 1.

(20) Li, G.; Dhinojwala, A.; Yeganeh, M. S. *Journal of Physical Chemistry B* **2009**, *113*, 2739–2747.

(21) Harp, G. P.; Rangwalla, H.; Li, G.; Yeganeh, M. S.; Dhinojwala, A. *Macromolecules* **2006**, *39*, 7464–7466.

(22) Harp, G. P.; Rangwalla, H.; Yeganeh, M. S.; Dhinojwala, A. *Journal of the American Chemical Society* **2003**, *125*, 11283–11290.

(23) Ringwald, S. C.; Pemberton, J. E. *Environmental Science and Technology* **1999**, *34*, 259–265.

(24) Zhang, C.; Wang, J.; Khmaladze, A.; Liu, Y.; Ding, B.; Jasensky, J.; Chen, Z. *Optics Letters* **2011**, *36*, 2272–2274.

(25) Calchera, A. R.; Curtis, A. D.; Patterson, J. E. *ACS Applied Materials and Interfaces* **2012**, *(submitted)*.

(26) Carter, R. L. *Molecular Symmetry and Group Theory*; John Wiley & Sons, Inc.: Hoboken, NJ, 1998.

7.7.1. *Spectra of Polystyrene in Additional Polarization Combinations*

Although the work presented in the main manuscript focuses on the peaks that are observed in *ssp* spectra, with their accompanying mode assignments, we have also collected *ppp* spectra. The *ppp* combination probes all nonzero elements of the $\chi^{(2)}$ tensor, so any peaks that are not discernible in *ssp* because of the molecular orientation should appear in *ppp* spectra. As shown in Figure 7-S1, the *ppp* spectrum is nearly identical to the *ssp* spectrum, showing that the contribution from other polarization combinations is effectively negligible in our experiments.

This result differs from previous studies for two main reasons: the magnitude of the nonresonant signal and the scanning geometry. More nonresonant signal is produced in *ppp* spectra because the nonresonant signal does not require a resonant response, and thus nonresonant signal will be generated from all four independent tensor elements regardless of the magnitude of the resonant response. We have previously shown that the nonresonant response invariably distorts the resonant spectrum, and both quantitative and qualitative comparison is greatly compromised.[1] However, when the nonresonant signal is removed, the resulting spectra for both *ssp* and *ppp* are essentially the same, showing that signal is dominated by the tensor element probed by the *ssp* configuration.

We did attempt to acquire spectra in the *sps* polarization combination, but were never able to observe a discernable resonant response. The only signal we could detect was nonresonant SFG. Because of the steep angle of incidence of the visible beam, there may be little discrimination between the interaction of the sample with *p* or *s* polarized visible light due to azimuthal symmetry. In *ppp*, however, though the resonant signal did not increase, the nonresonant signal from gold did, indicating that additional elements are being sampled. It may be possible to obtain better *sps* spectra by changing the incidence angle of the visible beam, but as discussed in the main text, this was not necessary for this work; all the needed information is contained in the *ssp* spectra.
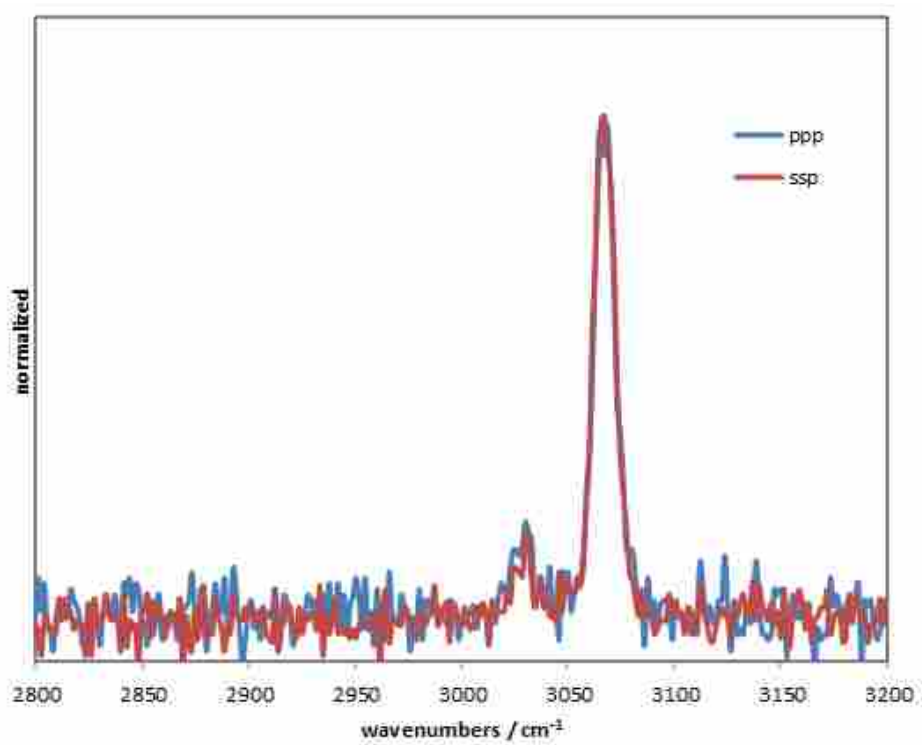
Figure 7-S1. Polystyrene scanned with *ppp* and *ssp* polarizations.

7.7.2. Specific Orientational Information for Polystyrene Spectra

Because the phenyl rings of polystyrene contain two vibrational modes with orthogonal transition dipole moments, the relative amplitudes of the two peaks can be used to determine the orientation according to the following equation:[2–4]

$$R = \left| \frac{A_{B1}}{A_{A1}} \right| = \left| \left(\frac{\beta_{caa,B1}}{\beta_{aac,A1}} \right) \left(\frac{2(\langle \cos 3\theta \rangle - \langle \cos \theta \rangle)}{(7+2r)\langle \cos \theta \rangle + (1-2r)\langle \cos 3\theta \rangle} \right) \right|$$

The above equation assumes a local C_{2v} symmetry with a random distribution of twist and azimuthal angles, allowing the tilt angle θ to be isolated and determined. R denotes the ratio between the amplitude A of a peak from a mode with B_1 symmetry to the amplitude of a peak from a mode with A_1 symmetry. r is the ratio of β_{ccc}/β_{aac} for the same A_1 vibration. The only peak that is definitively known as B_1 symmetry in polystyrene is the ν_{20b} peak and the most conclusive peak to use for A_1 symmetry is the ν_2 peak. The r ratio has been theoretically calculated for ν_2 as 1.13 by Briggman et al.[5]

Unfortunately, there is no agreement on the ratio of β values for the B_1 to A_1 modes, primarily due to our inability to accurately determine hyperpolarizabilities. As shown in the main paper, we can estimate relative hyperpolarizabilities, but due to uncertainty in the computed values we can only make qualitative comparisons. To determine absolute tilt angles, exact ratio values are needed. An additional complication is that previous determinations of polystyrene orientation used fit parameters for a peak at 3035 cm^{-1}, however we have shown that no peak is present at this location. Given the reported orientations and fit parameters, hyperpolarizability ratios for the observed peaks can be extrapolated. These hyperpolarizability ratios have been used to plot the anticipated amplitudes for a full range of orientation in Figure 7-S2, but it can easily be seen that these values do not agree and would result in different values for the tilt angle. Additionally, a self-consistency requirement shows the hyperpolarizabilty ratio cannot be accurate from either study. The spectra shown after plasma treatment only show the ν_{20b} mode, which requires that the amplitude ratio for ν_{20b}/ν_2 exceed 1, and neither of the hyperpolarizability determinations allow for such a response to occur; if the amplitude ratio exceeds 1, the hyperpolarizability ratio for the two modes must also be greater than 1.

Hyperpolarizability ratios could be determined from known orientations but such a system is not currently available. As can be seen in the chart, it is easy to identify when a
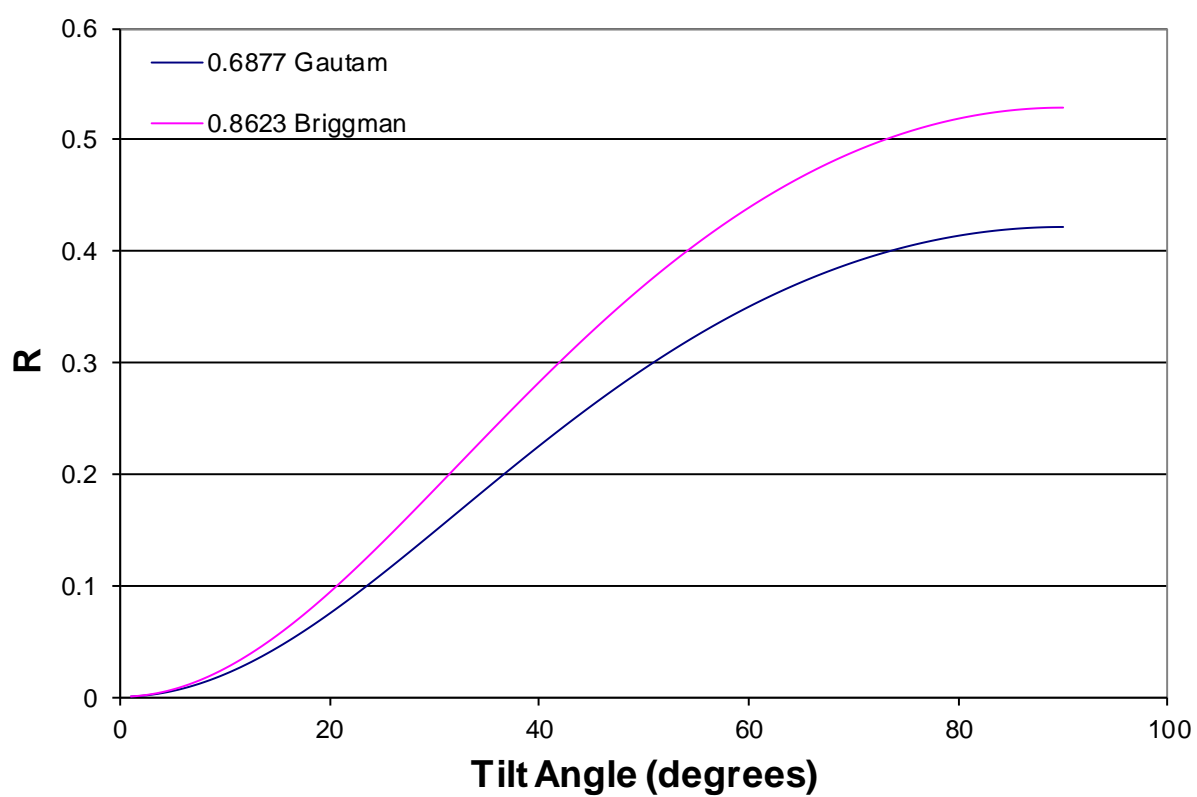
Figure 7-S2. Correlation of amplitude ratio R with tilt angle of phenyl groups using hyperpolarizability

ratios determined from Gautam[2] and Briggman[5].

molecule is standing straight up because the amplitude ratio will be 0, which we have seen in our phenylsilane samples; however, when the amplitude ratio is zero, it is impossible to determine the hyperpolarizabilty ratio of the two peaks because 0 divided by anything results in 0. A similar complication occurs for the other extreme where only the ν_{20b} peak is present. Furthermore, when only the ν_{20b} peak is present, that is the maximum tilt angle that can possibly be observed, but we know that the tilt angle cannot actually be 90° or no spectral response could be observed, independent of the polarization combination used. This sets a constraint on the accuracy of high tilt angle determinations. There is likely a constraint as well on lower tilt angle determinations in which anything below that angle will register as a ratio of 0. Because we do not independently know what this uncertainty is, we are not even definitively certain of the 0 or 90 degree angle determinations. The fact that the native polystyrene surface does show both ν_{20b} and ν_2 peaks fairly strongly, with the ν_2 peak significantly more intense than ν_{20b} means that the tilt angle is likely low, but more definitive quantification is not possible at this time.

7.7.3. References

(1) Curtis, A. D.; Burt, S. R.; Calchera, A. R.; Patterson, J. E. *Journal of Physical Chemistry C* **2011**, *115*, 11550–11559.

(2) Gautam, K. S.; Schwab, A. D.; Dhinojwala, A.; Zhang, D.; Dougal, S. M.; Yeganeh, M. S. *Physical Review Letters* **2000**, *85*, 3854–3857.

(3) Hirose, C.; Akamatsu, N.; Domen, K. *Applied Spectroscopy* **1992**, *46*, 1051–1072.

(4) Duffy, D. C.; Davies, P. B.; Bain, C. D. *Journal of Physical Chemistry* **1995**, *99*, 15241–15246.

(5) Briggman, K. A.; Stephenson, J. C.; Wallace, W. E.; Richter, L. J. *Journal of Physical Chemistry B* **2001**, *105*, 2785–2791.

CHAPTER 8:   ROLE OF NONRESONANT SUM-FREQUENCY GENERATION IN THE INVESTIGATION OF MODEL LIQUID CHROMATOGRAPHY SYSTEMS*

Although I am not the primary author of this paper, I was still a significant contributor to the majority of work presented herein (Dual primary authors were not used because I think it looks awkward in publications). This work was performed to show that the problems listed thus far are not isolated to polystyrene or to substrates that are known to produce large nonresonant signals. These complications are specifically illustrated in this chapter with octadecylsilane attached to fused silica substrates. This chapter provides direct evidence that even in systems that have been considered to possess negligible nonresonant contribution, the nonresonant signal is not negligible and can lead to faulty conclusions. This chapter further illustrates the fact that we really do not have an accurate model for the nonresonant response to correct in data processing procedures. Changes do occur in this study that could be reasonably treated as resonant changes if checks were not made, but such a conclusion would be inaccurate. Additionally, correction for nonresonant removal by the variable time-delay approach cannot be accomplished with this system as will be discussed.

8.1. ABSTRACT.

In vibrationally resonant sum-frequency generation (VR-SFG) spectra, the resonant signal contains information about the molecular structure of the interface, whereas the nonresonant signal is commonly treated as a background and has been assumed to be negligible on transparent substrates. The work presented here on model chromatographic stationary phases contradicts this assumption. Model stationary phases, consisting of functionalized fused silica windows, were investigated with VR-SFG spectroscopy, both with and without experimental suppression of the nonresonant response. When samples are moved from CD_3OD to D_2O, the VR-SFG spectrum was found to change over time when the nonresonant signal was present but not when the nonresonant signal was suppressed. No effect was seen when the solvent was changed and pressurized to 900 psi. These results suggest that the response to the new solvent manifests primarily in the nonresonant response, not the resonant response. Any structural changes caused by the new solvent environment appear to be minor. The nonresonant signal is significant and must be properly isolated from the resonant signal to ensure a correct interpretation of the spectral data. Curve-fitting procedures alone are not sufficient to guarantee a proper interpretation of the experimental results.

8.2. INTRODUCTION

Reversed-phase liquid chromatography (RPLC) remains one of the most popular methods for chemical separations. Despite its wide use, however, the detailed molecular mechanisms of chromatographic retention are not fully understood. The common models of retention involve adsorption and/or partitioning of the analyte from the mobile phase to the stationary phase and incorporate solvophobic and/or lipophilic interactions.[1-5] These models are useful in guiding thinking about retention, but do not fully describe the entire separation process. In fact, retention

time is a summative measure of all the interactions that take place along the length of the column. Development of more detailed mechanisms of retention requires knowledge about three main types of interactions: between the mobile and stationary phases, between the analyte and stationary phase, and between the analyte and mobile phase.[5] It must also be understood how these interactions are affected by experimental parameters, such as temperature, pressure, pH, and ionic strength. A better understanding of the detailed, molecular level interactions that lead to retention will aid in the design of separation programs and reduce the need for extensive empirical optimization.

Molecular spectroscopy, in a variety of forms, has been informative about many aspects of chromatographic retention. In particular, vibrational spectroscopy has been used to probe the structure of the stationary-phase/mobile-phase interface. For example, temperature-controlled FTIR studies revealed that the stationary phase does not undergo a discrete transition from an ordered "solid-like" phase to a disordered "liquid-like" phase.[6] Raman spectroscopy has been used to investigate the response of the stationary phase after exposure to elevated hydrostatic pressure[7] and some of the details of analyte binding.[8] Another technique that has been used in recent years is vibrationally resonant sum-frequency generation (VR-SFG) spectroscopy.[9,10]

VR-SFG is a nonlinear optical method that has inherent selectivity for interfaces and is thus well suited to the investigation of the molecular mechanisms of retention in RPLC. An overview of the principles has been given elsewhere,[11,12] but in brief, two laser beams overlap at the interface and produce a third beam at the sum of the two input frequencies. When one of the input beams is resonant with a molecular vibration at the interface, substantial enhancement occurs. Analysis of the relative intensities of various vibrational modes in VR-SFG spectra

provides information on molecular orientation and conformational order.[13] For this reason, proper measurement of peak intensities, free of distortion, is critically important.

VR-SFG has been applied to the study of model stationary phase systems consisting of fused silica flats functionalized with various alkylsilanes.[14,15] Conclusions have been drawn about the effect of molecular parameters, such as the degree of cross-linking between the alkylsilane chains,[15] and changes in molecular environment, such as solvent, on the structure of the interface.[16,17] As an example, Figure 8-1 shows results of our early work[18] with monolayers of octadecyldimethylsilane (ODMS) on fused silica; these spectra were acquired on a frequency scanning VR-SFG system. Clearly, the spectra in the three environments are different. These observations were interpreted in line with the stationary phase breathing model, whereby the effective volume of the stationary phase depends on solvent penetration[19] and are qualitatively similar to the results of others.[16] Further, they were interpreted as showing that a complete "phase collapse" does not occur in pure water, but rather that some conformational order is maintained even as the chains bend toward the surface;[18] other researchers[13,14] reached similar conclusions.

The interpretation of VR-SFG spectra of model stationary phases was based on certain assumptions that, at the time, had not been fully validated. In addition, VR-SFG spectra are complicated by two factors inherent to the technique. First, because VR-SFG is a coherent technique, overlap between peaks can lead to spectral distortion resulting in apparent changes to amplitude and center frequency. Second, the measurement contains a nonresonant signal that can also interfere with the resonant response. The overall VR-SFG intensity is represented mathematically as

$$I_{SFG} \propto \left| \chi_{NR}^{(2)} + \chi_{R}^{(2)} \right|^2 \tag{1}$$
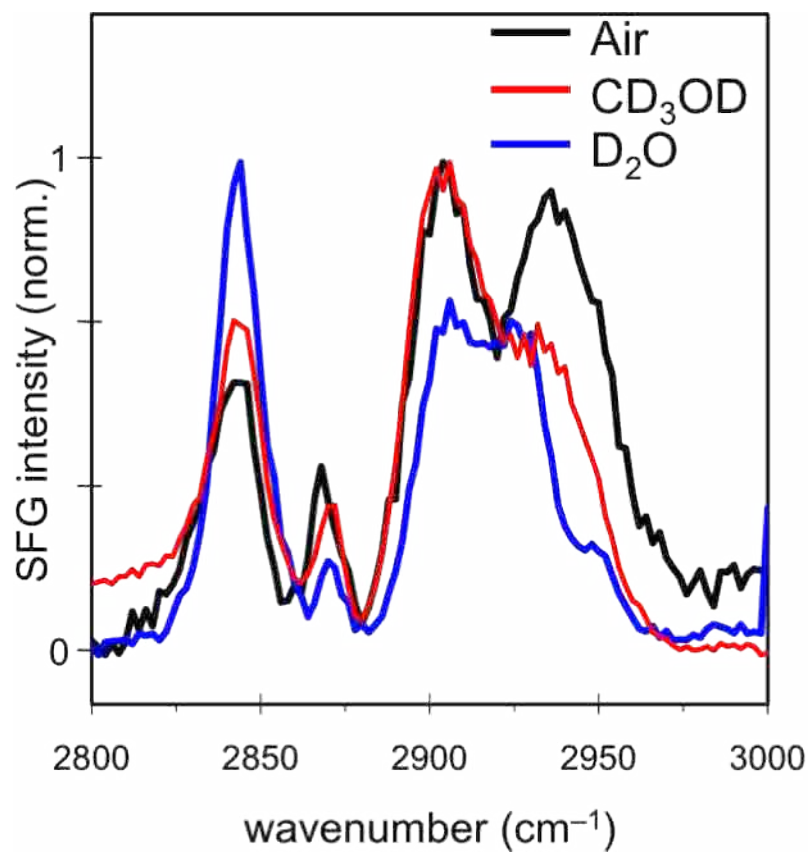
Figure 8-1. Monomeric C_{18} model stationary phases in various environments: air, CD_3OD and D_2O at ambient pressure.

where $\chi_{NR}^{(2)}$ and $\chi_{R}^{(2)}$ are the nonresonant and resonant susceptibilities, respectively. The resonant susceptibility is well modeled by a collection of Lorentzian profiles

$$\chi_{R}^{(2)} = \sum_{q} \frac{\Gamma_q \sqrt{A_q}}{\omega - \omega_q + i\Gamma_q} \tag{2}$$

where A_q, ω_q, and Γ_q represent the amplitude, central frequency, and Lorentzian half-width at half-max (HWHM) of each resonant vibrational mode. The first of these complications, regarding overlapping peaks, was appreciated and accounted for in the work cited above. However, the second issue involving the nonresonant response was not fully appreciated at the time. The fact that both the resonant and nonresonant susceptibilities are complex allows for interference between the two signals, as shown by

$$I_{SFG} \propto \left| \chi_{NR}^{(2)} + \chi_{R}^{(2)} \right|^2 = \left| \chi_{NR}^{(2)} \right|^2 + \left| \chi_{R}^{(2)} \right|^2 + 2 \left| \chi_{NR}^{(2)} \right| \left| \chi_{R}^{(2)} \right| \cos(\delta(\omega)) \tag{3}$$

In Equation (3), $\delta(\omega)$ is a frequency-dependent phase term that accounts for interference between the resonant and nonresonant signals and between overlapping resonant peaks. Interference between the resonant and nonresonant signals also leads to dramatic distortions of the resonant spectrum, which in turn can affect the determination of molecular orientations.

As we have discussed elsewhere,[20] it is not clear how best to model the nonresonant contribution. The conventional experiment measures the intensity of the total SFG response, but the amplitude and phase of the nonresonant signal are not measured independently without additional effort. Determination of the relative phase between various resonant peaks is possible with phase-sensitive or heterodyne-detection techniques,[21-23] but this requires additional experimental setup beyond the standard homodyne configuration. The relative amplitude and phase of the nonresonant signal have been determined for a very specific system on a conventional broadband VR-SFG system, but only through a series of experiments involving

suppression of the nonresonant signal.[24] As we show below, determination of the amplitude and phase of the nonresonant contribution through numerical processing or curve-fitting alone is not guaranteed to produce unique results; additional experimental data is essential.

When the substrate is nonconducting, a common practice has been to assume negligible interference by the nonresonant signal or to model it as a constant background. Either assumption can lead to misinterpretation of the experimental results, as was seen in a recent study of thin films of polystyrene on three different substrates.[25] Even though the nonresonant signal was weak from the fused silica and sapphire substrates, as compared to silicon, it had dramatic effects on the appearance of the VR-SFG spectra. When the nonresonant signal was experimentally suppressed, the spectra from all three substrates appeared identical, suggesting that the structure is independent of the substrate.

Although the nonresonant signal from fused silica may be weaker than from a conducting substrate, it cannot be treated as negligible, due to the cross term of Equation (3). This cross term can be advantageous in cases where $\left|\chi_N^{(2)}\right| > \left|\chi_R^{(2)}\right|$, such as with self-assembled monolayers (SAMs) on metallic substrates, because a weak resonant response is amplified by the cross term, although it is necessarily distorted from the true resonant response by this interference. This same effect can happen in reverse when $\left|\chi_R^{(2)}\right| > \left|\chi_N^{(2)}\right|$. Now the first term in Equation (3) is very small and the stronger resonant response will amplify the nonresonant response. This amplification, however, will be frequency-dependent; the nonresonant signal is only boosted at frequencies where there is a strong resonant signal.[20,26] In addition, not all the incident IR light can lead to generation of nonresonant signal because of absorption by the resonant vibrations. It is not currently known how to fully account for this frequency-dependent amplification of the nonresonant signal when analyzing VR-SFG spectra.[20] In earlier studies, narrow-band frequency

scanning systems were not capable of suppressing the nonresonant signal, but with a broad-band

VR-SFG system, the nonresonant signal can be experimentally suppressed by varying the delay

between the IR and visible probe pulses.[27] As we show here, suppression of the nonresonant

signal is critical to ensure proper interpretation of the VR-SFG spectra under varying conditions.

VR-SFG is a powerful technique for investigating interfaces; however, all aspects of the

measurement must be fully understood to ensure a proper interpretation of the data. For example,

it has been shown that the experimental configuration (e.g., incident angles of the probe beams)

can affect the measured intensities.[28-30] To fully account for these influences on the signal, proper

handling of the nonresonant response is necessary; the nonresonant response changes with

experimental configuration.[20] Furthermore, phase retrieval methods, which have been purported

to be useful in accounting for the nonresonant response, do not always produce results that agree

with direct experimental measurement.[31] Currently, the safest course of action is to

experimentally suppress the nonresonant signal, with subsequent correction for the resulting

time-domain distortions, although this correction may not always be necessary depending on the

level of detail that is desired.[20,26]

In this paper, we report VR-SFG measurements of model RPLC stationary phases both

with and without experimental suppression of the nonresonant SFG signal at ambient and

elevated hydrostatic pressure. We show that spectral changes that could be interpreted as arising

from structural modifications are actually due to changes in the nonresonant response. Contrary

to prior reports, we do not observe significant differences in the molecular structure of the

stationary phase upon change of the solvent. Some difference is observed with elevated

hydrostatic pressure conditions, with both the resonant and nonresonant signals being affected.

Because our aim is the development of models of retention in RPLC, the proper interpretation of

the spectra is critical. These results show that experimental suppression of the nonresonant response should be part of the full investigation to determine which observed changes are in fact structural. This work also raises intriguing questions about how the nonresonant response is affected by experimental conditions.

8.3. EXPERIMENTAL METHODS

8.3.1. Synthesis of Model Stationary Phases

To create model polymeric RPLC stationary phases, fused silica discs (rounds 1" diameter and 1/8" thick, Quartz Scientific), were functionalized with octadecyltrichlorosilane (OTS, $Cl_3SiC_{18}H_{37}$) with the following procedure, based on literature precedent.[32] (OTS monolayers are termed polymeric because each silane has three points of attachment, which enables cross-linking. This is not the case with octadecyldimethylchlorosilane (ODMS), which can only form a monolayer, hence the stationary phases are termed monomeric.) The discs were immersed in $CHCl_3$ and sonicated for ~5 minutes and then placed in 100+ °C *piranha* solution for 1 to 2 hours. (*Caution: Piranha solution, 3:1 concentrated H_2SO_4:30% H_2O_2, is highly corrosive and should be handled with extreme care.*) The *piranha*-treated discs were rinsed with copious amounts of ultrapure water from an 18 MΩ Millipore system, directly followed by sequential rinses with copious amounts of acetone, chloroform, and methylene chloride. All solvents were HPLC grade. The rinsed discs were placed in a beaker of ~100 mL methylene chloride. The discs were never allowed to dry out during this cleaning procedure to minimize the risk of surface contamination.

The beaker containing the cleaned discs, still immersed in methylene chloride, was placed in a nitrogen-purged glove box and approximately 1 mL of $Cl_3SiC_{18}H_{37}$ reagent (Gelest) was added. The beaker was placed on a shaker table and allowed to react for ~24 hours. The discs

were then removed and rinsed with copious amounts of methylene chloride, chloroform, acetone, ultrapure water, acetone, and chloroform and placed in a clean beaker of chloroform and sonicated for ~10 minutes to remove unreacted and self-polymerized material adhering to the surface. Again, the discs were never allowed to dry out during the rinsing procedure. The discs were stored in CD_3OD until examined by VR-SFG.

8.3.2.   VR-SFG Setup

The broad-band VR-SFG spectroscopy[33,34] system is based on an amplified Ti:sapphire laser (Quantronix, Integra C) that produces 2.7 mJ per pulse at 1 kHz with a pulse duration of ~130 fs. The output beam is split, with the major portion pumping a broad band IR optical parametric amplifier (Quantronix, TOPAS-C) and the remaining portion of the laser passing through two Fabry-Pérot étalons to provide a spectrally narrow (2.5 cm^{-1} Lorentzian half-width half-max) visible pulse at ~795 nm. The optical parametric amplifier produces ~22 µJ of IR light centered in the C-H stretch region, around 2900 cm^{-1}, with a bandwidth of 250 cm^{-1}. The visible pulse energy at the sample is 20 µJ, with the visible beam slightly defocused to prevent damage to the sample. Polarization control of both the IR and visible beams is accomplished with periscopes. All spectra reported in this paper were acquired with the *ssp* configuration: *s*-polarized SFG produced by *s*-polarized visible and *p*-polarized IR light. The incident angles, external to the sample cell, were 60° for the IR and ~17° for the visible beam. For optimized detection, the polarization of the *s*-polarized SFG beam was rotated 90° by a half waveplate prior to entering a spectrometer (Andor Shamrock) with attached CCD (Andor iDus). A short-pass optical filter was placed before the spectrometer to remove reflected or scattered visible light. Measurement of the profile of the IR light was accomplished with a back-surface Au mirror

placed in the sample cell.[35] This reference material was also used to account for varying laser power.

The sample cell, shown in Figure 8-2, was constructed in-house and can hold a single fused silica disc.[36] A horizontal slot in the cap allows for optical access while still providing mechanical strength. An o-ring behind the disc provides a liquid seal. The liquid chamber is connected to a Lee Scientific pump by metal tubing. The hydrostatic pressure is set by a LabView interface that controls the pump. With the current cell design, the maximum safe operating pressure is ~1000 psi (68 atm); above this pressure the disc is prone to crack.

8.3.3. *Experimental Suppression of Nonresonant Signal*

The nonresonant signal was experimentally suppressed by delaying the visible pulse relative to the IR pulse with a manual delay stage.[27] Two delay times were used for these measurements. The zero-time delay was established by maximizing the SFG intensity from a Au reference; this response is purely nonresonant and provides the most accurate determination of time zero. As we have previously shown, the maximum nonresonant signal from fused silica occurs at a slightly later (< 0.5 ps) time.[20] The second delay time was set to 2.04 ps to effectively suppress all the nonresonant signal. To verify that the delay time could be reproducibly changed, a series of measurements were taken at the two positions of the delay stage with repeated cycling between them. No significant differences were seen in the spectra acquired at each delay time, regardless of the number of times the delay stage was moved, confirming good reproducibility in the position of the stage.
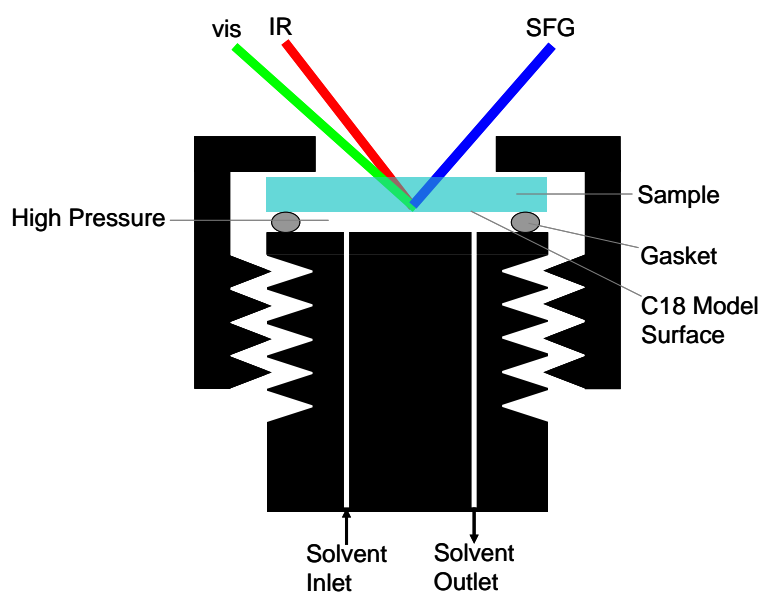
Figure 8-2. Diagram of the sample cell for VR-SFG probing of model RPLC stationary phases

8.4.1. *Ambient Pressure Measurements*

Model RPLC stationary phase samples that had previously been stored in CD_3OD were exposed to D_2O at ambient pressure. The sample was rinsed with D_2O and not allowed to dry out during placement in the sample cell. The samples were monitored *in situ* over time by VR-SFG to detect structural changes resulting from the change in the solvent environment. Multiple replicates of each measurement were performed over several months time, and the same trends were observed. As seen in Figure 8-3a, a noticeable change occurs in the spectrum after 1.5 hrs. The intensity of the band at 2945 cm^{-1}, assigned primarily to the Fermi resonance of the methyl symmetric stretch and methyl symmetric bend, has decreased relative to the intensity of the peak at 2885 cm^{-1}, assigned to the methyl symmetric stretch.[37] Figure 8-3a also includes a spectrum of a dried OTS-functionalized fused silica window that was dried under a nitrogen stream and exposed to air at ambient pressure; similar results were seen with freshly prepared samples that were dried after the rinsing procedure. Note that, in air, the 2945 cm^{-1} peak is more intense than the 2885 cm^{-1} peak; the 2945 cm^{-1} peak is relatively weaker in both solvent environments compared to a dry sample.

Figure 8-3b includes VR-SFG spectra of the same samples from Figure 8-3a but acquired with experimental suppression of the nonresonant response. The spectra with and without nonresonant suppression at each immersion time were acquired sequentially; there was a delay of 5-10 minutes between acquisitions because of the necessary integration times. Suppression of the nonresonant response changes the appearance of the spectrum as a result both of the elimination of interference with the nonresonant signal and effects in the time domain (discussed further below),[26] but for constant delay times, spectra can be directly compared. With suppression of the
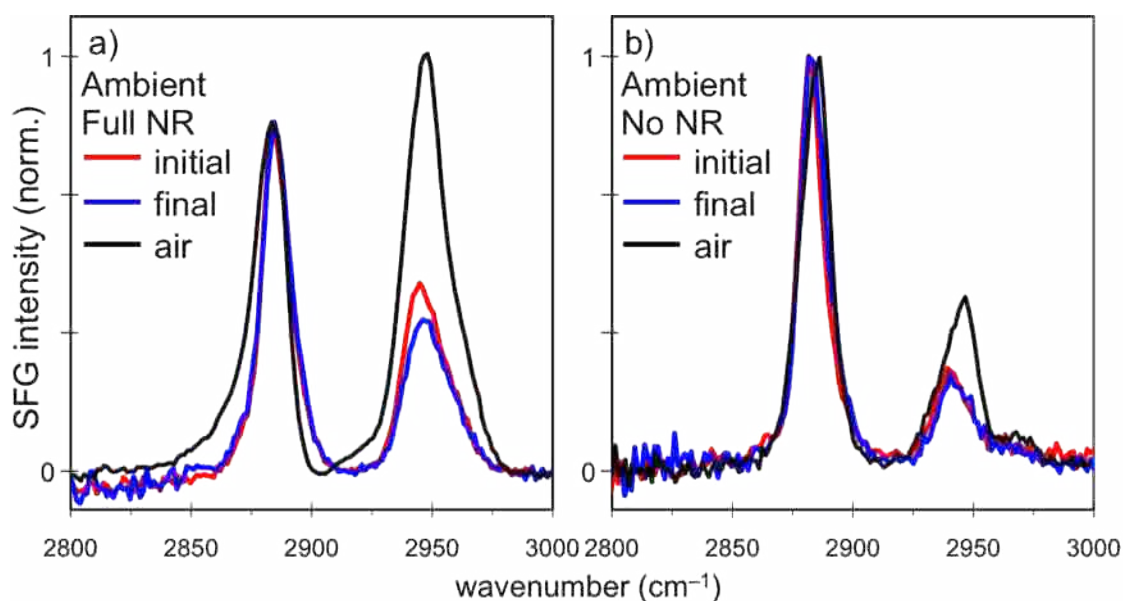
Figure 8-3. a) VR-SFG spectra of polymeric C_{18} model stationary phases in separate environments. "Initial" denotes a sample previously stored in CD_3OD and immersed in D_2O at ambient pressure. "Final" denotes spectra of the same sample acquired 1.5 hrs after immersion. "Air" denotes a dried sample exposed to ambient air. b) Spectra of the identical samples in the same three environments obtained with full suppression of the nonresonant signal. Each spectrum was acquired within 10 minutes of the corresponding spectrum in Figure 8-3a. Spectra are normalized to the feature at 2880 cm^{-1}.

nonresonant response, unlike what is seen in Figure 8-3a, after 1.5 hrs in D_2O, the relative intensities are virtually unchanged. Also included in Figure 8-3b is a spectrum from a sample exposed to air acquired with the nonresonant signal suppressed. Here the relative intensity of the 2945 cm^{-1} peak is higher than in either solvent. Note also that the 2945 cm^{-1} peak has significantly decreased in relative intensity compared to Figure 8-3a even though nothing was physically done to the sample. Some distortion of the line shape is also evident.

8.4.2. *Elevated Pressure Measurements*

Figure 4a contains VR-SFG spectra of polymeric OTS stationary phases exposed to D_2O at an elevated hydrostatic pressure of 900 psi to investigate the possible effects of pressure in an HPLC column. Samples were previously stored in CD_3OD, as in the ambient pressure studies. The first spectrum was acquired immediately after immersion and increase of the pressure, and the second was acquired after 3 hrs of exposure to high pressure D_2O. The spectra at elevated pressure differ from those at ambient pressure (compare the initial spectra in Figures 8-3a and 4a), but the relative peak intensities are virtually unchanged over the three-hour period. In other trials, no changes were observed up to 5 hrs after pressurization. Figure 8-4b shows VR-SFG spectra from the same sample in Figure 8-4a acquired with suppression of the nonresonant response. As at ambient pressure, no significant change in relative intensity is apparent over time when the nonresonant signal is suppressed.

8.5. DISCUSSION

As is readily seen from the results in Figures 8-3 and 8-4, the VR-SFG spectra appear very different depending on how they are acquired. Interpretation of these results must account for all these observations, which requires a separation of how both the resonant and nonresonant

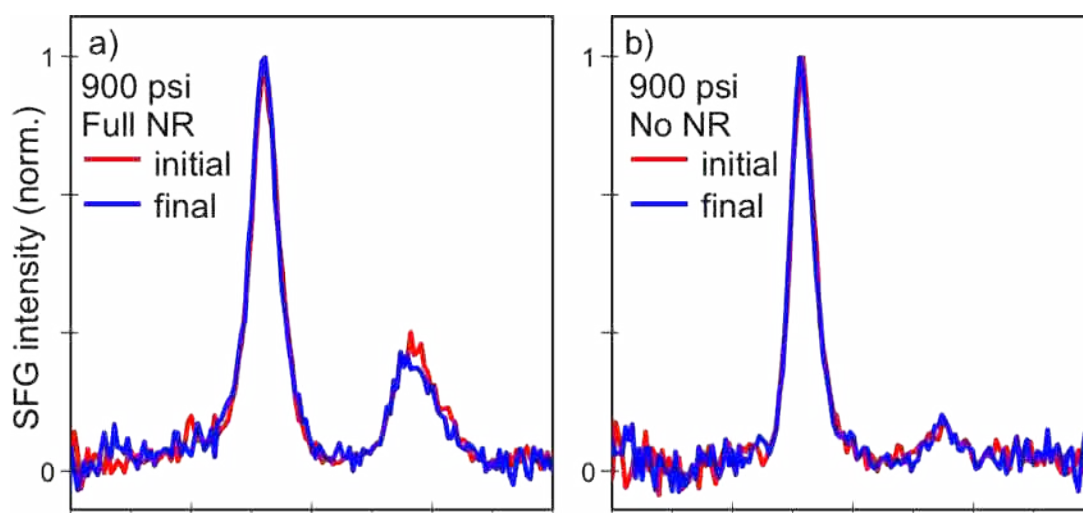**Figure 8-4.** Polymeric C_{18} model stationary phases previously stored in CD_3OD and immersed in D_2O at 900 psi hydrostatic pressure. Spectra acquired upon initial immersion and pressurization (initial) and after 3 hrs (final). a) Spectra obtained with no suppression of the nonresonant signal. b) Spectra obtained with full suppression of the nonresonant signal. Spectra are normalized to the feature at 2880 cm^{-1}.

signals respond to the changing environment. These environments include a change of solvent and a change of pressure, which we now discuss in turn.

8.5.1.   *Spectral Changes at Ambient Pressure*

As seen in Figure 8-3a, when the VR-SFG spectra are acquired in the conventional manner – i.e., no nonresonant suppression – they exhibit changes that may be interpreted as structural differences in various environments. As an OTS-functionalized sample goes from air to methanol to water, the intensity of the 2945 cm^{-1} peak decreases relative to the 2885 cm^{-1} peak. Such changes could be interpreted as resulting from reorientation of the methyl terminus in response to the new environment. However, when the nonresonant signal is experimentally suppressed in Figure 8-3b, no intensity changes are observed from initial to final, suggesting a structure that doesn't change over time. There is, however, still a difference in the spectrum of the sample that was exposed to air.

These results indicate that greater caution must be taken in interpreting changes in VR-SFG spectra; factors other than the molecular structure influence the measured spectrum of the OTS-functionalized samples. In particular, the nonresonant signal has been shown to cause dramatic spectral changes,[25] and these results appear to be another example of this effect. Previous studies of OTS-functionalized surfaces have assumed that the nonresonant signal is either constant or negligible. Our results show the possibility that the apparent changes seen in the VR-SFG spectrum after exposure to the new solvent environment are due not to changes in the resonant response, which would indicate structural changes, but to changes in the nonresonant response, which then manifest as a change in relative intensity of the resonant features. To better understand the interplay between the resonant and nonresonant signals, we

analyzed the spectra with conventional curve fitting and simulated the spectra with different amounts of resonant and nonresonant signal.

Figure 8-5 shows two attempts to fit the initial spectrum of OTS-functionalized fused silica in Figure 8-3a. The parameters from these fits, and one additional fit (shown in Supporting Information) are summarized in Table 8-1. Only two Lorentzian peaks were used in this fit, because that is all that can be experimentally resolved. All three attempts give statistically "good" fits; however, the resulting data sets are not at all consistent with each other. Most notably, the signs of the two peaks can be changed at will and a good fit is still obtainable. The sign and magnitude of the nonresonant amplitude and phase also change among the various fits. Clearly, multiple minima in the parameter space give equally good fits, but we have no real way to determine which set of parameters is physically meaningful. We could attempt to fit the spectrum with more fit functions, but that would introduce additional local minima, resulting in even more "good" fits but providing no physically meaningful information. What is needed is a unique set of parameters determined with the minimal number of fit functions bounded with experimentally validated constraints.

Table 8-2 includes the parameters from fits to the Final spectrum in Figure 3a. As before, multiple sets of parameters give equally good fits, making it difficult if not impossible to determine what is actually changing upon exposure to the new solvent environment. Note that the signs of the amplitudes in Trial 2 are reversed from the parameters in Table 8-1. Again, this is a fundamental problem in that we do not have enough independent data to uniquely determine all the parameters in the VR-SFG spectrum. Additional fit parameters will always improve the statistical quality of the fit, but the physical meaning is often lost.[38] The choice of fit parameters
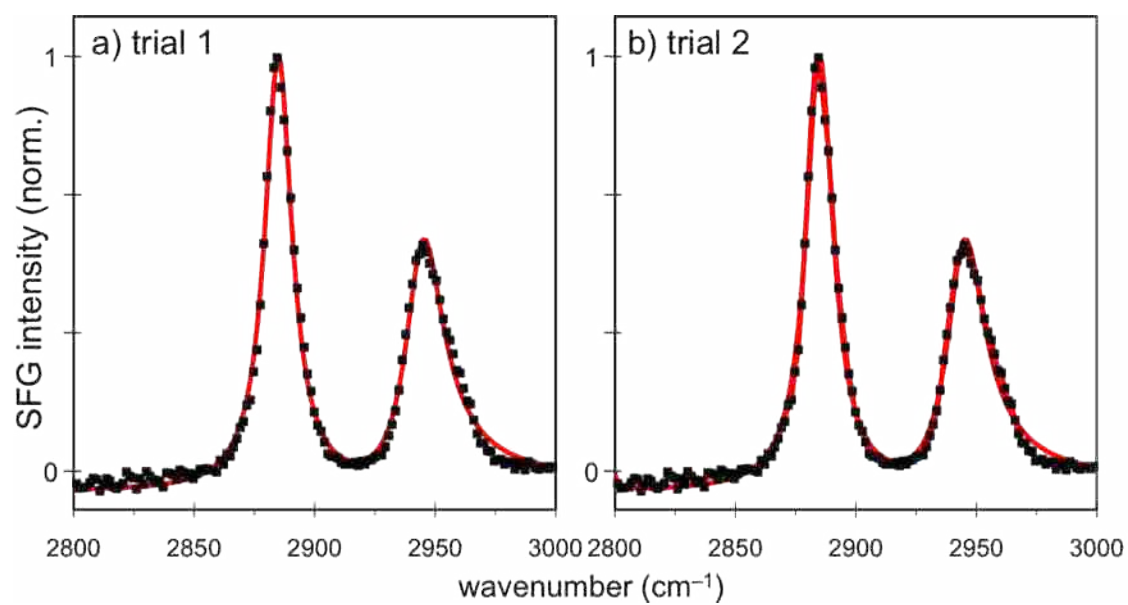
Figure 8-5. Attempts to fit the Initial spectrum in Figure 3a. The resulting fit parameters are summarized in Table 8-1.

Table 8-1. Attempted fits of Initial spectrum from Figure 8-3a.

	Trial 1		Trial 2		Trial 3	
	Value	95% conf.	Value	95% conf.	Value	95% conf.
A_1	0.5566	(0.4633, 0.65)	1.184	(1.12, 1.25)	–0.9387	(–1.044, –0.8331)
ω_1 / cm^{-1}	2885	(2885, 2885)	2885	(2885, 2885)	2885	(2885, 2886)
Γ_1 / cm^{-1}	6.908	(6.654, 7.162)	6.908	(6.654, 7.162)	7.070	(6.736, 7.404)
A_2	0.2418	(0.1915, 0.2922)	–0.4488	(–0.48, –0.42)	–0.4606	(–0.5262, –0.3949)
ω_2 / cm^{-1}	2944	(2944, 2945)	2944	(2944, 2945)	2943	(2942, 2943)
Γ_2 / cm^{-1}	9.636	(9.064, 10.21)	9.636	(9.064, 10.21)	9.141	(8.384, 9.899)
B_{NR}	0.3321	(0.2432, 0.421)	0.1563	(0.13, 0.18)	0.0863	(0.0532, 0.1194)
ϕ / rad	–1.309	(–1.391, –1.227)	–4.584	(–4.694, –4.474)	1.085	(0.468, 1.703)
sum of squared errors	0.0709		0.0709		0.11398	
R^2	0.99108		0.9906		0.98567	

Table 8-2. Attempted fits of Final spectrum from Figure 8-3a.

	Trial 1		Trial 2		Trial 3	
	Value	95% conf.	Value	95% conf.	Value	95% conf.
A_1	0.6042	(0.514, 0.694)	−1.301	(−1.355, −1.248)	−0.8998	(−0.9955, −0.8041)
ω_1 / cm^{-1}	2885	(2885, 2886)	2885	(2885, 2886)	2885	(2885, 2886)
Γ_1 / cm^{-1}	7.299	(7.045, 7.553)	7.31	(7.056, 7.565)	7.594	(7.277, 7.911)
A_2	0.2132	(0.1705, 0.2559)	0.7616	(0.7309, 0.7923)	−0.3477	(−0.3971, −0.2983)
ω_2 / cm^{-1}	2945	(2945, 2946)	2945	(2945, 2946)	2943	(2943, 2944)
Γ_2 / cm^{-1}	10.72	(10.01, 11.43)	10.76	(10.05, 11.48)	9.981	(9.101, 10.86)
B_{NR}	0.2758	(0.1973, 0.3543)	0.0479	(0.0332, 0.0626)	0.0970	(0.0625, 0.1314)
ϕ / rad	4.921	(4.833, 5.009)	0.6799	(0.4179, 0.9418)	0.931	(0.430, 1.43)
sum of squared errors	0.06404		0.06405		0.08908	
R^2	0.99145		0.99094		0.98811	

should be governed by the underlying physical model of the system, such as which resonances should be observed, and not on the quality of the fit alone.

To explore these issues further, simulated data sets were created based on Eq. (1) using the conventional model for the nonresonant signal of $\chi_{NR}^{(2)} = B_{NR}e^{i\phi}$. For these simulations, the resonant parameters were fixed, as was the nonresonant phase, ϕ, and only the nonresonant amplitude, B_{NR}, was changed. This was done for multiple values of the phase, two of which are shown in Figure 8-6. These simulated spectra illustrate how changes in the nonresonant amplitude can affect the spectrum in a way that could be interpreted as a change in the resonant response, and hence a structural change. The only way to definitively determine whether the resonant response, and by implication the structure, has changed is to remove the nonresonant response. In this study, with the nonresonant response suppressed, there is no significant difference in the resonant spectrum when the solvent changes from methanol to water, as seen in Figure 8-3b, suggesting no significant structural difference after long-term exposure to the new solvent. The structure in a liquid environment is likely different than when the sample is exposed to air; the relative intensities in air that are observed with the nonresonant signal suppressed are different from the liquid spectra, suggesting that this structure is, in fact, different.

One criticism of experimentally suppressing the nonresonant signal is that information about the nonresonant amplitude and phase are lost through this process. Similar to the approach taken in reference 24, we attempted to determine the resonant parameters from the suppressed spectra and then go back to determine the nonresonant amplitude and phase. In that study a silver substrate was used, which provided a strong nonresonant response, and the molecules attached to the surface only exhibited a single resonance. With our samples, the fused silica has a weaker nonresonant response, and the attached layer has multiple resonances. These factors frustrate any
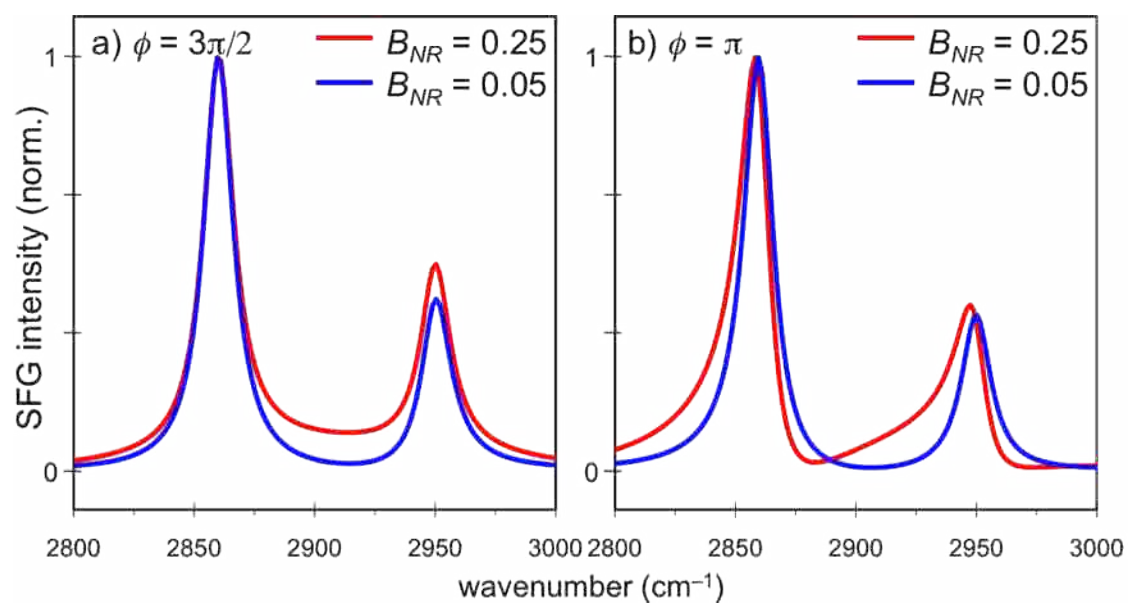
Figure 8-6. Simulation of a VR-SFG spectrum with fixed resonant parameters but variable nonresonant phase and nonresonant amplitude. Spectra are normalized to the feature at 2880 cm^{-1}.

attempt to uniquely determine the nonresonant parameters; there is effectively an infinite combination of amplitudes and phase that could be used. (This is discussed further in the Supporting Information.)

The problem rests in part on the assumed model of the nonresonant response, $\chi^{(2)}_{N\ R} = B_N\ e^{i\phi}$. As we found in our work on polystyrene,[20] this model is not always valid, and OTS-functionalized fused silica is another case where it does not work well. For the system in the current study, a single amplitude and phase do not accurately describe the nonresonant response. We can only comment qualitatively on how it changes with the solvent environment. In fact, one trend that is observed in the spectra and all the fits summarized in Tables 8-1 and 8-2 is that the amplitude of the nonresonant signal decreases over the course of time in the new solvent environment. With a nonresonant signal, unless the exact form of the nonresonant response is known, even the parameters of well resolved peaks cannot be determined. Removing the nonresonant signal reveals that the resonant signal, however, does not change.

8.5.2.   *Spectral Changes at Elevated Pressure*

The response of the OTS-functionalized fused silica windows to elevated hydrostatic pressure was significantly different from the response at ambient pressure in two main ways. First, the initial spectra, both with and without nonresonant suppression, are different than at ambient pressure. Specifically, the intensity of the 2945 cm^{-1} peak has decreased even further relative to the 2885 cm^{-1} peak. Second, no significant change in the spectrum occurs over time, either with or without inclusion of the nonresonant signal. These results suggest that pressure does have an effect on the interface, which may manifest in two ways. First pressure may affect the structure, but any structural changes must take place quickly – the delay between the sample placement and the initial measurements was about 10 minutes. Second, the different relative

intensities in Figure 8-3b compared to 8-4b could be due to time-domain effects, particularly of the Fermi resonance, and not actual structural changes.

Effects of elevated pressure are also manifested in the nonresonant response, which causes some of the changes seen when comparing Figures 8-3a and 8-4a. The nonresonant response appears to be somewhat weaker and does not change with time. Without the separation of the two contributions, we could erroneously conclude that whatever structural changes take place in the new solvent environment are inhibited by elevated pressure. Full comparison of the spectra obtained both with and without nonresonant suppression reveals that some change is occurring, and that this change manifests in the nonresonant response; the nonresonant-suppressed spectra alone would not fully show all the responses to elevated pressure.

Although we cannot definitively identify the cause of the observed changes in the nonresonant signal, it seems reasonable that this response reflects the local solvent environment at the interface. One hypothesis is that when the sample is stored in methanol, some solvent molecules diffuse to the substrate where they can hydrogen bond with unfunctionalized surface silanol groups. If this is true, then switching the solvent to water would result in swapping of the molecules that penetrated the alkyl layer, which in turn would change the local dielectric environment at the substrate. Whether this hypothesis proves to be correct or not, different solvent environments clearly result in different degrees of nonresonant signal, but may not significantly affect the structure of the alkyl chains. Comparing our spectra to those of Henry, *et al.*,[16] it appears that our OTS layers are of high surface coverage, which likely does not allow for much conformational freedom. It is possible that elevated hydrostatic pressure inhibits this solvent exchange to some degree as the alkyl chains reorient, and likely become less mobile. If methanol remains trapped at the substrate, the dielectric environment will not change and the

nonresonant signal will also remain unchanged. Indeed, in our earlier study,[18] the possibility of solvent penetration through the chains to the substrate was hinted at but not fully explored. This is a hypothesis that we are investigating further.

8.5.3. *Additional Challenges in Interpreting VR-SFG Spectra*

Even with suppression of the nonresonant response, unambiguous structure determination is still difficult. In a time-domain picture, the IR pulse resonantly excites the C-H stretches of the OTS molecules, and these vibrations then dephase over time. The resonant free-induction decay (FID) is sampled by the visible pulse to produce the measured VR-SFG spectrum. Because the duration of the visible pulse is shorter than the FID, incomplete sampling, or apodization, occurs, which leads to changes in the frequency-domain spectrum. We have recently developed a methodology that exploits these time-domain effects to better determine the parameters of the resonant spectrum, although some limitations remain.[26]

Despite these improvements in data collection and analysis, VR-SFG spectra of OTS-functionalized surfaces still present a challenge for proper interpretation. In particular, the peak at 2945 cm^{-1} is problematic. Its mode assignment varies in the literature, which will influence any structural determinations; it has been assigned as a single mode or as multiple overlapping modes.[14,15,32,39-41] We have recently shown[37] that this peak in fact contains two identifiable features, the Fermi resonance between the methyl symmetric stretch and methyl symmetric bend at 2945 cm^{-1} and a weaker feature, assigned as the methyl asymmetric stretch, at ~2960 cm^{-1}. (These assignments are based on work with ODMS, but also apply to OTS.) Simply assigning the peak at 2945 cm^{-1} to a single vibrational mode will undoubtedly affect any interpretations of the data. The 2885 cm^{-1} peak is assigned as the methyl symmetric stretch, and the relative intensity of these features should change with a structural change.

Because the 2945 cm^{-1} peak has strong Fermi-resonance character,[37] it dephases much more quickly than would be anticipated based on its line width;[42] thus, when the latter portions of the FID are sampled, this mode exhibits a dramatic decrease in the observed amplitude.[26] (This decrease in amplitude with delay time allows for the observation of the 2960 cm^{-1} mode and causes the asymmetric line profile seen in Figure 8-3b.) The mixed character of the 2945 cm^{-1} mode also makes it difficult to reconstruct the FID to determine the proper resonant parameters because the relationship between linewidth and lifetime is no longer described by a simple Lorentzian model.[42] Consider a case where the relative orientation of the methyl groups does not change, but the environment does change in a way affects the coupling of the stretch and bend modes that create the Fermi resonance. The alteration of this coupling will then cause the 2945 cm^{-1} peak to dephase more quickly than in another environment. This would in turn lead to a reduction in intensity of the 2945 cm^{-1} mode, either with our without nonresonant suppression, but this observation would not be indicative of a structural change. The Fermi coupling also affects the intensity of the 2885 cm^{-1} mode through intensity borrowing, which presents additional complications. Use of the 2945 cm^{-1} mode for structural determination is problematic and, until these issues are resolved, challenges remain in determining absolute molecular structures of these systems. We continue to work on ways to unambiguously determine the molecular structure of OTS surfaces.

8.6. Conclusions

VR-SFG is a powerful probe of surface and interfacial structure, but the interpretation of the spectra is not always straightforward. The presence of nonresonant signal can significantly affect the measured spectra and potentially result in a misleading understanding of the system under study. For model chromatographic stationary phases, we have shown that the nonresonant

signal changes in response to environmental conditions. This different nonresonant response can cause changes in the VR-SFG spectra that could be attributed to structural changes. Rather than being a background signal, the nonresonant signal is valuable because it may reflect the local solvent environment and/or other symmetry considerations at the interface.

We explored the response of model polymeric C_{18} stationary phases to changes of solvent, from CD_3OD to D_2O, both at ambient pressure and 900 psi hydrostatic pressure. When the nonresonant signal is included in the measurement, the VR-SFG spectrum changes in a way that can be interpreted as a time-dependent structural change as the interface responds to the new solvent environment. These types of changes are not observed at elevated pressure. However, when the nonresonant signal is experimentally suppressed, time-dependent spectral changes are not observed, either at ambient or elevated pressure. Whatever changes take place at the interface when the solvent is changed manifest significantly in the nonresonant response, but not in the resonant response. These changes might be due to penetration of the solvent to the substrate, which may be inhibited by elevated pressure; such processes, and their detailed kinetics, are still being investigated.

Given the different interpretation that arises from spectra obtained either with or without the nonresonant signal, we urge caution in interpreting VR-SFG spectra of these and other systems. In investigating model chromatography samples on fused silica substrates, as well as other interfaces on dielectric substrates, the nonresonant response is not negligible. The safest course is to experimentally suppress the nonresonant contribution. However, the nonresonant signal is not without value, as it is indicative of some type of change, still to be determined, in response to environmental conditions. All contributions to the SFG intensity, both resonant and nonresonant, need to be fully studied for a complete understanding of the interfacial system.

Work is ongoing with other types of stationary phases and other solvent and pressure conditions to determine what structural changes do take place and identify links between the structure of the interface and chromatographic retention.

Supporting Information Available. Additional discussion about the difficulty of using curve-fitting analysis when nonresonant signal is present. This material is available free of charge via the Internet at http://pubs.acs.org.

8.7. REFERENCES

(1) Horvath, C.; Melander, W.; Molnar, I. *Journal of Chromatography* **1976**, *125*, 129-156.

(2) Sentell, K. B.; Dorsey, J. G. *Analytical Chemistry* **1989**, *61*, 930-4.

(3) Dill, K. A. *Journal of Physical Chemistry* **1987**, *91*, 1980-8.

(4) Carr, P. W.; Li, J.; Dallas, A. J.; Eikens, D. I.; Tan, L. C. *Journal of Chromatogrophy, A* **1993**, *656*, 113-33.

(5) Ranatunga, R. P. J.; Carr, P. W. *Analytical Chemistry* **2000**, *72*, 5679-5692.

(6) Doyle, C. A.; Vickers, T. J.; Mann, C. K.; Dorsey, J. G. *Journal of Chromatography, A* **2000**, *877*, 41-59.

(7) Liao, Z.; Orendorff, C. J.; Pemberton, J. E. *Chromatographia* **2006**, *64*, 139-146.

(8) Doyle, C. A.; Vickers, T. J.; Mann, C. K.; Dorsey, J. G. *Journal of Chromatography, A* **1997**, *779*, 91-112.

(9) Zhu, X. D.; Suhr, H.; Shen, Y. R. *Physical Review B: Condensed Matter* **1987**, *35*, 3047-3050.

(10) Shen, Y. R. *Nature* **1989**, *337*, 519-25.

(11) Bain, C. D. *Journal of the Chemical Society: Faraday Transactions* **1995**, *91*, 1281-1296.

(12) Goates, S. R.; Schofield, D. A.; Bain, C. D. *Langmuir* **1999**, *15*, 1400-1409.

(13) Zhuang, X.; Miranda, P. B.; Kim, D.; Shen, Y. R. *Physical Review B: Condensed Matter* **1999**, *59*, 12632-12640.

(14) Pizzolatto, R. L.; Yang, Y. J.; Wolf, L. K.; Messmer, M. C. *Analytical Chimica Acta* **1999**, *397*, 81-92.

(15) Li, X.-Q.; Messmer, M. C. *Journal of Chromatography, A* **2003**, *984*, 19-28.

(16) Henry, M. C.; Wolf, L. K.; Messmer, M. C. *Journal of Physical Chemistry B* **2003**, *107*, 2765-2770.

(17) Henry, M. C.; Piagessi, E. A.; Zesotarski, J. C.; Messmer, M. C. *Langmuir* **2005**, *21*, 6521-6526.

(18) Horn, B. A. *Dissertation – Spectroscopic Investigations of Chromatographic Processes*; Brigham Young University: Provo, UT, **2001**.

(19) Yonker, C. R.; Zwier, T. A.; Burke, M. F. *Journal of Chromatography* **1982**, *241*, 257-68.

(20) Curtis, A. D.; Burt, S. R.; Calchera, A. R.; Patterson, J. E. *Journal of Physical Chemistry C* **2011**, *115*, 11550-11559.

(21) Ji, N.; Ostroverkhov, V.; Chen, C.-Y.; Shen, Y.-R. *Journal of the American Chemical Society* **2007**, *129*, 10056-10057.

(22) Stiopkin, I.; Jayathilake, H. D.; Bordenyuk, A.N.; Benderskii, A. V. *Journal of the American Chemical Society* **2008**, *130*, 2271-2275.

(23) Yamaguchi, S.; Tahara, T. *Journal of Chemical Physics* **2008**, *129*, 101102/1-101102/4.

(24) Shaw, S. K.; Lagutchev, A.; Dlott, D. D.; Gewirth, A. A. *Analytical Chemistry* **2009**, *81*, 1154-1161.

(25) Curtis, A. D.; Reynolds, S. B.; Calchera, A. R.; Patterson, J. E. *Journal of Physical Chemistry Letters* **2010**, *1*, 2435-2439.

(26) Curtis, A. D.; Asplund, M. C.; Patterson, J. E. *Journal of Physical Chemistry C* **2011**, *115*, 19303-19310.

(27) Lagutchev, A.; Hambir, S. A.; Dlott, D. D. *Journal of Physical Chemistry C* **2007**, *111*, 13645-13647.

(28) Gan, W.; Wu, B.-h.; Chen, H.; Guo, Y.; Wang, H.-f. *Chemical Physics Letters* **2005**, *406*, 467-473.

(29) Wang, H.-F.; Gan, W.; Lu, R.; Rao, Y.; Wu, B.-H. *International Reviews in Physical Chemistry* **2005**, *24*, 191-256.

(30) Gan, W.; Wu, B.-h.; Zhang, Z.; Guo, Y.; Wang, H.-f. *Journal of Physical Chemistry C* **2007**, *111*, 8716-8725.

(31) Chen, X.; Hua, W.; Huang, Z.; Allen, H. C. *Journal of the American Chemical Society* **2010**, *132*, 11336-11342.

(32) Liu, Y.; Wolf, L. K.; Messmer, M. C. *Langmuir* **2001**, *17*, 4329-4335.

(33) Van Der Ham, E. W. M.; Vrehen, Q. H. F.; Eliel, E. R. *Optics Letters* **1996**, *21*, 1448-1450.

(34) Richter, L. J.; Petralli-Mallow, T. P.; Stephenson, J. C. *Optics Letters* **1998**, *23*, 1594-1596.

(35) Quast, A. D.; Zhang, F.; Linford, M. R.; Patterson, J. E. *Applied Spectroscopy* **2011**, *65*, 634-641.

(36) Baker, L. R. *Thesis – Spectroscopic Study of Compressible Mobile Phase and Stationary Phase Behavior in Chromatography*, Brigham Young University, **2008**.

(37) Quast, A. D.; Wilde, N. C.; Matthew, S. S.; Maughan, S. T.; Castle, S. L.; Patterson, J. E. *Vib. Spectrosc.* **2011**, **DOI:** 10.1016/j.vibspec.2012.03.003.

(38) Meier, R. J. *Vibrational Spectroscopy* **2005**, *39*, 266-269.

(39) Lambert, A. G.; Neivandt, D. J.; Briggs, A. M.; Usadi, E. W.; Davies, P. B. *Journal of Physical Chemistry B* **2002**, *106*, 10693-10700.

(40) Nihonyanagi, S.; Eftekhari-Bafrooei, A.; Borguet, E. *Journal of Chemical Physics* **2011**, *134*, 084701/1-084701/7.

(41) Sagle, L. B.; Cimatu, K.; Litosh, V. A.; Liu, Y.; Flores, S. C.; Chen, X.; Yu, B.; Cremer, P. S. *Journal of the American Chemical Society* **2011**, *133*, 18707-18712.

(42) Fendt, A.; Fischer, S. F.; Kaiser, W. *Chemical Physics* **1981**, *57*, 55-64.

8.8. Supporting Information

8.8.1. *Attempts to Fit Individual Spectra that Include Nonresonant Signal*

Three attempts at fitting the initial spectrum from Figure 8-4a are summarized in Figure 8-S1 and Table 8-S1.

Figure 8-S1. Three separate curve-fits of the initial spectrum from Figure 4a.

Table 8-S1. Results of three attempts to fit the initial spectrum from Figure 4a.

Initial	Trial 1		Trial 2		Trial 3	
	Value	95% conf.	Value	95% conf.	Value	95% conf.
A_1	0.5566	(0.4633, 0.65)	1.184	(1.12, 1.25)	–0.9387	(–1.044, –0.8331)
w_1 / cm^{-1}	2885	(2885, 2885)	2885	(2885, 2885)	2885	(2885, 2886)
Γ_1 / cm^{-1}	6.908	(6.654, 7.162)	6.908	(6.654, 7.162)	7.070	(6.736, 7.404)
A_2	0.2418	(0.1915, 0.2922)	–0.4488	(–0.48, –0.42)	–0.4606	(–0.5262, –0.3949)
w_2 / cm^{-1}	2944	(2944, 2945)	2944	(2944, 2945)	2943	(2942, 2943)
Γ_2 / cm^{-1}	9.636	(9.064, 10.21)	9.636	(9.064, 10.21)	9.141	(8.384, 9.899)
B_{NR}	0.3321	(0.2432, 0.421)	0.1563	(0.13, 0.18)	0.0863	(0.0532, 0.1194)
ϕ / rad	–1.309	(–1.391, –1.227)	–4.584	(–4.694, –4.474)	1.085	(0.468, 1.703)
sum of squared errors	0.0709		0.0709		0.11398	
R^2	0.99108		0.9906		0.98567	

Figure 8-S2 and Table 8-S2 summarize the results of the curve-fitting analysis of the final
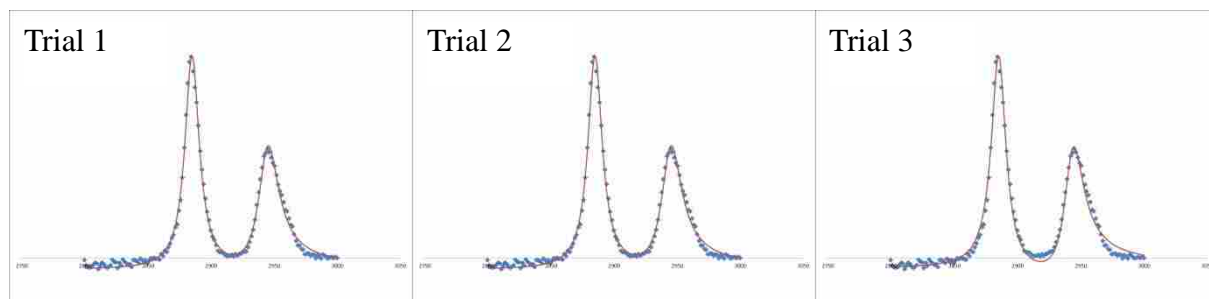
spectrum from Figure 8-4a.
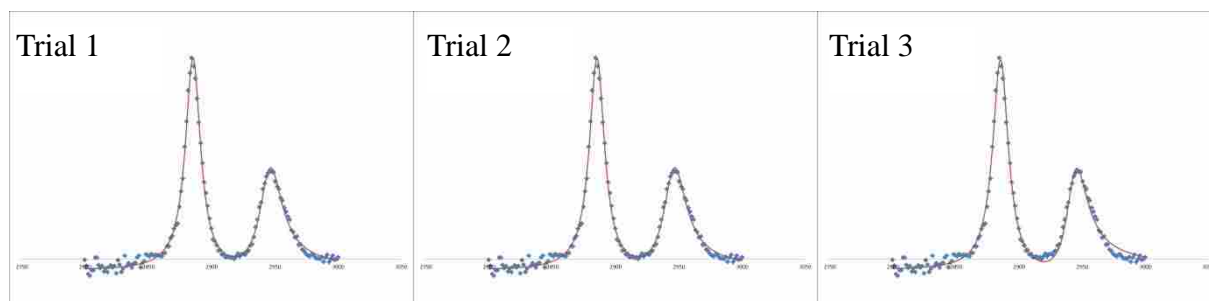
Figure 8-S2. Three separate curve-fits of the final spectrum from Figure 4a.

Table 8-S2. Results of three attempts to fit the final spectrum from Figure 4a.

Final	Trial 1		Trial 2		Trial 3	
	Value	95% conf.	Value	95% conf.	Value	95% conf.
A_1	0.6042	(0.514, 0.694)	−1.301	(−1.355, −1.248)	−0.8998	(−0.9955, −0.8041)
w_1 / cm^{-1}	2885	(2885, 2886)	2885	(2885, 2886)	2885	(2885, 2886)
Γ_1 / cm^{-1}	7.299	(7.045, 7.553)	7.31	(7.056, 7.565)	7.594	(7.277, 7.911)
A_2	0.2132	(0.1705, 0.2559)	0.7616	(0.7309, 0.7923)	−0.3477	(−0.3971, −0.2983)
w_2 / cm^{-1}	2945	(2945, 2946)	2945	(2945, 2946)	2943	(2943, 2944)
Γ_2 / cm^{-1}	10.72	(10.01, 11.43)	10.76	(10.05, 11.48)	9.981	(9.101, 10.86)
B_{NR}	0.2758	(0.1973, 0.3543)	0.0479	(0.0332, 0.0626)	0.0970	(0.0625, 0.1314)
ϕ / rad	4.921	(4.833, 5.009)	0.6799	(0.4179, 0.9418)	0.931	(0.430, 1.43)
sum of squared errors	0.06404		0.06405		0.08908	
R^2	0.99145		0.99094		0.98811	

As can be seen in the figures and corresponding tables above, multiple fits to the same data

set produce different solutions that are of good statistical quality. The resulting parameters are,

however, very different, thus these fits provide no physically meaningful results. All three fits are

nearly identical as judged by the sum of squared errors and R^2 and visual inspection, but produce very different resonant parameters, both in amplitude and sign. (We do admit that it is arguable that trial 3 does not fit as well as trials 1 and 2, but such a fit is still of comparable quality to what is typically seen in the literature.) Other sets of parameters were also obtained, but only these three are shown for illustration purposes. All these problems arise from the interference of the nonresonant signal. A common criticism of the nonresonant suppression technique is the loss of phase information; however, as seen in the different fits shown here, we never actually had any phase information to lose because the phase extracted from the fitting with the conventional model is highly variable, which likewise produces variable resonant parameters.

8.8.2.   Attempt to Simultaneously Fit the Initial and Final Spectra

Guided by the approach of reference 1, and knowing that the resonant spectrum does not change, we attempted to use a single set of resonant parameters to simultaneously fit the initial and final spectra and thus determine how the nonresonant signal changes. These results are summarized in Figure 8-S3 and Table 8-S3.
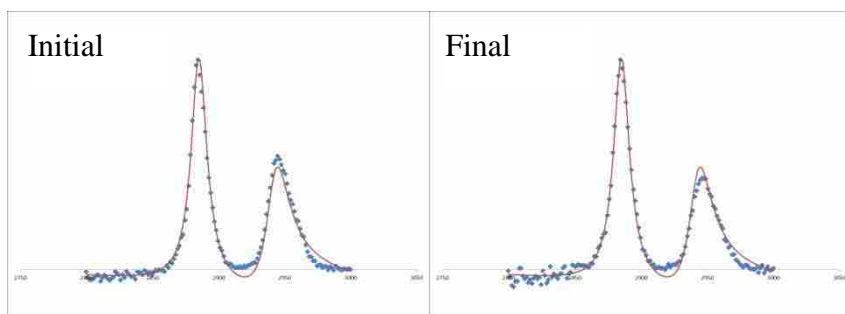

Figure 8-S3. Simultaneous fitting of the initial and final spectra from Figure 4a.

Table 8-S3. Results from the simultaneous fitting shown in Figure S3.

	Value	95% conf.
A_1	1.0	fixed
w_1 / cm^{-1}	2885	(2885, 2885)
Γ_1 / cm^{-1}	7.363	(7.090, 7.640)
A_2	0.4267	(0.0.4000, 0.4500)
w_2 / cm^{-1}	2942	(2941, 2942)
Γ_2 / cm^{-1}	10.51	(9.70, 11.32)
B_{NR} initial	0.1216	(−1.28e6, 1.28e6)
Φ initial	2.67e−14	(−1.06e6, 1.06e6)
B_{NR} final	0.1216	(−1.28e6, 1.28e6)
Φ final	2.67e−14	(−1.06e6, 1.06e6)

As seen in Figure 8-S3 and Table 8-S3, this simultaneous fitting approach does not work for our spectra. In fact, the results for the nonresonant amplitude and phase indicate that the values for these parameters are essentially arbitrary. The failure of this approach in this situation is due to the faulty assumption of a single-valued amplitude and/or phase of the nonresonant response. The fit line in both initial and final spectra is actually identical because, with the model of $\chi_{N}^{(2)}{}_R = B_N \, e^{i\phi}$ for the nonresonant response, the only minimum that can be found is to treat the difference in the spectral signal as noise and fit the average of the two responses; however, the signal-to-noise and reproducibility of the data clearly show that the two spectra are different.

The same difficulty arises, and the same result is obtained, when trying to fit either a single nonresonant amplitude and phase simultaneously for both spectra, or allowing for two different nonresonant amplitudes and phases (a separate amplitude and phase for each spectrum) because the model of the nonresonant response is inaccurate. It should also be noted that the discrepancies shown in this fit line to the data are identical to the discrepancies seen in

comparing theoretical modeling of the response to the actual data, again due to inaccurate

modeling of the nonresonant response and illustrating the important point that computer-assisted

curve-fitting cannot do anything beyond what a person can manually accomplish without the

fitting program.[2]

8.8.3.   References

(1) Shaw, S. K.; Lagutchev, A.; Dlott, D. D.; Gewirth, A. A. *Analytical Chemistry* **2009**, *81*, 1154-1161.
(2) Meier, R. J. *Vibrational Spectroscopy* **2005**, *39*, 266-269.

CHAPTER 9: ADDITIONAL CONSIDERATIONS AND FUTURE WORK

9.1. ASSUMPTIONS ABOUT LINESHAPES AND AMPLITUDES

As I have shown throughout this dissertation, accurate analysis of sum frequency spectroscopy cannot occur unless spectra are acquired with experimental conditions that more fully isolate the desired resonant response. However, even with the work that has been shown, a couple important points regarding lineshapes are still assumed and lack discussion.

One assumption that has been made throughout is that the underlying lineshapes of spectra collected with SFG are Lorentzian, but this is currently unconfirmed by direct experiment. Lorentzians are the natural lineshape if only lifetime broadening is present, which is the assumption invoked with SFG on solid materials. We know that the suppressed spectra adopt a Gaussian profile, but even when fitting unsuppressed spectra, better fits can often be obtained if using Gaussian lineshapes. The figures in chapter 8 reveal that the fits do not reach baseline for the ~2945 cm^{-1} peak of octadecylsilane samples when the experimental data does. This can be corrected to provide a better fit if Gaussian profiles are used, but it is not the commonly accepted assumption that such profiles represent the actual underlying physics.

The difficulty in determining the underlying lineshape is that it is impossible to determine an accurate peakshape from the tips only,[1] but the tips are all that is available when interference with other signal is present, whether from additional peaks or the broad nonresonant response. Because removing the nonresonant signal induces an apodization that definitively imposes a Gaussian profile, it is currently unknown whether the underlying peak parameters actually match a Lorentzian profile. If SFG peaks are not Lorentzian, the parameters determined from the variable time-delay approach are inaccurate, but the methodology is still valid.

The second consideration I wish to note is that SFG practitioners seem to be using peak amplitudes instead of peak areas. Peak areas are always the accurate comparison of the response from the vibrational modes, but amplitude ratios will be the same as long as the peak widths are identical. Often times this requirement seems to be forgotten as peak amplitudes from different widths are compared, or the fitting may assume all peak widths are the same and force the unverified assumption on the analysis. For an accurate analysis seeking quantitative information, peak areas should be used unless it has been unambiguously determined that the peak widths are the same for the two amplitude values being compared.

9.2. ADHESION STUDIES HAVE BEEN ENABLED

Despite the difficulties in obtaining absolute orientation information, quantifying relative change is still possible and the setup for adhesive studies has been built. This setup contains a direct attachment of an Instron testor to the sample mount on the optics table for SFG studies. The Instron is able to apply stress to samples with quantified force loads to provide the stress and record additional information as adhesive bonds are broken on samples. The adhesive of study is used to attach a fused silica window (which provides the spectroscopic access) to a metal post that is pulled by the Instron. We have tested samples of polystyrene dissolved in small amounts of chloroform to make an adhesive paste and have tested superglue between the fused silica and metal post. Sample preparation procedures are still being developed because our current adhesive bonds are breaking at forces lower than the Instron tester can accurately apply and measure, but the optical setup enabling the studies has been completed.

One of the pieces of information that has already been provided confirms the determination made in chapters 1 and 4 regarding the orientational order at buried interfaces. As the sample being probed is in between the fused silica substrate and metal post used for pulling,

no signal is observed. This absence of resonant signal has been verified by using control samples that do maintain a free surface and maintain signal in the same sample mount. This confirms the previous hypothesis that there is no ordering, or insufficiently detectable ordering, at a buried interface to cause an additional resonant interference to what is observed from the free surface.

9.3. SOURCE OF THE NONRESONANT SIGNAL

Progress is also being made toward determining the physical source of the nonresonant signal. The nonresonant signal unarguably results from fast responses, otherwise the suppression technique could not work. I do not doubt the electronic nature, but I believe it be an entropically driven indicator of disorder in the sample. Fresh samples possess more resonant and less nonresonant signal than aged or annealed samples, which suggests that the nonresonant signal is generated from randomly oriented areas of broken symmetry. The random orientation causes cancellation of the resonant signal; however, because the nonresonant signal is not resonant with anything to indicate ordering, it may not be subject to cancellation by the random orientations.

In recent work, primarily led by Angela Calchera, SFG signal has been observed in the *psp* polarization for atactic polystyrene and polymethylmethacrylate, which is considered to be a forbidden polarization. Neither polymer should possess any chirality or form any crystalline bulk, which are the two common explanations for such a phenomenon. The signal seems to be dominated by nonresonant generation, but this is still indicative that the polymer bulk may not be as isotropic as has been assumed. The fact that resonant signal is not observed may provide new insights into the physical generation of the nonresonant signal, such as randomly oriented domains of order. If nonresonant signal can be used as an indicator of relative disorder, it can provide additional information regarding interfacial interactions of interest, such as adhesive interactions or chromatography retention mechanisms.

APPENDICES

CURVE FITTING ROUTINES

This appendix will give the direct scripts used for a variety of curve fitting routines. For fitting a single spectrum, a single script is used dependent on whether you would like to fit with either Gaussian or Lorentzian lineshapes and confidence intervals are calculated automatically with the fit command. Gaussian functions are built into Matlab, so only the programming for the Lorentzian lineshapes and simultaneous fitting with the variable time-delay method will be shown. The number of peaks is determined by how many profiles you add to the fittype command. Simultaneous fitting with the variable time-delay approach is more complicated and involves nested functions to generate the multiple fit profiles. The multiple profiles are used to minimize residuals, and the command must be directly given to calculate the confidence intervals using the residuals and the Jacobian matrix (these are used in determination of confidence intervals with the fit command as well, but does not have to be explicitly requested). The Jacobian matrix is what contains all the parameter and confidence information, with the diagonal of the matrix containing the parameter values. Off-diagonal elements indicate the amount of covariance of the parameters and are used in calculating the confidence intervals.

FITTING TO LORENTZIAN LINESHAPES

```
cd R:\data\chromatography;              %loads directory containing data

%open gold reference file
disp('Select the Gold File')
[fname, dname]=uigetfile('*.asc','Read Spectrum File');
fid=fopen([dname,fname],'r');
data=fscanf(fid,'%f %f',[2,Inf]);
NR=data(2,:)';
gold=NR./max(NR);

    %open Sample file
    cd(dname);
    disp('Select the Sample File')
    [fname, dname]=uigetfile('*.asc','Read Spectrum File');
```

```matlab
fid=fopen([dname,fname],'r');
data=fscanf(fid,'%f %f',[2,Inf]);
wavelength=data(1,:)';
raw=data(2,:)';
freq=(1./wavelength-1/796).*10^7;
spectrum=(raw./max(raw)*0.1);

%Plot Spectrum
spectrum(freq<2600|freq>3400)=[]; %\
gold(freq<2600|freq>3400)=[];        %-removes excess baseline
freq(freq<2600|freq>3400)=[];      %/
plot(freq,spectrum,'.')
xlabel('wavenumbers')
ylabel('arb. units')
hold on
NR=ones(length(freq),1);          %establishes the assumed NR response
SFG=fittype('reference.*abs(sqrt(a1).*c1./((x-b1)+1i*c1)+...
sqrt(a2).*c2./((x-b2)+1i*c2)+sqrt(a3).*NR.*exp(1i.*phase))^2',...
'problem','reference');          %Fits two lorentzian peaks with nonres
                                  %Problem denotes the variable (reference)
                                  that will have predetermined values, not a
                                  fit parameter, and will be given to the
                                  fit command line.
                                  %Note: fittype must be on single line, not
                                   what is shown here.
start=[    .1    .1  0     2960 3025 5.00  5.00    0  3.60];
low = [-10.0 -10.0  0     2950 3015 0.00  0.00 -Inf  0.00];
high= [ 10.0  10.0  0.10  2990 3055 50.0  50.0  Inf  2*pi];
[sample,gof]=fit(freq,spectrum,SFG,'problem',gold,'Weights',weight,...
'StartPoint',start,'Lower',low,'Upper',high,'Robust','off','MaxFunEvals',...
1800);
disp(sample)
disp(gof)
```

VARIABLE TIME-DELAY

The variable time-delay uses three functions to perform simultaneous fitting. The master function is listed first with the name bigsolverconf.m This function provides initial parameter guesses and constraints to the function called nonlin5.m and receives feedback of the final paramters and statistical information required to calculate confidence intervals. Nonlin5 sets up the system of equations to simultaneously solve and provides the parameter information to sfgexp5.m from which it receives the theoretical fits to the multiple spectra. Sfgexp5 models the

response of a spectrum apodized with a given delay using the parameters provided by the above

functions.

bigsolverconf.m

```
cd S:/jeplab/data/polystyrene;
%open gold reference file
disp('Select the Gold File')
[fname, dname]=uigetfile('*.asc','Read Spectrum File');
fid=fopen([dname,fname],'r');
data=fscanf(fid,'%f %f',[2,Inf]);
goldraw=data(2,:)';
fclose(fid);
goldn=goldraw./max(goldraw);

%load multiple spectra for simultaneous fitting
    %open Sample file
    cd(dname);
    disp('Select the Sample File')
    [fname, dname]=uigetfile('*.asc','Read Spectrum File');
    fid=fopen([dname,fname],'r');
    data2=fscanf(fid,'%f %f',[2,Inf]);
    wavelength=data2(1,:)';
    raw=data2(2,:)';
    fclose(fid);
    freq=(1./wavelength-1/793.8).*10^7;
    scaled=freq.*2.998e10/10^13;
    spectrum=(raw./max(raw));
    newfreq=linspace(freq(1),freq(1024),2048)';
    hz=newfreq.*2.998e10;
    newscaled=hz./10^13;
    newspectrum=interp1(freq,spectrum,newfreq);


    disp('Select the Sample with less delay2')
    cd(dname)
    [fname, dname]=uigetfile('*.asc','Read Spectrum File');
    fid=fopen([dname,fname],'r');
    data3=fscanf(fid,'%f %f',[2,Inf]);
    fclose(fid);
    raw2=data3(2,:)';
    spectrum2=(raw2./max(raw2));
    newspectrum2=interp1(freq,spectrum2,newfreq);

    disp('Select the Sample with less delay3')
    cd(dname)
    [fname, dname]=uigetfile('*.asc','Read Spectrum File');
    fid=fopen([dname,fname],'r');
    data4=fscanf(fid,'%f %f',[2,Inf]);
    raw3=data4(2,:)';
    fclose(fid);
    spectrum3=(raw3./max(raw3));
    newspectrum3=interp1(freq,spectrum3,newfreq);
```

```matlab
    disp('Select the Sample with less delay4')
    cd(dname)
    [fname, dname]=uigetfile('*.asc','Read Spectrum File');
    fid=fopen([dname,fname],'r');
    data5=fscanf(fid,'%f %f',[2,Inf]);
    raw4=data5(2,:)';
    fclose(fid);
    spectrum4=(raw4./max(raw4));
    newspectrum4=interp1(freq,spectrum4,newfreq);

    disp('Select the Sample with less delay5')
    cd(dname)
    [fname, dname]=uigetfile('*.asc','Read Spectrum File');
    fid=fopen([dname,fname],'r');
    data6=fscanf(fid,'%f %f',[2,Inf]);
    raw5=data6(2,:)';
    fclose(fid);
    spectrum5=(raw5./max(raw5));
    newspectrum5=interp1(freq,spectrum5,newfreq);

    gold1=interp1(freq,goldn,newfreq);
    gold=abs(goldfit(newfreq,gold1)).^2;

%fit spectrum with gold reference
start=[ 0.1 3027 9.0 -0.1 3045 1.0  .10 3058 2.0  0.1 3069 4.0 -0.0 3085
3.0];
low = [-Inf 3025 0.5 -Inf 3040 0.5 -Inf 3055 0.5 -Inf 3065 0.5 -Inf 3080
0.5];
high= [ Inf 3030 9.9  Inf 3050 9.9  Inf 3060 9.9  Inf 3075 9.9  Inf 3090
9.9];
    options=optimset('MaxFunEvals',1e101,'MaxIter',1e10);
    format short g
    delay=[-25 -32 -39 -46 -50];

%fit data set simultaneously according to nonlin5 function
    [sample,resnorm,residual,exitflag,output,lambda,jacobian]=
lsqnonlin(@nonlin5,start,low,high,options,newfreq,gold,newspectrum,newspectru
m2,newspectrum3,newspectrum4,newspectrum5,delay);

%ci=confidence intervals from the residuals and the jacobian matrix. Default
value is used, which is 95% confidence
    ci=nlparci(sample,residual,jacobian);

    %Plot Fit
    figure(1)
    ww=sfgexp5(sample,newfreq,gold,delay(1));
    plot(freq,spectrum,'.')
    axis([2900 3200 -0.2 1.2])
    hold on
    SFGfit = plot(newfreq,ww,'r');
    legend('data','SFGfit')
    hold off

    figure(2)
    xx=sfgexp5(sample,newfreq,gold,delay(2));
    plot(freq,spectrum2,'.')
    hold on
```

```
SFGfit2=plot(newfreq,xx,'r');
axis([2900 3200 -0.2 1.2])
hold off

figure(3)
yy=sfgexp5(sample,newfreq,gold,delay(3));
plot(freq,spectrum3,'.')
hold on
SFGfit3=plot(newfreq,yy,'r');
axis([2900 3200 -0.2 1.2])
legend('data','SFGfit')
hold off

figure(4)
zz=sfgexp5(sample,newfreq,gold,delay(4));
plot(freq,spectrum4,'.')
hold on
SFGfit4=plot(newfreq,zz,'r');
axis([2900 3200 -0.2 1.2])
legend('data','SFGfit')
hold off

figure(5)
aa=sfgexp5(sample,newfreq,gold,delay(5));
plot(freq,spectrum5,'.')
hold on
SFGfit5=plot(newfreq,aa,'r');
axis([2900 3200 -0.2 1.2])
legend('data','SFGfit')
hold off

%Output Values
amplitudes=[sample(1),sample(4),sample(7),sample(10),sample(13)];
frequencies=[sample(2),sample(5),sample(8),sample(11),sample(14)];
HWHM=[sample(3),sample(6),sample(9),sample(12),sample(15)];
results=nan(5,3);
results(:,1)=amplitudes;
results(:,2)=frequencies;
results(:,3)=HWHM;
disp(results)
disp(ci)
```

nonlin5.m
```
function chisquare=nonlin5(a,x,ref,y1,y2,y3,y4,y5,delay)
s1=sfgexp5(a,x,ref,delay(1));
s2=sfgexp5(a,x,ref,delay(2));
s3=sfgexp5(a,x,ref,delay(3));
s4=sfgexp5(a,x,ref,delay(4));
s5=sfgexp5(a,x,ref,delay(5));
ytot=[y1;y2;y3;y4;y5];
stot=[s1;s2;s3;s4;s5];
chisquare=ytot-stot; %here chisquare really means residuals, squared errors
are already built into the lsqnonlin command if residuals are set up.
```

sfgexp5.m
```matlab
function s1=sfgexp5(a,x,ref,delay)

lorentzians=sqrt(a(1)).*a(3)./(x-a(2)+1i.*a(3))+sqrt(a(4)).*a(6)./(x-
a(5)+1i.*a(6))+sqrt(a(7)).*a(9)./(x-a(8)+1i.*a(9))+sqrt(1).*a(11)./(x-
a(10)+1i.*a(11))+sqrt(a(12)).*a(14)./(x-a(13)+1i.*a(14));

%in the Fourier transform, the length of the time axis is dependent on the
spacing between points in the frequency domain, so the axis is set to go from
0 to 1/(x2-x1) to obtain the proper time length
t=linspace(0,1/(112083213513110-112061692153739),2048)';
    gauss=abs(gaussian([2.2898e-12 1.0561e-12 .41961],t)).^2;
    decay1=exp(-10.08e11.*t);
    decay2=exp(-10.08e11.*t);
    g1=ifft(fft(gauss).*fft(decay1)); %the above functions generate
    g2=ifft(fft(g1).*fft(decay2));        visible line profile in time
    shift=circshift(g2,delay);       %shifts the profile in time
    vt=fft(ifft(lorentzians).*shift); %convolutes the resonant resonse with
s0=ref.*abs(vt).^2;                    the visible profile
  s1=s0./max(s0);
```

DETERMINATION OF THE INNATE LORENTZIAN PHASE FOR GAUSSIAN FITTING

Complex form of a Gaussian is obtained by multiplying by $e^{i\Phi(x)}$. This allows for interference with multiple peaks, but still maintains the same Gaussian function after a modulus squared. However, unless additional interferences are known, the phase $\Phi(x)$ should match the phase inherent in Lorentzian lineshapes for complex Gaussians to interfere in a coherent technique.

A Lorentzian is expressed by $\left| \dfrac{\sqrt{A} \times \Gamma}{\omega - \omega_0 + i\Gamma} \right|^2$ which has no readily apparent phase term, but actually does contain a frequency dependent phase term by nature of being complex. Any complex function can be modeled as $\mathbf{a} + \mathbf{b}i$ which can then be algebraically manipulated to extract the phase directly by modeling as $\left| function \right| e^{i\Phi(x)}$

The Lorentzian phase can be extracted by solving for $e^{i\Phi(x)}$ where x is now the frequency, expressed as ω, in the following relation:

$$\frac{\sqrt{A} \times \Gamma}{\omega - \omega_0 + i\Gamma} = a + bi = \left| \frac{\sqrt{A} \times \Gamma}{\omega - \omega_0 + i\Gamma} \right| e^{i\Phi(\omega)} \tag{1}$$

$$\frac{\sqrt{A} \times \Gamma}{\omega - \omega_0 + i\Gamma} = \frac{\sqrt{A}\Gamma(\omega - \omega_0)}{(\omega - \omega_0)^2 + \Gamma^2} - \frac{\sqrt{A}\Gamma^2}{(\omega - \omega_0)^2 + \Gamma^2} i = \sqrt{\frac{A\Gamma^2}{(\omega - \omega_0)^2 + \Gamma^2}} e^{i\Phi(\omega)}$$

After dividing by the modulus we are left with

$$\frac{\omega - \omega_0}{\sqrt{(\omega - \omega_0)^2 + \Gamma^2}} - \frac{i\Gamma}{\sqrt{(\omega - \omega_0)^2 + \Gamma^2}} = e^{i\Phi(\omega)} \tag{2}$$

After factoring the denominator this can be simplified to:

$$e^{i\Phi(\omega)} = \sqrt{\frac{\omega - \omega_0 - i\Gamma}{\omega - \omega_0 + i\Gamma}} \tag{3}$$

This phase function, which is inherent in the complex form of the Lorentzian lineshape, can now

be used for fitting Gaussian peaks as well.

The phase can also be directly solved for:

$$e^{i\Phi(\omega)} = \sqrt{\frac{\omega - \omega_0 - i\Gamma}{\omega - \omega_0 + i\Gamma}} \tag{4}$$

$$i\Phi(\omega) = \frac{1}{2}[\ln(\omega - \omega_0 - i\Gamma) - \ln(\omega - \omega_0 + i\Gamma)]$$

The ln of a complex number can be calculated by $\ln z = \ln|z| + i \arg(z)$ where

$\arg(x+iy) = \tan^{-1}(y/x)$. So

$$\frac{1}{2}[\ln(\omega - \omega_0 - i\Gamma) - \ln(\omega - \omega_0 + i\Gamma)] = \frac{1}{2}[\ln\sqrt{(\omega - \omega_0)^2 + \Gamma^2} + i\tan^{-1}(\frac{-\Gamma}{\omega - \omega_0}) - \ln\sqrt{(\omega - \omega_0)^2 + \Gamma^2} - i\tan^{-1}(\frac{\Gamma}{\omega - \omega_0})$$

$$= \frac{1}{2}[-2i\tan^{-1}(\frac{\Gamma}{\omega - \omega_0})] = -i\tan^{-1}(\frac{\Gamma}{\omega - \omega_0}) = i\Phi(\omega)$$

therefore, $\Phi(\omega) = -\tan^{-1}(\frac{\Gamma}{\omega - \omega_0})$. \tag{5}